1-1-2012

Synthesis and Self-Assembly of Polymeric Hybrid Nanomaterials

Amanda C. Kamps
University of Pennsylvania, amanda.kamps@gmail.com

Recommended Citation

Kamps, Amanda C., "Synthesis and Self-Assembly of Polymeric Hybrid Nanomaterials" (2012). *Publicly Accessible Penn Dissertations*. 648.
http://repository.upenn.edu/edissertations/648

Synthesis and Self-Assembly of Polymeric Hybrid Nanomaterials

Abstract

The ability to construct functional polymeric hybrid nanomaterials is critically important for many applications. In this thesis I present the synthesis of amphiphilic polymers of various compositions including insulating coil-coil, semiconducting rod-coil, semiconducting brush-coil, and bioconjugated rod-coil polymers. The self-assembly of these polymers is presented along with methodologies for controlling the organization of nanomaterials and polymers towards the construction of functional hybrid materials with controllable structures and properties.

In this thesis, an analysis of the conditions necessary to stabilize the cooperative self-assembly of nanoparticles and amphiphilic block copolymers into a unique cavity-like structure is presented. This work reveals the mechanism behind the formation of the structure and presents experimental and theoretical phase maps that show the conditions required to stabilize this structure for a range of nanoparticle sizes. These self-assembly guidelines provide an essential foundation for the generation of functional composites with predesigned structures and properties.

A high-yield click chemistry synthesis of an amphiphilic conjugated block copolymer with systematic block lengths that self-assembles into well-defined nanofibers whose length can be effectively controlled by varying the relative block-lengths is also presented. Furthermore, superstructures of bundled and branched nanofibers with tunable shapes, lengths, and densities were fabricated through hierarchical self-assembly. This work demonstrates that complex superstructures of organic semiconductors can be fabricated via bottom-up self-assembly approach using preformed nanofibers as building blocks.

The solution phase self-assembly of an amphiphilic conjugated brush copolymer into an elongated nanoribbon structure is also reported. The subtle effects of hydrogen bonding and pi-pi stacking interactions were investigated and found to be critical in the formation of this unusual structure which has not been reported for amphiphilic conjugated block copolymers and is important because it could offer insight into how internal packing structures affect the electronic properties of the polymer.

The synthesis and self-assembly of a bio-conjugated rod-coil block copolymer into distinct nanostructures is also presented. These functional bio-conjugated polymers combine the optoelectronic properties of semiconducting polymers with the bio-recognition properties of DNA and is important because it offers a new approach to forming semiconducting nanostructures with controllable geometries by self-assembly and to interface with biological molecules.

Degree Type
Dissertation

Degree Name
Doctor of Philosophy (PhD)

Graduate Group
Chemistry

First Advisor
So-Jung Park

Second Advisor
Mike Fryd

Keywords
amphiphilic block copolymers, conjugated polymers, nanocomposite materials, nanoparticles, self-assembly, supramolecular

Subject Categories
Chemistry | Nanoscience and Nanotechnology | Polymer Chemistry

SYNTHESIS AND SELF-ASSEMBLY OF POLYMERIC HYBRID NANOMATERIALS

Amanda C. Kamps

A DISSERTATION
in
Chemistry

Presented to the Faculties of the University of Pennsylvania
in
Partial Fulfillment of the Requirements for the
Degree of Doctor of Philosophy
2012

Supervisor of Dissertation	Co-Supervisor of Dissertation
So-Jung Park, Associate Professor of Chemistry	Mike Fryd, Adjunct Professor of Chemistry

Graduate Group Chairperson

Gary A. Molander, Professor of Chemistry

Dissertation Committee

Christopher B. Murray, Professor of Chemistry
Cherie Kagan, Professor of Materials Science and Engineering
Larry G. Sneddon, Professor of Chemistry

DEDICATION

to my best friend, Sean Anthony O'Loughlin,

the one I laugh with,

dream with,

live for,

love.

ACKNOWLEDGEMENTS

I'd like to thank my advisor, Dr. So-Jung Park for her mentorship and support. I'm appreciative of all the time and effort she has put into my thesis projects and into my professional development.

I'd also like to thank my advisor Dr. Mike Fryd. Your guidance, perspective, and scientific insight were invaluable to me. I am very grateful for our weekly discussions and I am greatly appreciative of the opportunity to learn about both science and life from such a great scientist and an amazing person.

I'd like to thank my committee members, Professor Chris Murray, Professor Cherie Kagan, and Professor Larry Sneddon. Thanks you for your advice, encouragement, constructive comments, and time.

I would also like to thank all the current and past members of the Park group. I've learned a lot from all of you and it has been a privilege to work with such talented people; Dr. Tim Duncan, Dr. Yeongri Jung, Dr. Sang-Jae Park, Dr. Zaki Estephan, Xi-Jun Chen, Rob Hickey, Helen Cativo, Zhaoxia Qian, and Qingjie Luo. I'd especially like to thank my undergraduate students Benjamin Young and Angela Mu. I'm very proud of both of you and it was a pleasure to work with you.

I'd especially like to thank Dr. Brenda Sanchez, Xi-Jun Chen, and Helen Cativo for being such great friends and such inspiring scientists. I greatly respect and admire your passion for life (and science), your compassion and strength.

I'd also like to thank my siblings, Rebecca, Brian and Sara for always reminding me that I work too hard and wondering why I'm still in school and why I don't get summers off. Thanks to my nieces, Helena and Elizabeth, for letting me be the 'cool out of town aunt' and for sticking up for me, 'Aunt Amanda's not a nerd!'. Thanks to my dad, Mark Kamps, for always encouraging me to be strong and independent. I'd also like to thank the Tesmers; Meghann, Matt, Tom, and Karen. You've always been there for me and I am so grateful for your support and encouragement.

I'd especially like to thank my husband, Sean O'Loughlin. You're my inspiration and my 'constant'. I'm so grateful for the last seven years and I am excited for our next journey together.

ABSTRACT

SYNTHESIS AND SELF-ASSEMBLY OF POLYMERIC HYBRID NANOMATERIALS

Amanda C. Kamps

So-Jung Park

Mike Fryd

The ability to construct functional polymeric hybrid nanomaterials is critically important for many applications. In this thesis I present the synthesis of amphiphilic polymers of various compositions including insulating coil-coil, semiconducting rod-coil, semiconducting brush-coil, and bioconjugated rod-coil polymers. The self-assembly of these polymers is presented along with methodologies for controlling the organization of nanomaterials and polymers towards the construction of functional hybrid materials with controllable structures and properties.

In this thesis, an analysis of the conditions necessary to stabilize the cooperative self-assembly of nanoparticles and amphiphilic block copolymers into a unique cavity-like structure is presented. This work reveals the mechanism behind the formation of the structure and presents experimental and theoretical phase maps that show the conditions required to stabilize this structure for a range of nanoparticle sizes. These self-assembly guidelines provide an essential foundation for the generation of functional composites with predesigned structures and properties.

A high-yield click chemistry synthesis of an amphiphilic conjugated block copolymer with systematic block lengths that self-assembles into well-defined nanofibers whose length can be effectively controlled by varying the relative block-lengths is also presented. Furthermore, superstructures of bundled and branched nanofibers with tunable shapes, lengths, and densities were fabricated through hierarchical self-

assembly. This work demonstrates that complex superstructures of organic semiconductors can be fabricated via bottom-up self-assembly approach using preformed nanofibers as building blocks.

The solution phase self-assembly of an amphiphilic conjugated brush copolymer into an elongated nanoribbon structure is also reported. The subtle effects of hydrogen bonding and pi-pi stacking interactions were investigated and found to be critical in the formation of this unusual structure which has not been reported for amphiphilic conjugated block copolymers and is important because it could offer insight into how internal packing structures affect the electronic properties of the polymer.

The synthesis and self-assembly of a bio-conjugated rod-coil block copolymer into distinct nanostructures is also presented. These functional bio-conjugated polymers combine the optoelectronic properties of semiconducting polymers with the bio-recognition properties of DNA and is important because it offers a new approach to forming semiconducting nanostructures with controllable geometries by self-assembly and to interface with biological molecules.

TABLE OF CONTENTS

List of Abbreviations

ACN	acetonitrile
AFM	atomic force microscope
ATRP	atom transfer radical polymerization
DCM	dichloromethane
DNA	deoxyribonucleic acid
DLS	dynamic light scattering
DMF	N,N-dimethylformamide
GPC	gel permeation chromatography
GRIM	grignard metathesis method
MW	molecular weight
ODN	oligodeoxynucleotide
PAA	poly(acrylic acid)
PAT	poly(alkylthiophene)
PBS	phosphate buffered saline
PDI	polydispersity index
PEG	poly(ethylene glycol)
PHT	poly(hexylthiophene)
PL	photoluminescence
PS	poly(styrene)
PTOTT	poly(tetra-oxo-tridecanyl-thiophene**)**
RAFT	reversible addition-fragmentation chain transfer
TEM	transmission electron microscope
THF	tetrahydofuran

LIST OF TABLES

LIST OF SCHEMES

LIST OF FIGURES

Chapter 1

Chapter 2

Chapter 3

Chapter 4

Chapter 5.

Chapter 1: Introduction

1.1 Synthesis of Block Copolymers

1.1.1 Living Radical Polymerization Techniques. In general the control in living radical polymerizations is achieved via a fast initiation event which provides a constant concentration of growing polymer chains. Another critical aspect of maintaining control in living radical polymerizations is the dynamic equilibrium between propagating radicals and dormant species. Termination in controlled living radical polymerizations is suppressed because of the low concentration of active species and propagating radicals. The near instantaneous growth of all the polymer chains in controlled living polymerizations provides critical control over the polymer chain architecture and polydispersity (typically < 1.2).[1]

The mechanism of living radical polymerization is very different from that of conventional radical polymerizations. Conventional radical polymerizations are basically chain reactions with the sequential addition of monomer units to form propagating radicals. Chains are initiated by radicals formed from an initiator adding to monomers. Chain termination occurs when the propagating radicals self-react via combination or disproportionation which results in polydispersities of >1.5 or >2.0 respectively.

Both controlled living radical polymerizations and conventional radical polymerizations grow though initiation, propagation, and termination pathways. However, there are many key differences between the two techniques that aptly demonstrate the advantages of living radical polymerization techniques. The first difference is that initiation is slow in conventional radical polymerizations whereas in controlled living radical polymerizations the initiation is very fast. Overall, the steady state of growing radicals is established by the activation-deactivation process in living radical polymerization techniques instead of the initiation-termination process used in conventional radical polymerizations. Another key difference between the two techniques is that termination in conventional radical polymerization occurs between longer chains, whereas in controlled living radical polymerizations the chains all grow over time and termination rates decrease significantly with time due to the persistent radical effect.[1]

1.1.1.1 RAFT. Reversible addition-fragmentation chain transfer (RAFT) polymerization was invented at CSIRO in the 1990s and gained popularity by 1998.[2] The RAFT polymerization method is advantageous because it can be used with a majority of monomers (including (meth)acrylates, (meth)acrylamides, acrylonitrile, styrenes, dienes, and vinyl monomers) and is tolerant of various functional groups and can therefore be run in aqueous or protic solvents.[3] RAFT has also gained popularity because it is relatively simple to implement and is cost-effective relative to other technologies. The success of a RAFT polymerization is dependent on the selection of a RAFT agent that is suitable for the monomer and the reaction conditions. RAFT chain transfer agents are typically thiocarbonylthio compounds (Scheme 1) that are typically composed of a C=X double bond that is reactive toward radical addition. The groups A and X are often either both CH_2 or both S, and the Z group is chosen to give the chain transfer agent the appropriate reactivity to propagating radicals. The R group is a homolytic leaving group and the R-radical must also be capable of reinitiating polymerizations.[4] The overall effectiveness of RAFT agents are determined by the R and Z substituents and have been extensively studied to provide guidelines for controlled RAFT polymerizations.[3, 5, 6] The RAFT agent is chosen to ideally have all the living chains grow simultaneously because the equilibration of dormant and active chain ends is rapid with respect to propagation.

The thiocarbonylthio groups present in the RAFT chain transfer agent are retained at the end of the polymers and allows for sequential synthesis of block copolymers and end-functionalized polymers.[7, 8] The thiocarbonylthio group can also be cleaved yielding thiol terminated polymers that can also be used as ligands for gold nanoparticles[9, 10], for surface attachment[11], or as building blocks for other syntheses[12].

Scheme 1. General mechanism of RAFT polymerization.

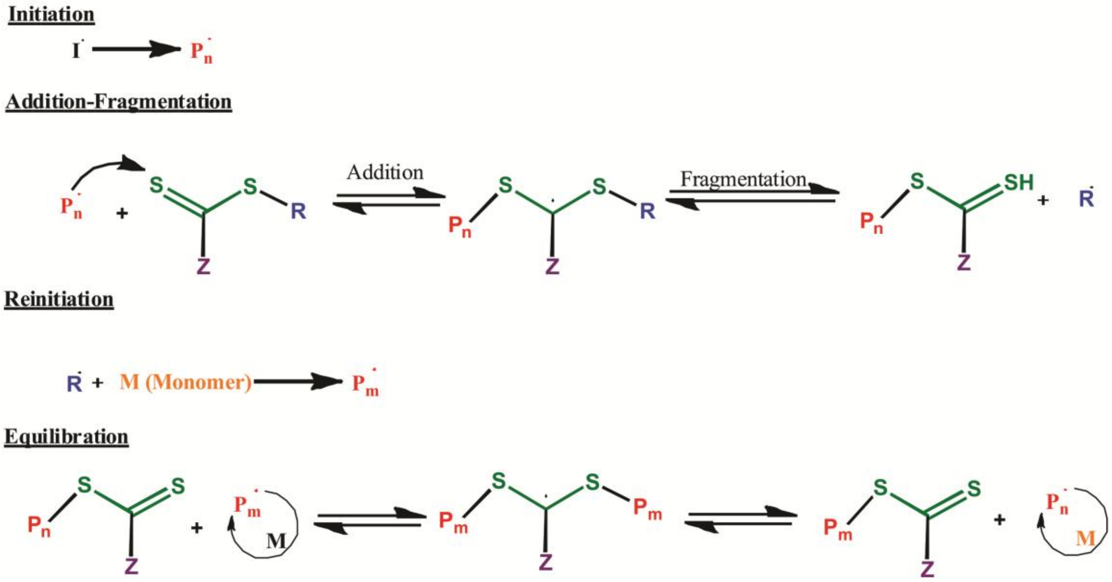

1.1.1.2 GRIM. The Grignard metathesis method (GRIM) is a polymerization method first developed in 1999 by McCullough[13] for the synthesis of highly regioregular poly(alkylthiophenes) with low polydispersities. Compared to other earlier methods for synthesizing poly(thiophenes), such as Rieke[14] and McCullough[13], the GRIM method is advantageous because it is a facile method that does not require cryogenic temperatures or highly reactive metals. GRIM is a transition metal catalyzed cross-coupling reaction. The polymerization proceeds through a catalytic cycle of transmetalation, reductive elimination, and oxidative addition (Scheme 2). The polymer chain growth occurs by an insertion of one monomer at a time as shown in the reaction mechanism cycle and the Ni(dppp) moiety is incorporated into the polymer chain as an end group via the formation of a *π*-complex.[15] The GRIM polymerization was originally thought of as proceeding by a step growth mechanism[16], however more recent reports describe the GRIM method as proceeding by a chain-growth and living polymerization[15, 17] Evidence for GRIM as a living polymerization is given by the fact that the monomer conversion is dependent on the molar ratio between the monomer and the nickel initiator, and by the ability to grow different polymer blocks by sequential polymerization.[15]

One of the main advantages of the GRIM method in regards to synthesis of amphiphilic block copolymers is the ease of end-group functionalization. In-situ functionalization of poly(thiophenes) is achieved by adding a Grignard reagent to both terminate and end-group functionalize the reaction (Scheme 2). A number of different Grignard reagenets (ethynyl, allyl, vinyl, phenyl) can be used to terminate the reaction.[18] Furthermore, the nature of the end capping reaction in which the end-group is formed through a nickel-π complex insures that the resultant polymer has only one functional end-group instead of two. This in-situ end-capping capability of the GRIM polymerization method is very advantageous because it is critical for poly(thiophenes) use as building blocks for the synthesis of amphiphilic block copolymers.

Scheme 2. General mechanism of GRIM polymerization and end-capping reaction.

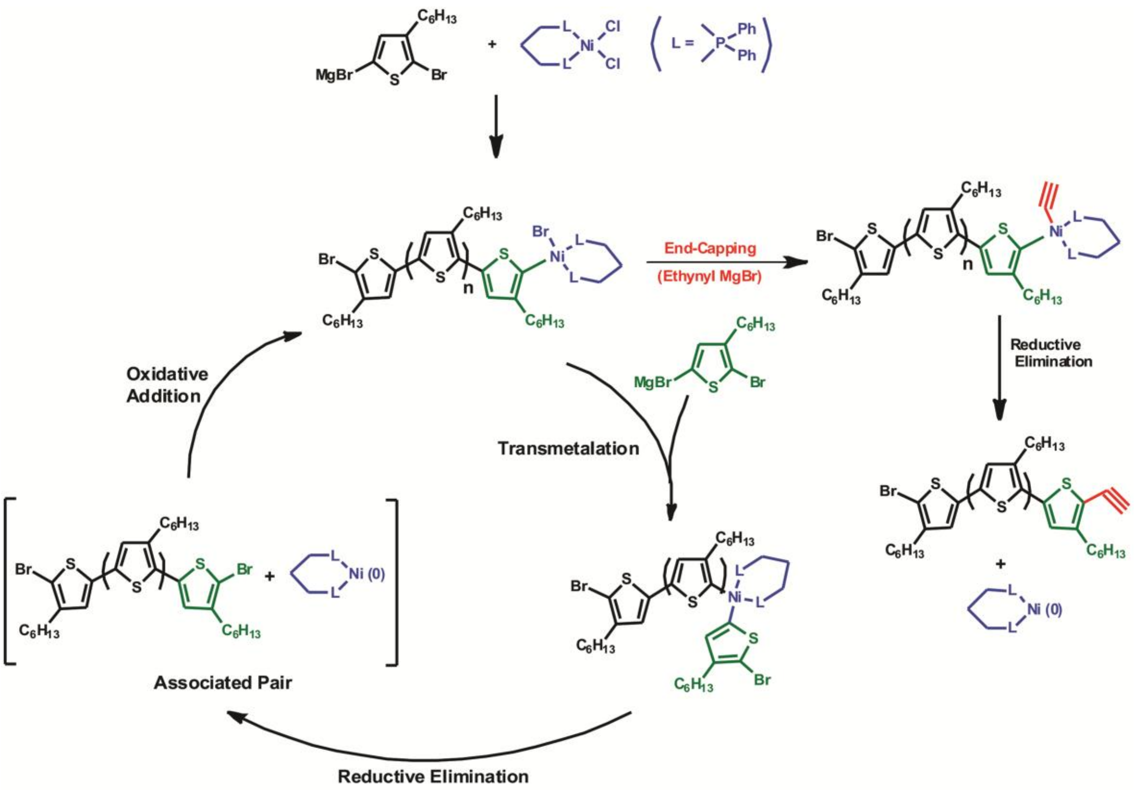

1.1.1.3 ATRP. Atom transfer radical polymerization (ATRP) is one of the most successful living radical polymerization methods especially in regards to the synthesis of styrenes, methacrylates, and a variety of other monomers.[19] The ATRP process yields low polydispersity polymers whose molecular weight is determined by the relative ratio of monomer and inititiator concentrations. ATRP is based on a copper halide/nitrogen ligand catalyst complex that establishes a reversible equilibrium between growing radicals and dormant species as shown in Scheme 3. The persistent radical effect means that the majority of the growing polymer chains in ATRP are dormant species that grow due to the dynamic equilibrium between dormant species and growing radicals.[20] The equilibrium is determined by the choice of the ligand and the ligand also provides increased solubility for the catalyst complex in the appropriate solvent. The initiators used in ATRP must have a large initiation rate constant and are typically alkyl halides with resonance stabilizing substituents that can also be chosen for their end-group functionalization of the resultant polymer.

One of the main advantages of ATRP is that the functionality and architecture of the polymer can be precisely controlled. In particular, the initiator used in the ATRP process determines the end group of the polymer. Thus functional initiators can be chosen to yield the appropriate end-group functionality on one end of the polymer. The other end of the polymer consists of an alkyl halide group that can either be dehalogenated in a one-pot process or transformed into other functionalities via a variety of nucleophilic substitution or electrophilic addition reactions.[21] The halogen end-groups can also be re-activated by an ATRP catalyst system and can be used as macroinitiators for further polymerizations. The precise control offered by ATRP polymerization method has been used to synthesize a multitude of polymers with various architectures,[22, 23] such as block copolymers, star polymers, hyperbranched polymers, and also various functionalities that have been combined with other coupling methods such as click chemistry.[24-26] Some of the many applications of these polymers include drug-delivery, electroactive materials, surfactants, coatings, adhesives, biomaterials, and other nanomaterials.[27]

Scheme 3. General mechanism of ATRP.

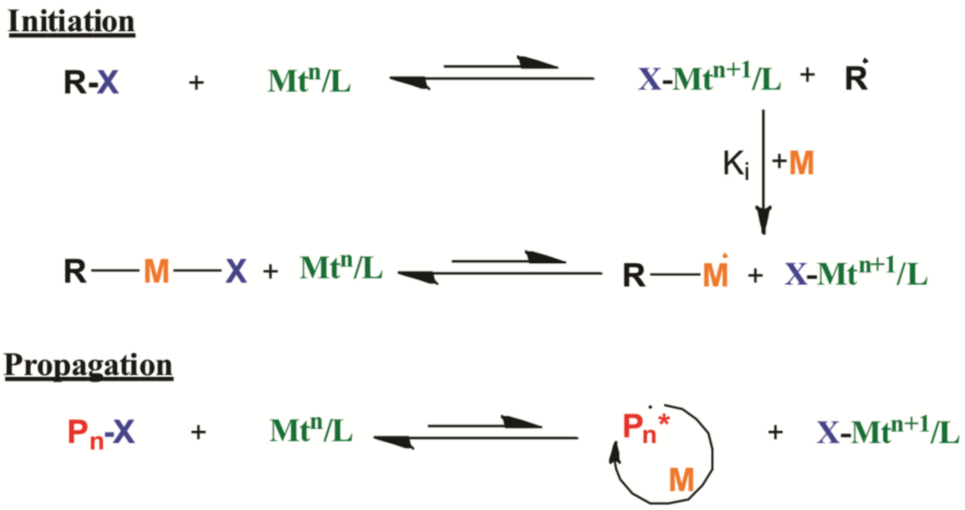

1.1.2 Macroinitiation Methods.

One of the most widely used techniques for the synthesis of block copolymers is via the sequential addition of monomers. This approach is typically called the macroinitiation method because the first polymer is used as a macroinitiator for the synthesis of the second polymer block. In the macroinitiation approach, the second polymer length is controlled by adjusting reaction conditions such as time, temperature, and the monomer concentration.[28] The macroinitiation approach can be used in conjunction with a number of the aforementioned radical polymerization methods (ie. ATRP, RAFT, and GRIM).[29] The macroinitiation method cannot be used for all block copolymers and is limited to polymers with compatible polymerization mechanisms, reactivities, and solvent compatibilities.

1.1.3 Coupling Methods.

Block copolymers can also be synthesized by coupling two functional homopolymers together via a covalent chemical reaction. Coupling methods are advantageous because the relative block-length of the block copolymer can be precisely controlled by the choice of parent homopolymers. The choice of solvent is very important in coupling reactions because both homopolymers need to be well solvated, not aggregated, and accessible to each other for efficient coupling to occur.

Some of the most commonly used coupling methods fall under the aptly named "click chemistry" category. The term "click chemistry" was first introduced by Sharpless in 2001 as a chemical philosophy referring to reactions that could quickly and reliably covalently bind two molecules together.[30] Nowadays, click reactions have become ubiquitous in the literature and more specifically refer to reactions with a high degree of selectivity, straightforward experimental set-ups, a tolerance to a variety of functional groups, quantitative yields, and minimal synthetic work-ups.[31] Despite, the stringency of these requirements, there have actually been a number of examples of reactions that fulfill these requirements including the azide-nitrile cycloaddition reaction, thiolene reactions, diel-alder cyloaddition reactions, and the copper catalyzed azide-alkyne cycloaddition reaction.[12, 26, 32, 33]

Although “click coupling” reactions are among the more widely used coupling reactions, there are other methods that don’t necessarily meet all the strict requirements for this classification, but have also been used for the synthesis of block copolymers. The coupling reaction can be used to synthesize typical block copolymers, but are more often used for the coupling of less typical polymers such as peptide or DNA block copolymers. For example, phosphoramidite chemistry has been used to couple oligodeoxynucleotide strands to end-functionalized polymers.[34, 35] The michael addition reaction has also been used to couple peptides and polymers via the reaction of thiols from cysteine side chains of peptides onto activated alkenes on polymers.[36, 37]

1.2 Solution Phase Self-Assembly of Block Copolymers

1.2.1 Non-Covalent Interactions as Driving Forces for Self-Assembly. In general, self-assembly is the spontaneous and reversible organization of molecular components into ordered structures. Non-covalent interactions are critical driving forces in self-assembly. Some examples of non-covalent interactions in order of increasing strength include; van der waals forces, π-π interactions, hydrogen bonding, hydrophobic interactions, ion-dipole, ion-ion, and metal-ligand interactions. In a given self-assembled system, multiple interactions can contribute to a self-assembled structure. Often, the tuning of these interactions can be used to yield specific functionalities and to yield predesigned composite structures.

In nature, these non-covalent interactions are used to mediate biological interactions and fulfill critical functions. For example, the DNA double helix structure is driven by hydrogen bonding between complementary base pairs and further stabilized by aromatic stacking interactions between bases. The structure of proteins is critically important to their function and the main driving forces behind the folding process is hydrogen bonding between amino acids and the minimization of the number of hydrophobic side chains exposed to water.[38] The assembly of the actin polymer which is responsible for muscle contraction and cell division is highly dependent on environmental factors such as ion and ATP concentration.[39] Overall, it is clear that nature has yielded many elegant examples of non-covalent interactions as driving forces for the self-assembly of simple building blocks into complex and functional architectures.

Inspired by nature, there are many examples in synthetic polymer science that take advantage of the toolbox of noncovalent interactions to program specific functionalities into polymer systems. The ion-dipole and hydrogen bonding interactions were used to drive the self-assembly of a urea functionalized methacrylate amphiphilic block copolymer into a crosslinked nanostructure as shown in Figure 1.1A.[8] Programmed self-assembly of metal nanoparticles onto hybrid nanowires was achieved by the molecular recognition between p-electron rich 1,5-dioxynaphthalene (DNP) as the guest molecule and p- electron deficient cyclobis(paraquat-p-phenylene) (CBPQT4+) as the host molecule (Figure 1.1B).[40] The metal-ligand non-covalent interaction has been used to self-assemble metallo-supramolecular polymers which combine the functionality of the metal ion with the processablity of the polymer (Figure 1.1C).[41] The aforementioned examples all incorporate a molecular recognition element that dominates the self-assembly process. This is a powerful tool that has found promise in the preparation of stimuli-responsive smart materials.[42] However, even self-assembly without an addressable recognition element has high potential for many applications and will be described in more detail in the following sections.

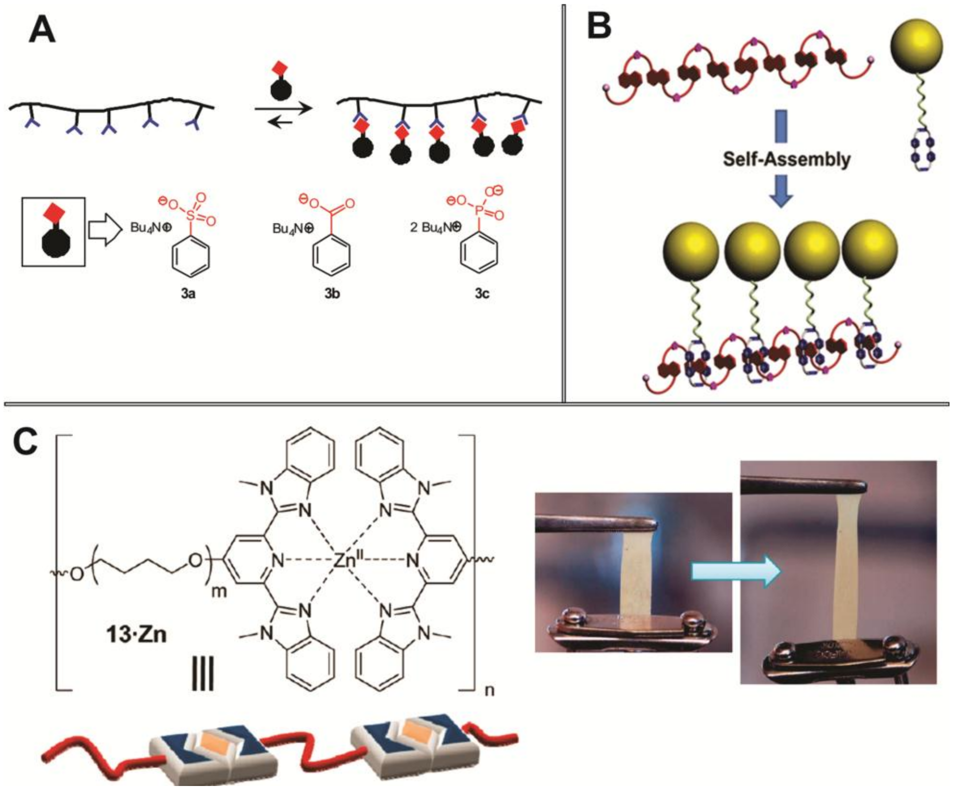

Figure 1.1. (A) Schematic representation of urea bearing polymers binding, sulfonate 3a, carboxylate 3b, and phosphonate 3c guest molecules. (B) Schematic representation of hybrid nanowires formed from electron rich guest molecule and electron deficient host molecules. (C) Structure of a metallo-supramolecular polymer and the proposed AB multiblock-like phase segregation present in the solid state. Pictures highlighting the elastic nature of the metallosupramolecular polymer. Reproduced with permission from (A) Chemical Communications, (B) Macromolecules, and (C) Chemistry - A European Journal.

1.2.2 Self-Assembly of Coil-Coil and Rod-Coil Block Copolymers. Coil-coil amphiphilic block copolymer systems are typically composed of a hydrophilic flexible polymer covalently attached to a hydrophobic flexible polymer. The self-assembly of these systems is rather well understood and well-documented due to extensive studies from research groups such as Eisenberg.[43] The factors that determine the self-assembly structure of these systems include the relative block lengths, the block copolymer concentration, the solvent content, and the interaction parameter. The interaction parameter is known as the Flory Huggins interaction parameter and is a measure of the dissimilarity between the two polymer blocks.[44] These factors have been varied extensively to form diverse morphologies of block copolymers with potential applications in fields such as biomedicine, catalysis, and microelectronics.[45, 46]

Rod-coil block copolymers are an increasingly important class of molecules for the self-assembly of functional polymer systems.[47] The self-assembly behavior of rod-coil block copolymer systems differs from that of the conventional coil-coil block copolymer systems. The microphase separated supramolecular structures for coil-coil block copolymers can be predicted by factoring in the volume ratio of each block and the interaction parameter between the two blocks. However, the self-assembly behavior of rod-coil block copolymers is more complex due to the added driving force towards liquid crystalline alignment and π-π stacking of the rigid block.[48] The rod block also has a limited ability to stretch to accommodate packing arrangements within self-assembled structures.[49] This effect along with the tradeoff between the microphase separation of the rod and coil blocks and the liquid crystalline alignment of the rigid rods can often result in novel structures both in solution and in melts.[50]

1.2.3 Incorporation of Nanomaterials into Block Copolymer Composites. Amphiphilic block copolymers and nanomaterials can be used as building blocks for the formation of nanocomposite structures. Depending on the functional groups of the block copolymer, the polymer can associate with the nanomaterial through noncovalent interactions such as hydrogen bonding, electrostatic and hydrophobic interactions. These interactions can lead to complex self-assembly behavior which has led to a number of interesting nanocomposite structures.[51, 52] The block copolymer building blocks can induce ordering of the nanomaterials, increase the stability of the nanomaterials, and can act as an element for further functionalization of the nanocomposite.[53] Nanocomposite structures have many advantages over the individual constituent components. Nanocomposite formation is often reversible and can also provide enhanced stability for the nanomaterials. Furthermore, the structure of the nanocomposite can be very important for providing specific functions for certain applications. The nanocomposite itself can also act as a building block for the formation of even more complex structures. In general, nanocomposite structures have also been found to have new properties that can act collectively and can be enhanced relative to that of individual building blocks.[54, 55] The properties and functions of the nanocomposite structure can be dependent on the location of the nanomaterial within the amphiphilic block copolymer matrix.

Nanoparticles are one of the most powerful and widely used building blocks that have been incorporated into amphiphilic block copolymer nanomaterials. Nanoparticles have size dependent optical and conductive properties and have found potential applications in single electron devices, nanoelectronics, sensing, catalysis, and biodiagnostics.[56] Nanoparticles can be incorporated into amphiphilic block copolymer matrices, thus forming nanocomposite structures with properties that are often dependent on the location and ordering of the incorporated nanoparticle. The location of the nanoparticle is dependent on the nanoparticle's coordinating ligand, size, shape, volume fraction, and its interaction energy relative to both the solvent and the polymer. Efforts in the development of nanoparticle synthesis techniques has afforded strict control over these parameters for many types of nanoparticles including: gold[57], magnetic[58], and semiconducting nanoparticles[59]. One of the requirements for solution phase incorporation of nanoparticles into block copolymers is that the affinity of the nanoparticles must be greater than it's affinity for the solvent. This can be achieved by incorporating molecular recognition elements into the polymer and nanoparticle. For example, Russell *et al.* built a nanoparticle-polymer composite through the hydrogen bonding interaction between triazine functionalized polystyrene polymer and thymine functionalized gold nanoparticles.[60] Nanoparticles can also be incorporated into block copolymers without molecular recognition elements by instead taking advantage of hydrophobic interactions. For example, the quantum dots selectively incorporated at the interface of the amphiphilic block copolymer presented in Chapter 2 relies on entropic and enthalpic interactions to dictate the position of the nanoparticle and the structure of the block copolymer assembly.[61, 62]

It is important to note that nanoparticles are not simply passively incorporated into block copolymer nanocomposites, but instead can play a very active role in the self-assembly process and resultant structure. For example, Taton *et al.* incorporated citrate-stabilized gold nanoparticles into poly(methacrylate)-*block*-poly(acrylic acid) (PMMA-*b*-PAA) block copolymer micelles.[63] In this case, a small amount of 1-dodecanethiol was added in order to hydrophobically coat the surface of gold nanoparticles and to ensure their incorporation into the hydrophobic core of the block copolymer micelle. In another example, Eisenberg *et al.* incorporated gold nanoparticles functionalized with poly(styrene)-*b*-PAA (PS-*b*-PAA) into the walls of PS-*b*-poly(ethylene oxide) (PS-*b*-PEO) vesicles due to hydrophobic interactions.[64]

Nanoparticles may be one of the more popular nanomaterials that have been incorporated into block copolymer nanocomposites, but they are certainly not the only possibility. Other nanomaterials such as carbon nanotubes, graphene, and homopolymers are also potent building blocks that have been self-assembled with block copolymers. Homopolymers can be incorporated into hydrophobic cores of amphiphilic block copolymer assemblies which can induce changes to the size and the structure of the nanocomposite. For example, addition of PS homopolymer to PS-*b*-PAA assemblies increases the diameter of the micelle because the homopolymer is solubilized in the core and addition of PS to vesicle forming PS-*b*-PAA reduces the core chain stretching of the system and drives the formation of micelles instead of vesicles or rods.[65] Experimental and theoretical evidence shows that the maximum amount of homopolymer that can be incorporated in nanocomposites increases linearly with the concentration of diblock copolymer chains.[66] Not only does the homopolymer effect the conformation of the assembly, but it can also afford functionality to the nanocomposite. For example, the incorporation of poly(thiophene) homopolymer into an amphiphilic glycopolymer afforded water solubility to the poly(thiophene) and yielded superior optical functionalities because the poly(thiophene) formed long conjugated π orbitals without self-quenching due to its encapsulation.[67]

Single-walled carbon nanotubes (SWNT) composite materials have been investigated for such applications as electrostatic discharge, structural reinforcement, and electron emitters in field effect displays.[68, 69] Block copolymers can be used to encapsulate SWNTs which affords a non-destructive method to stabilize and disperse carbon nanotubes. In one example, PS-*b*-poly(4-vinylpyridine) (PS-*b*-P4VP) dispersed SWNTs and selectively synthesized metal nanoparticles within the nanocomposite which was then used in the fabrication of transparent, low-electric resistance devices.[70, 71] In general SWNTs have been dispersed in a variety of block copolymers in which the block copolymer serves to both protect and solubilize the SWNTs.[72, 73]

1.3 Thesis Overview.

This dissertation will focus on the synthesis of amphiphilic block copolymers of varying functionalities and their subsequent controlled self-assembly with other nanomaterials into hybrid nanocomposites with controlled structures and functions. The overall goal of this work has been to develop methods to control the structure and properties of these functional hybrid materials by controlling the organization of polymers and nanomaterials. Such control over the supramolecular self-assembly of a amphiphilic block-copolymer systems is a critical step towards the generation of materials with tunable electronic and optical properties. Chapter 1 gives a brief overview of current methods in the synthesis of amphiphilic block copolymers and an overview of some of the most important considerations in the solution phase self-assembly of amphiphilic block copolymers. Each subsequent chapter will focus on both the synthesis and the self-assembly of a different functional amphiphilic block copolymer moiety. Chapter 2 focuses on the self-assembly of a prototypical insulating coil-coil amphiphilic block copolymer (PS-*b*-PAA) with nanoparticles into a unique cavity-like structure.[61, 74] An in-depth analysis of the conditions necessary to stabilize the cooperative self-assembly of the nanoparticles and amphiphilic block copolymer in a selective solvent is presented along with the enthalpic and entropic interactions that drive the self-assembly process. In Chapter 3 the synthesis and self-assembly of a semiconducting rod-coil amphiphilic block copolymer (PHT-*b*-PEG) into isolated, bundled, and branched nanofibers is presented.[75] In this work the shape, length, and density of hierarchical assembly structures is efficiently controlled by varying the solvent quality, polymer length, and relative polymer concentrations. Chapter 4 also presents the synthesis and self-assembly of a semiconducting rod-coil amphiphilic block copolymer with a different composition, PTOTT-*b*-PEG. The interaction of the polar substituents of the conjugated polymer with polar protic common solvents dominate the self-assembly process and provide a facile route to achieve stable conjugated polymer nanoribbons in aqueous solvents. Investigations of how the concentration and solvent composition affects the packing of the polymer provides insight into subtle effects of hydrogen bonding interactions and π-π stacking interactions on the self-assembly process. The work presented in Chapter 5 focuses on the synthesis and self-assembly of a bioconjugated rod-coil amphiphilic block copolymer (PTOTT-*b*-DNA). This conjugated DNA block copolymer system is interesting because it self-assembles into a distinct vesicle nanostructure and is capable of exploiting both the recognition properties of the DNA and the responsiveness of the polymer to tailor the structural and physiochemical properties of the system.

1.4 References

1. Braunecker, W. A.; Matyjaszewski, K., Controlled/Living Radical Polymerization: Features, Developments, and Perspectives. *Prog. Polym. Sci.* 2007, 32, 93-146.
2. Chiefari, J., *et al.*, Living Free-Radical Polymerization by Reversible Addition-Fragmentation Chain Transfer: The Raft Process. *Macromolecules* 1998, 31, 5559-5562.
3. Moad, G.; Rizzardo, E.; Thang, S. H., Toward Living Radical Polymerization. *Acc. Chem. Res.* 2008, 41, 1133-42.
4. Moad, G.; Rizzardo, E.; Thang, S. H., Radical Addition-Fragmentation Chemistry in Polymer Synthesis. *Polymer* 2008, 49, 1079-1131.
5. Moad, G.; Rizzardo, E.; Thang, S. H., Living Radical Polymerization by the Raft Process. *Aust. J. Chem.* 2005, 58, 379-410.
6. Moad, G.; Rizzardo, E.; Thang, S. H., Living Radical Polymerization by the Raft Process – a Second Update. *Aust. J. Chem.* 2009, 62, 1402.

7. Li, G.; Song, S. E. N.; Guo, L. E. I.; Ma, S., Self-Assembly of Thermo- and Ph-Responsive Poly (Acrylic Acid) -B-Poly (N-Isopropylacrylamide) Micelles for Drug Delivery. *Polymer* 2008, 5028-5035.

8. Kamps, A. C.; Magbitang, T.; Nelson, A., Urea-Bearing Copolymers for Guest-Dependent Tunable Self-Assembly. *Chem. Commun.* 2007, 954-6.

9. Liang, M.; Lin, I.-C.; Whittaker, M. R.; Minchin, R. F.; Monteiro, M. J.; Toth, I., Cellular Uptake of Densely Packed Polymer Coatings on Gold Nanoparticles. *ACS Nano* 2010, 4, 403-13.

10. Shan, J.; Nuopponen, M.; Jiang, H.; Viitala, T.; Kauppinen, E.; Kontturi, K.; Tenhu, H., Amphiphilic Gold Nanoparticles Grafted with Poly(N -Isopropylacrylamide) and Polystyrene. *Macromolecules* 2005, 38, 2918-2926.

11. Lokitz, B. S.; Messman, J. M.; Hinestrosa, J. P.; Alonzo, J.; Verduzco, R.; Brown, R. H.; Osa, M.; Ankner, J. F.; Kilbey, S. M., Dilute Solution Properties and Surface Attachment of Raft Polymerized 2-Vinyl-4,4-Dimethyl Azlactone (Vdma). *Macromolecules* 2009, 42, 9018-9026.

12. Quémener, D.; Davis, T. P.; Barner-Kowollik, C.; Stenzel, M. H., Raft and Click Chemistry: A Versatile Approach to Well-Defined Block Copolymers. *Chemical Communications (Cambridge)* 2006, 5051-3.

13. Loewe, R. S.; Khersonsky, S. M.; McCullough, R. D., A Simple Method to Prepare Head-to-Tail Coupled, Regioregular Poly(3-Alkylthiophenes) Using Grignard Metathesis. *Adv. Mater.* 1999, 11, 250-253.

14. Chen, T. A.; Wu, X. M.; Rieke, R. D., Regiocontrolled Synthesis of Poly(3-Alkylthiophenes) Mediated by Rieke Zinc - Their Characterization and Solid-State Properties. *J. Am. Chem. Soc.* 1995, 117, 233-244.

15. Iovu, M. C.; Sheina, E. E.; Gil, R. R.; McCullough, R. D., Experimental Evidence for the Quasi-"Living" Nature of the Grignard Metathesis Method for the Synthesis of Regioregular Poly(3-Alkylthiophenes). *Macromolecules* 2005, 38, 8649-8656.

16. Yokoyama, A.; Miyakoshi, R.; Yokozawa, T., Chain-Growth Polymerization for Poly(3-Hexylthiophene) with a Defined Molecular Weight and a Low Polydispersity. *Macromolecules* 2004, 37, 1169-1171.

17. Sheina, E. E.; Liu, J. S.; Iovu, M. C.; Laird, D. W.; McCullough, R. D., Chain Growth Mechanism for Regioregular Nickel-Initiated Cross-Coupling Polymerizations. *Macromolecules* 2004, 37, 3526-3528.

18. Jeffries-El, M.; Sauve, G.; McCullough, R. D., Facile Synthesis of End-Functionalized Regioregular Poly(3-Alkylthiophene)S Via Modified Grignard Metathesis Reaction. *Macromolecules* 2005, 38, 10346-10352.

19. Matyjaszewski, K.; Xia, J. H., Atom Transfer Radical Polymerization. *Chem. Rev.* 2001, 101, 2921-2990.

20. Fischer, H., The Persistent Radical Effect: A Principle for Selective Radical Reactions and Living Radical Polymerizations. *Chem. Rev.* 2001, 101, 3581-3610.

21. Coessens, V.; Pintauer, T.; Matyjaszewski, K., Functional Polymers by Atom Transfer Radical Polymerization. *Prog. Polym. Sci.* 2001, 26, 337-377.

22. Matyjaszewski, K.; Tsarevsky, N. V., Nanostructured Functional Materials Prepared by Atom Transfer Radical Polymerization. *Nature Chemistry* 2009, 1, 276-288.

23. Yi, Z.; Liu, X.; Jiao, Q.; Chen, E.; Chen, Y., Synthesis , Characterization , and Self-Assembly of Comb-Dendronized Amphiphilic Block Copolymers. *Polymer* 2008, 6-15.

24. Sumerlin, B. S.; Tsarevsky, N. V.; Louche, G.; Lee, R. Y.; Matyjaszewski, K., Highly Efficient “Click” Functionalization of Poly(3-Azidopropyl Methacrylate) Prepared by Atrp. *Macromolecules* 2005, 38, 7540-7545.

25. Bolognesi, A.; Galeotti, F.; Mróz, W.; Gancheva, V.; Terlemezyan, L., Towards Semiconducting Graft Copolymers: Switching from Atrp to “Click” Approach. *Macromol. Chem. Phys.* 2010, 211, 1488-1495.

26. Lutz, J.-F.; Börner, H. G.; Weichenhan, K., Combining Atrp and “Click” Chemistry: A Promising Platform toward Functional Biocompatible Polymers and Polymer Bioconjugates. *Macromolecules* 2006, 39, 6376-6383.

27. Pyun, J.; Matyjaszewski, K., Synthesis of Nanocomposite Organic/Inorganic Hybrid Materials Using Controlled/"Living" Radical Polymerization. *Chem. Mater.* 2001, 13, 3436-3448.

28. Wu, Z.-Q.; Ono, R. J.; Chen, Z.; Bielawski, C. W., Synthesis of Poly(3-Alkylthiophene)-Block-Poly(Arylisocyanide): Two Sequential, Mechanistically Distinct Polymerizations Using a Single Catalyst. *J. Am. Chem. Soc.* 2010, 132, 14000-14001.

29. Matthews, J. R.; Goldoni, F.; Schenning, A. P. H. J.; Meijer, E. W., Non-Ionic Polythiophenes: A Non-Aggregating Folded Structure in Water. *Chemical Communications (Cambridge)* 2005, 5503-5.

30. Kolb, H. C.; Finn, M. G.; Sharpless, K. B., Click Chemistry: Diverse Chemical Function from a Few Good Reactions. *Angew. Chem. Int. Ed.* 2001, 40, 2004-2021.

31. Binder, W. H.; Sachsenhofer, R., 'Click' Chemistry in Polymer and Materials Science. *Macromol. Rapid Commun.* 2007, 28, 15-54.

32. Gil, M.; Arévalo, M.; López, Ó., Click Chemistry - What's in a Name? Triazole Synthesis and Beyond. *Synthesis* 2007, 2007, 1589-1620.

33. Binder, W. H.; Sachsenhofer, R., 'Click' Chemistry in Polymer and Material Science: An Update. *Macromol. Rapid Commun.* 2008, 29, 952-981.

34. Chen, X. J.; Sanchez-Gaytan, B. L.; Hayik, S. E. N.; Fryd, M.; Wayland, B. B.; Park, S. J., Self-Assembled Hybrid Structures of DNA Block-Copolymers and Nanoparticles with Enhanced DNA Binding Properties. *Small* 2010, 6, 2256-2260.

35. Noro, A.; Nagata, Y.; Tsukamoto, M.; Hayakawa, Y.; Takano, A.; Matsushita, Y., Novel Synthesis and Characterization of Bioconjugate Block Copolymers Having Oligonucleotides. *Biomacromolecules* 2005, 6, 2328-33.

36. Lutolf, M. P.; Tirelli, N.; Cerritelli, S.; Cavalli, L.; Hubbell, J. A., Systematic Modulation of Michael-Type Reactivity of Thiols through the Use of Charged Amino Acids. *Bioconjugate Chem.* 2001, 12, 1051-1056.

37. Heggli, M.; Tirelli, N.; Zisch, A.; Hubbell, J. A., Michael-Type Addition as a Tool for Surface Functionalization. *Bioconjugate Chem.* 2003, 14, 967-973.

38. Wong, G. C. L.; Pollack, L., Electrostatics of Strongly Charged Biological Polymers: Ion-Mediated Interactions and Self-Organization in Nucleic Acids and Proteins. *Annu. Rev. Phys. Chem.* 2010, 61, 171-89.

39. Pollard, T. D.; Borisy, G. G., Cellular Motility Driven by Assembly and Disassembly of Actin Filaments. *Cell* 2003, 112, 453-465.

40. Basu, S., *et al.*, Donor-Acceptor Oligorotaxanes Made to Order. *Chemistry-a European Journal* 2011, 17, 2107-2119.

41. Fox, J. D.; Rowan, S. J., Supramolecular Polymerizations and Main-Chain Supramolecular Polymers. *Macromolecules* 2009, 42, 6823-6835.

42. Yerushalmi, R.; Scherz, A.; van der Boom, M. E.; Kraatz, H. B., Stimuli Responsive Materials: New Avenues toward Smart Organic Devices. *J. Mater. Chem.* 2005, 15, 4480-4487.

43. Zhang, L.; Eisenberg, A., Multiple Morphologies and Characteristics of " Crew-Cut " Micelle-Like Aggregates of Polystyrene-B-Poly (Acrylic Acid) Diblock Copolymers in Aqueous Solutions. *Macromolecules* 1996, 3168-3181.

44. Wolf, B. A., Chain Connectivity and Conformational Variability of Polymers: Clues to an Adequate Thermodynamic Description of Their Solutions, 2 - Composition Dependence of Flory-Huggins Interaction Parameters. *Macromol. Chem. Phys.* 2003, 204, 1381-1390.

45. Lindman, B.; Alexandridis, P., *Amphiphilic Block Copolymers: Self-Assembly and Applications*. Elsevier: 2000.

46. Blanazs, A.; Armes, S. P.; Ryan, A. J., Self-Assembled Block Copolymer Aggregates: From Micelles to Vesicles and Their Biological Applications. *Macromol. Rapid Commun.* 2009, 30, 267-277.

47. Lim, Y.-b.; Moon, K.-S.; Lee, M., Rod–Coil Block Molecules: Their Aqueous Self-Assembly and Biomaterials Applications. *J. Mater. Chem.* 2008, 18, 2909.

48. Olsen, B. D.; Segalman, R. a., Structure and Thermodynamics of Weakly Segregated Rod−Coil Block Copolymers. *Macromolecules* 2005, 38, 10127-10137.

49. Chou, S.-H.; Tsao, H.-K.; Sheng, Y.-J., Structural Aggregates of Rod-Coil Copolymer Solutions. *J. Chem. Phys.* 2011, 134.

50. Tenneti, K. K.; Chen, X.; Li, C. Y.; Wan, X.; Fan, X., Competition between Liquid Crystallinity and Block Copolymer Self Assembly in Core-Shell Rod-Coil Block Copolymers. *New York* 2007, 1-9.

51. Cui, H.; Chen, Z.; Zhong, S.; Wooley, K. L.; Pochan, D. J., Block Copolymer Assembly Via Kinetic Control. *Science (New York, N.Y.)* 2007, 317, 647-50.

52. Pochan, D. J.; Chen, Z.; Cui, H.; Hales, K.; Qi, K.; Wooley, K. L., Toroidal Triblock Copolymer Assemblies. *Science (New York, N.Y.)* 2004, 306, 94-7.

53. Shenhar, R.; Norsten, T. B.; M Rotello, V., Polymer-Mediated Nanoparticle Assembly: Structural Control and Applications. *Adv. Mater.* 2005, 17, 657-669.

54. Guo, Z.; Pereira, T.; Choi, O.; Wang, Y.; Hahn, H. T., Surface Functionalized Alumina Nanoparticle Filled Polymeric Nanocomposites with Enhanced Mechanical Properties. *J. Mater. Chem.* 2006, 16, 2800-2808.

55. Stone, D. A.; Korley, L. T. J., Bioinspired Polymeric Nanocomposites. *Macromolecules* 2010, 43, 9217-9226.

56. Kinge, S.; Crego-Calama, M.; Reinhoudt, D. N., Self-Assembling Nanoparticles at Surfaces and Interfaces. *ChemPhysChem* 2008, 9, 20-42.

57. Sun, Y. G.; Xia, Y. N., Shape-Controlled Synthesis of Gold and Silver Nanoparticles. *Science* 2002, 298, 2176-2179.

58. Gupta, A. K.; Gupta, M., Synthesis and Surface Engineering of Iron Oxide Nanoparticles for Biomedical Applications. *Biomaterials* 2005, 26, 3995-4021.

59. Murray, C. B.; Kagan, C. R.; Bawendi, M. G., Synthesis and Characterization of Monodisperse Nanocrystals and Close-Packed Nanocrystal Assemblies. *Annu. Rev. Mater. Sci.* 2000, 30, 545-610.

60. Boal, A. K.; Ilhan, F.; DeRouchey, J. E.; Thurn-Albrecht, T.; Russell, T. P.; Rotello, V. M., Self-Assembly of Nanoparticles into Structured Spherical and Network Aggregates. *Nature* 2000, 404, 746-748.

61. Kamps, A. C.; Sanchez-Gaytan, B. L.; Hickey, R. J.; Clarke, N.; Fryd, M.; Park, S.-J., Nanoparticle-Directed Self-Assembly of Amphiphilic Block Copolymers. *Langmuir* 2010, 26, 14345-50.

62. Sanchez-Gaytan, B. L.; Cui, W. H.; Kim, Y. J.; Mendez-Polanco, M. A.; Duncan, T. V.; Fryd, M.; Wayland, B. B.; Park, S. J., Interfacial Assembly of Nanoparticles in Discrete Block-Copolymer Aggregates. *Angew. Chem. Int. Ed.* 2007, 46, 9235-9238.

63. Kang, Y.; Taton, T. A., Core/Shell Gold Nanoparticles by Self-Assembly and Crosslinking of Micellar, Block-Copolymer Shells. *Angew. Chem. Int. Ed.* 2005, 44, 409-412.

64. Mai, Y.; Eisenberg, A., Controlled Incorporation of Particles into the Central Portion of Vesicle Walls. *J. Am. Chem. Soc.* 2010, 132, 10078-10084.

65. Choucair, A.; Eisenberg, A., Control of Amphiphilic Block Copolymer Morphologies Using Solution Conditions. *European Physical Journal E* 2003, 10, 37-44.

66. Izzo, D.; Marques, C. M., Solubilization of Homopolymers in a Solution of Diblock Copolymers. *J. Phys. Chem. B* 2005, 109, 6140-5.

67. Fukuda, T.; Inoue, Y.; Koga, T.; Matsuoka, M.; Miura, Y., Encapsulation of Polythiophene by Glycopolymer for Water-Soluble Nanowire. *Chem. Lett.* 2011, 40, 864-866.

68. Bose, S.; Khare, R. A.; Moldenaers, P., Assessing the Strengths and Weaknesses of Various Types of Pre-Treatments of Carbon Nanotubes on the Properties of Polymer/Carbon Nanotubes Composites: A Critical Review. *Polymer* 2010, 51, 975-993.

69. Fujigaya, T.; Nakashima, N., Soluble Carbon Nanotubes and Nanotube-Polymer Composites. *Journal of Nanoscience and Nanotechnology* 2012, 12, 1717-1738.

70. Sung, J.; Jo, P. S.; Shin, H.; Huh, J.; Min, B. G.; Kim, D. H.; Park, C., Transparent, Low-Electric-Resistance Nanocomposites of Self-Assembled Block Copolymers and Swnts. *Adv. Mater.* 2008, 20, 1505-1510.

71. Shin, H.-i.; Min, B. G.; Jeong, W.; Park, C., Amphiphilic Block Copolymer Micelles: New Dispersant for Single Wall Carbon Nanotubes. *Macromol. Rapid Commun.* 2005, 26, 1451-1457.

72. Shvartzman-Cohen, R.; Florent, M.; Goldfarb, D.; Szleifer, I.; Yerushalmi-Rozen, R., Aggregation and Self-Assembly of Amphiphilic Block Copolymers in Aqueous Dispersions of Carbon Nanotubes. *Langmuir* 2008, 24, 4625-4632.

73. Zou, J.; Liu, L.; Chen, H.; Khondaker, S. I.; McCullough, R. D.; Huo, Q.; Zhai, L., Dispersion of Pristine Carbon Nanotubes Using Conjugated Block Copolymers. *Adv. Mater.* 2008, 20, 2055.

74. Sanchez-Gaytan, B. L.; Li, S.; Kamps, A. C.; Hickey, R. J.; Clarke, N.; Fryd, M.; Wayland, B. B.; Park, S.-J., Controlling the Radial Position of Nanoparticles in Amphiphilic Block-Copolymer Assemblies. *J. Phys. Chem. C* 2011, 115, 7836-7842.

75. Kamps, A. C.; Fryd, M.; Park, S.-J., Hierarchical Self-Assembly of Amphiphilic Semiconducting Polymers into Isolated, Bundled, and Branched Nanofibers. *ACS Nano* 2012, 6, 2844-2852.

Chapter 2: Nanoparticle-Directed Self-Assembly of Amphiphilic Block Copolymers[1,2]

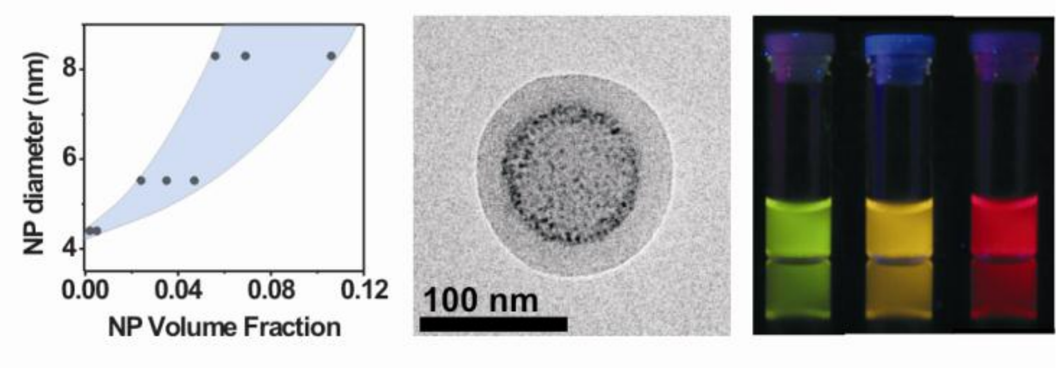

Nanoparticles can form cavity-like structures in core-shell type assemblies of poly(acrylic acid)-b-polystyrene block copolymers through the cooperative self-assembly of nanoparticles and block copolymers. We show that the unique self-assembly behavior is general for as-synthesized alkyl-terminated nanoparticles for a range of nanoparticle sizes. We examined various self-assembly conditions such as solvent compositions, nanoparticle coordinating ligands, volume fraction of nanoparticles, and nanoparticle sizes to elucidate the mechanism of the radial assembly formation.

---

[1] Reproduced in part with permission from Kamps, A. C., Sanchez-Gaytan, B. L., Hickey, R. J., Clarke, N., Fryd, M., and Park, S.-J. (2010) Nanoparticle-Directed Self-Assembly of Amphiphilic Block Copolymers, *Langmuir 26*, 14345-14350. Copyright 2010 American Chemical Society.

[2] Reproduced in part with permission from Sanchez-Gaytan, B. L., Li, S., Kamps, A. C., Hickey, R. J., Clarke, N., Fryd, M., Wayland, B. B., and Park, S.-J. (2011) Controlling the Radial Position of Nanoparticles in Amphiphilic Block copolymer Assemblies, *The Journal of Physical Chemistry C 115*, 7836-7842. Copyright 2011 American Chemical Society.

2.1 Introduction

For the past decade, there has been a considerable effort towards combining nanoparticles and polymers in materials synthesis and device fabrication in order to take advantage of the unique physical properties of nanoparticles and the excellent processibility of polymers.[1-6] An important issue in this area is to develop efficient ways to control the arrangement of nanoparticles in the polymer matrix because the dispersion of nanoparticles significantly impacts the electronic, transport, and mechanical properties of the composite materials.[7, 8] Recently, it has been shown that the cooperative self-assembly of nanoparticles and block copolymers can produce a range of well-ordered arrays of nanoparticles in polymer thin films.[9, 10] In this approach, nanoparticles are segregated into a favorable polymer domain or to the interface between polymer domains, and the arrangement of nanoparticles can be directed by controlling the interaction between nanoparticles and polymers.[11, 12]

The self-assembly of block copolymers in a selective solvent is a well-studied phenomena with a multitude of potential applications, such as cosmetics, emulsification, drug delivery, and environmental purification.[13] Some of the factors that control the morphology and size of block copolymers in a selective solvent include the relative block lengths of the block copolymer, the nature of the common solvent, the copolymer concentration, and the water content.[14] Utilizing the controlled morphology of amphiphilic block copolymers as templates for nanoparticle organization is an attractive method for the development of block copolymer/nanoparticle composites. However, the presence of nanoparticles can significantly impact the assembly of block copolymers. In thin film studies, it has been found that the presence of nanoparticles can alter the morphology of the block copolymer. For example, the incorporation of nanoparticles was found to lead to a morphological transition of block copolymer from cylindrical to lamellar phases.[15] Theoretical reports on polymer-nanocomposites also predicted that the size, shape, and volume fraction of nanoparticles along with the interaction energies between the nanoparticles and polymer, will all be important factors for controlling the morphology and distribution of nanoparticles within nanoparticle-block copolymer composites.[16]

The macroscopic electrical, optical, and mechanical properties of polymer-nanocomposites are affected by the morphology of the polymer and the spatial distribution of the nanoparticles within the polymer-composite.[11] Most reports of nanoparticle-polymer composites involve thin film structures,[7, 12, 17] and less is known about the specific effects of nanoparticle incorporation within a block copolymer matrix in a selective solvent. In the solution phase, the self-assembly of block copolymers and nanoparticles has been explored as a promising synthetic tool for generating multifunctional nanostructures.[18-25] In particular, Taton and coworkers have developed a simple way to prepare well-defined, water-soluble multicomponent nanoparticles by the self-assembly of nanoparticles of varying compositions and amphiphilic block copolymers composed of polystyrene and polyacrylic acid (PAA-*b*-PS).[20, 21, 23] In this body of work, the self-assembly process produced block copolymer micelles that encapsulated various types of nanoparticles in the hydrophobic core of the micelles, but the nanoparticles acted as simple solutes. Indeed, most previous studies have relied on the solubilization of nanoparticles into the core of block copolymer micelles, and the nanoparticles were often functionalized with one of the polymer blocks for encapsulation.[24, 25] Thus, little is known about the impact of nanoparticle loading on the self-assembly formation and the organization of nanoparticles within the self-assembled structure.

Recently, we have shown that the cooperative self-assembly of as-synthesized quantum dots and amphiphilic block copolymers can yield an unusual cavity-like assembly structure of quantum dots in spherical block copolymer assemblies.[26] In this approach, nanoparticles are prepared by well-established synthetic procedures and used for the self-assembly without further surface functionalization. This capability not only eliminates one synthetic step, but also reduces the chance of damaging the physical properties of nanoparticles that could be affected by the surface chemistry, such as photoluminescence quantum yields of quantum dots. This work showed that ordered arrays of nanoparticles can be formed by the solution phase self-assembly of nanoparticles and amphiphilic block copolymers. It also showed that nanoparticles can play an active role in the self-assembly process rather than being passively incorporated as a solute. Moreover, this approach also offers a critical strategy to control the spatial arrangement of nanoparticles in block copolymer micelles. Here, we demonstrate that the radial assembly is a general behavior for typical as-synthesized alkyl-terminated nanoparticles of varying sizes and reveal what drives the formation of the unique assembly structure. Furthermore, we present experimental and theoretical phase maps constructed for a range of different sized CdSe nanoparticles. These findings provide important practical guidelines for reproducibly fabricating nanoparticle/block copolymer hybrid materials with desired structures and optical properties.

2.2 Experimental Section

2.2.1 Synthesis of PS-*b*-PAA Block Copolymers (BCP). Poly(*t*-butyl acrylate)$_{38}$-*block*-poly(styrene)$_{154}$ was synthesized using the reversible addition-fragmentation chain transfer (RAFT) polymerization method.[26, 27] Typically, a 10 mL acetone solution of RAFT reagent, 4-cyano-4(dodecylsulfanythiocarbony)sulfanyl pentanoic acid (161.5 mg, 0.4 mmol), 4,4'azobis(4-cyanovaleric acid) (22.4 mg, 0.08 mmol), and freshly distilled *tert*-butyl acrylate (2.3 mL, 15.8 mmol) was added to a 50 mL bulb with a vacuum adapter. The solution was degassed using three freeze-pump-thaw cycles and then heated at 80 ºC for five hours. The reaction product was collected by concentrating the solution to approximately 1 mL and precipitating the product with methanol. The light, yellow precipitate of poly(*t*-butyl acrylate) was filtered and washed twice with 2 mL of methanol. The precipitate was then dried under vacuum to a constant weight. Gel permeation chromatography (GPC) was used to determine the number average molecular weight and molecular weight distribution of the poly(*t*-butyl acrylate) product.

A 1.5 mL acetone solution of 4,4'azobis(4-cyanovaleric acid) (5.6 mg, 0.02 mmol) and styrene (6.9 mL, 60 mmol) was then added to the poly(*t*-butyl acrylate) product in a 100 mL bulb with a vacuum adapter. The mixture was then degassed by three freeze-pump-thaw cycles and heated at 80 ºC for 3 hours. After the reaction, the solution was concentrated to approximately 1 mL and slowly added into 20 mL of methanol, yielding an off-yellow precipitate of poly(*t*-butyl acrylate)-*block*-poly(styrene). This precipitate was washed with methanol and dried under vacuum to a constant weight. GPC was used to determine the number average molecular weight and molecular weight distribution of the poly(*t*-butyl acrylate)-*block*-poly(styrene) product.

The synthesized poly(*t*-butyl acrylate)-*block*-poly(styrene) was then hydrolyzed to yield poly(acrylic acid)-*block*-poly(styrene) following a literature method.[28] Typically, a 0.2 mL concentrated aqueous solution of hydrochloric acid ($N_{HCl} = 12.1$) was added to a 3 mL freshly distilled THF solution of 5 x 10^{-3} mmol of poly(*t*-butyl acrylate)-*block*-poly(styrene). This solution was heated to reflux for 2.5 hours and then concentrated by rotary evaporation. The oily residue was slowly added to 10 mL of methanol, yielding an off-yellow precipitate. This precipitate was then filtered, washed twice with 2 mL of methanol, and dried under vacuum to a constant weight.

2.2.2 Synthesis of ZnS Coated CdSe Nanoparticles.

A modified literature procedure was used for the synthesis of ZnS-coated CdSe quantum dots.[29] All chemicals used in the synthesis were purchased from Aldrich, except for tetradecylphosphonic acid (TDPA, Alfa Aesar) and tetramethyldisilathiane ((TMS)2S, Fluka). Typically, 1 g of trioctylphosphine oxide (TOPO), 0.5 g of hexadecylamine (HDA), 0.12 g of tetradecylphosphonic acid (TDPA), and 26 mg of CdO were added to a three-neck flask. The system was purged with nitrogen and then heated to 290 ºC. When the solution became clear, a Se-TOP solution (1 mL, 1.0 M) was rapidly injected into the reaction mixture and then the temperature was set to 250 ºC. The reaction was then quenched at different times to yield different sized CdSe quantum dots. The synthesized quantum dots were precipitated with methanol, washed with hexanes and acetone, and then redispersed in chloroform for characterization.

For ZnS coating, 2 g TOPO, 0.5 g HDA, and 2 g TOP were added to dried CdSe nanoparticles (2 x 10^{-7} mol) in a 3-neck flask. A ZnS precursor stock solution was prepared by dissolving 65 μL of $Zn(Et)_2$ and 130 μL of $(TMS)_2S$ in 10 mL TOP. The amount of ZnS precursor needed to grow a desired ZnS shell thickness was determined using a literature procedure.[30] The solution containing CdSe nanoparticles and surfactants was heated to 160 ºC and the ZnS precursor solution was added in a drop-wise fashion over about 10 minutes. After the ZnS precursor addition, the mixture was cooled to 90 ºC and stirred for 3 hours. The synthesized ZnS-coated CdSe nanoparticles were purified by a series of precipitations with methanol and acetone, and then dispersed into chloroform.

The CdSe@ZnS nanoparticles consist of a CdSe core, a ZnS shell and TOPO as the surrounding ligand. The CdSe nanoparticles were synthesized by fast injection of metal organic precursors to a flask with the hot TOPO coordinating liquid. The growth of nanoparticles requires a discrete nucleation event (fast injection) followed by a slower controlled growth onto the existing nuclei. Therefore, different sized CdSe nanoparticles were synthesized by varying the reaction time. The diameters of the nanoparticles used for most of the experiments presented herein were determined to be 3.0 ± 0.4 nm, 4.1 ± 0.4 nm, and 6.9 ± 0.7 nm by TEM and were synthesized at reaction times of 1.5, 6, and 13 minutes, respectively). The ZnS shell was grown onto the CdSe nanoparticles in order to passivate the emission trap sites caused by defects in the surface and therefore enhance the stability and fluorescence quantum yield of the nanoparticles.[30] The CdSe@Zns nanoparticles typically had a quantum yield that was approximately ten times larger than that of the CdSe nanoparticles and were very bright in solution (Figure 2.1 C). The narrow absorption and emission spectra (Figure 2.1 A-B) of the CdSe@ZnS nanoparticles along with TEM analysis confirms that the nanoparticles are uniform in size and shape and have well-formed crystalline cores.

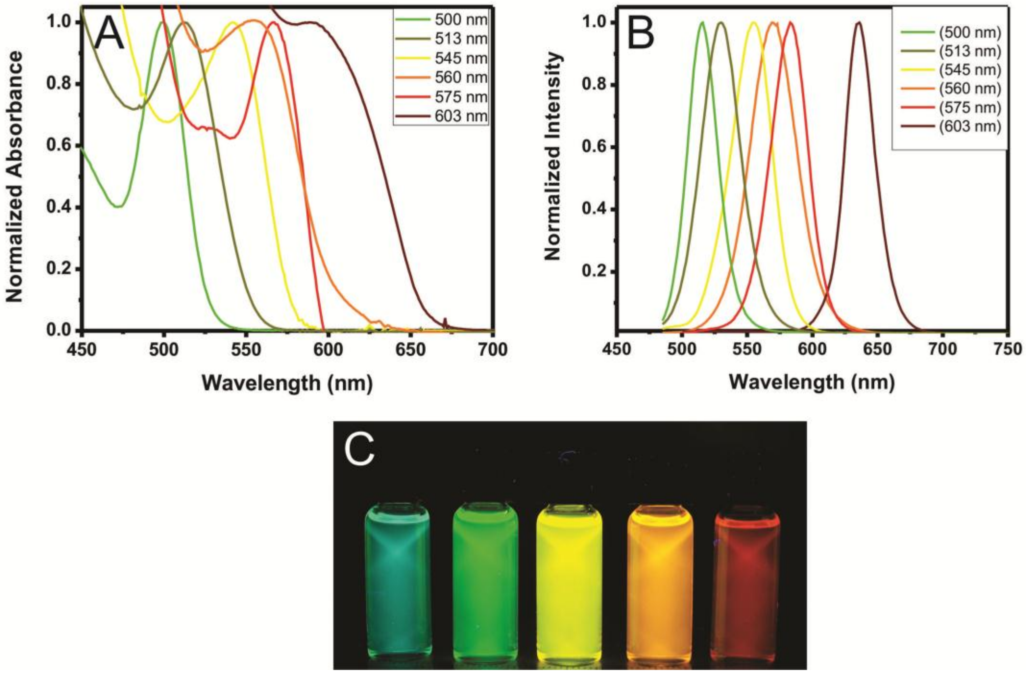

Figure 2.1. Normalized (A) absorbance and (B) PL spectra of different sized CdSe@ZnS quantum dots. PL spectra were collected using an excitation wavelength of 470 nm. (C) Picture of different sized CdSe@ZnS quantum dots in chloroform solutions under UV illumination.

2.2.3 Preparation of Iron Oxide Nanoparticles. Oleic acid functionalized iron oxide nanoparticles were synthesized using oleic acid and oleylamine as stabilizing agents following a modified literature method.[31] First, the iron oleate complex was synthesized by reacting iron chloride and sodium oleate. Typically, 1.5 g of iron chloride ($FeCl_3 \cdot 6H_2O$, 5.5 mmol, Aldrich, 97%) and 5.2 g of sodium oleate (17 mmol, TCI, 95%) were added in a 100 mL flask. Then, a mixture of 20 mL of hexane, 11.5 mL of ethanol, and 8.8 mL of nanopure water were added to the flask. The two phase mixture was placed under reflux (~70 °C) for four hours. The upper organic layer containing the iron-oleate complex was washed three times with 30 mL of water and separated by centrifugation (8,000 rpm, 10 min). Then, the hexane was evaporated from the mixture by rotary evaporation and kept under vacuum overnight (~ 12 hours).

Typically, 5.6 nm iron oxide nanoparticles were synthesized by reacting 5.5 g of iron-oleate and 1.5 g of oleic acid (5.3 mmol, Aldrich, 90%) in 31 g of 1-octadecene (Aldrich, 90%) in a 100 mL round-bottom flack. The mixture was heated to 320 °C at a rate of 200 °C/hour, and then aged for 30 minutes. The dark brown color characteristic of the iron-oleate complex turns black upon the formation of nanoparticles. Finally, the solution was cooled to room temperature and nanoparticles were purified by three rounds of precipitation with 35 mL of ethanol and acetone. The precipitated nanoparticles were collected by centrifugation (8,000 rpm, 10 min) and then redispersed in hexane (10 mL). After the final washing step, the nanoparticles were dissolved in chloroform (10 mL) and centrifuged at low speed (3,000 rpm, 5min) to remove nanoparticle aggregates.

Polystyrene coated magnetic nanoparticles were prepared by the ligand exchange method.[32] Typically, 0.5 mL of 4.1 nm oleic acid functionalized iron oxide nanoparticles (1 mg/mL) were mixed with 0.5 mL of carboxyl-terminated polystyrene ($HOOC\text{-}(PS)_{190}$) in chloroform (20 mg/mL) for 15 hours. The polymer contained approximately one anthracene molecule per chain. The resulting PS-modified nanoparticles were precipitated with acetone, centrifuged at 5000 rpm for 10 minutes and then redispersed in chloroform. The procedure was repeated until there was no detectable anthracene in the supernatant. Finally, the nanoparticles were dried and finally redispersed in DMF.

2.2.4 Synthesis of Nanoparticle/Block Copolymer Co-Assemblies. Nanoparticles and block copolymers were self-assembled as described previously.[26] In a typical experiment, 25 μL of a PAA_{38}-*b*-PS_{154} solution (1.6×10^{-4} M) in DMF was mixed with 25 μL of a ZnS coated CdSe nanoparticle solution (1.6×10^{-6} M) in chloroform. While stirring, 1 mL of DMF is added to the solution followed by a slow addition of 300 μL of water (18 MΩ-cm) at a rate of 10 μL per 30 s. The mixture was kept under stirring for 12 h before additional water (1.5 mL) was added over 15 min. Then, the samples were dialyzed against water for 24 h and further purified by a series of centrifugations. The nanoparticle/block copolymer assemblies were purified from larger block copolymer aggregates by centrifuging the solution at 7,000 rpm for 10 minutes and discarding precipitates. Then, the supernatant was centrifuged again at 16,000 rpm for 1 hr, and precipitates were collected and redispersed in water (1 mL). For further purification, the solution was centrifuged for 1 hr at 16,000 rpm after 24 hr stirring. Finally, the precipitates were collected and redispersed in water (100 μL) and used for TEM analysis. The volume fraction of nanoparticles is defined by the total volume of nanoparticles over the combined volume of the nanoparticles and block copolymer. The volume fraction of nanoparticles was varied by changing the amount of nanoparticles while keeping the amount of block copolymer constant.

2.2.5 Strong Segregation Theory Calculations. The strong segregation model assumes a high degree of dissimilarity between the two blocks, therefore yielding a strongly segregated interface. In the strong segregation limit the free energies of all microphases scale the same way with chain length and interfacial tension, so the phase boundaries become independent of the strength of the repulsion between A and B blocks and depend only on the composition.[33]

The free energy per chain, f_{chain}, corresponding to the core-shell structure is given by,

$$\frac{1}{\left(\Omega\gamma_{AB}/b\right)} f_{\text{chain}} = \frac{V_{\text{c}}\left(f_{\text{Ac}}^{\text{str}} + f_{\text{Bc}}^{\text{str}} + f_{\text{c}}^{\text{int}}\right) + V_{\text{s}}\left(f_{\text{As}}^{\text{str}} + f_{\text{Bs}}^{\text{str}} + f_{\text{s}}^{\text{int}}\right)}{V_{\text{c}} + V_{\text{s}}} \qquad (0.1)$$

where Ω is the volume of a single chain, γ_{AB} is the A/B (i.e., PAA/PS) interfacial tension, and *b* is a reference length scale, which we take to be equal to one nanometer. The volume of the core (V_{c}) and the shell (V_{S}) are related to the various radii defined in Figure 7 as $V_{\text{c}}/\left(V_{\text{c}} + V_{\text{s}}\right) = R_{\text{c}}^3/\left(R_{\text{c}}^3 + R_{\text{s}}^3 - R_{np}^3\right)$ and $V_{\text{s}}/\left(V_{\text{c}} + V_{\text{s}}\right) = \left(R_{\text{s}}^3 - R_{np}^3\right)/\left(R_{\text{c}}^3 + R_{\text{s}}^3 - R_{np}^3\right)$. The subscripts, A, B, *c* and *s* refer to blocks A and B, the core and the shell, respectively, and the superscripts, *str* and *int* refer to stretching and interfacial energies. There are four contributions to the overall free energy per chain from chain stretching given by,

$$f_{\mathrm{Ac}}^{\mathrm{str}} = \kappa \frac{\left(R_c/b\right)^2}{\phi^2} \int_0^{\beta_c} \left(\beta_c - y\right)^2 y^2 \mathrm{d}y \qquad (0.2)$$

$$f_{\mathrm{Bc}}^{\mathrm{str}} = \kappa \frac{\left(R_c/b\right)^2}{\left(1-\phi\right)^2} \int_0^{1-\beta_c} \left(\beta_c + y\right)^2 y^2 \mathrm{d}y \qquad (0.3)$$

$$f_{\mathrm{As}}^{\mathrm{str}} = \kappa \frac{\left(R_s/b\right)^2}{\phi^2 \left[1-\left(R_{np}/R_s\right)^3\right]} \int_0^{1-\beta_s} \left(\beta_s + y\right)^2 y^2 \mathrm{d}y \qquad (0.4)$$

$$f_{\mathrm{Bs}}^{\mathrm{str}} = \kappa \frac{\left(R_s/b\right)^2}{\left(1-\phi\right)^2 \left[1-\left(R_{np}/R_s\right)^3\right]} \int_0^{\beta_s - R_{np}/R_s} \left(\beta_s - y\right)^2 y^2 \mathrm{d}y \qquad (0.5)$$

The parameters, β_{c} and β_{s}, are defined by,

$$\beta_c = z_c/R_c \equiv \phi^{1/3}; \quad \beta_s = z_s/R_s \equiv \left(1-\phi\left(1-\left(R_{np}/R_s\right)^3\right)\right)^{1/3} \qquad (0.6)$$

Since we assume that the nanoparticle layer is filled with nanoparticles, we also have a further relation between R_{s} and R_{c},

$$\Phi_{np} R_s^3 = R_{np}^3 - R_c^3 \qquad (0.7)$$

There are four contributions to the interfacial energy, two from each of the A-B interfaces, with an interfacial energy per unit area of γ_{AB}, and the other two from the B-nanoparticle interfaces. In the calculations presented below, we ignore the contributions from the latter since they are significantly smaller than the A-B interfacial energy.

$$f_c^{\text{int}} = 3\frac{(z_c/b)^2}{(R_c/b)^3} \qquad (0.8)$$

$$f_s^{\text{int}} = 3\frac{(z_s/b)^2}{(R_s^3 - R_{np}^3)/b^3} \qquad (0.9)$$

The dimensionless parameter, κ, in equations (0.2)-(0.5) is defined by,

$$\kappa = \frac{9\pi^2 (l_A l_B)^{1/2}}{8\Omega^2 \gamma_{AB}} b^3 \qquad (0.10)$$

where, l_A and l_B are monomer segment lengths. Assuming that the monomer lengths are approximately the same ($l_A \approx l_B = l$), and that the interfacial tension depends on the dimensionless polymer-polymer interaction parameter, χ, as shown in equation 1.11.[34]

$$\gamma \approx \left(\frac{\chi}{6}\right)^{1/2} l^{-2} \qquad (0.11)$$

Then, κ can be written as

$$\kappa \approx \frac{9\pi^2\sqrt{6}}{8}\frac{1}{N^2\chi^{1/2}}\left(\frac{b}{l}\right)^3 \qquad (0.12)$$

where N is the degree of polymerization of the entire copolymer. The minimized total free energy was calculated for the self-assembled structure in order to determine whether the introduction of a nanoparticle layer lowers the free energy of the core-shell structure. The free energy for the core-shell structure without a nanoparticle layer is found by taking the limit of $R_{np} \to R_c$ in equations (0.2)-(0.9).

2.2.6 Instrumentation. The molecular weight of synthesized polymers were determined using a gel permeation chromatography (GPC) system from Shimadzu equipped with Polymer Laboratories columns (guard; 10^6, 10^4 and 5 x 10^2 A), a UV detector (SPD-10AV) at 600 nm, and a refractive index detector (RID-10A) calibrated against linear polystyrene standards in THF. Proton NMR spectra were obtained using a Bruker-DMX300 interfaced to an Aspect 3000 computer at ambient temperature. The IR spectra were obtained on a Perkin-Elmer system 2000 FTIR spectrometer. The UV-vis spectra were measured using a Hewlett Packard 8452A diode array spectrometer. The synthesized nanoparticles and block copolymer/nanoparticle co-assemblies were characterized by TEM (Technai $G^2$12TWIN) operating at an 80 kV accelerating voltage and JEOL TEM-2010F operating at a 200 kV accelerating voltage.

2.3 Nanoparticle-Directed Self-Assembly of Amphiphilic Block Copolymers

2.3.1 Interfacial Assembly Structure. As described in Figure 2.2 A, nanoparticles were incorporated into amphiphilic block copolymer micelles by slowly adding water to a N,N-dimethylformamide (DMF) solution of nanoparticles and block copolymers. The resulting co-assemblies were then dispersed in water by dialysis and centrifugation, and characterized by transmission electron microscopy (TEM). Amphiphilic block copolymers of polyacrylic acid and polystyrene (PAA_{38}-*b*-PS_{154}) were synthesized by the reversible addition-fragmentation chain transfer (RAFT) polymerization method[26, 27] and used throughout the study. Zinc sulfide coated cadmium selenide quantum dots[29] and iron oxide magnetic nanoparticles[31] were synthesized by literature procedures using trioctyl phosphine oxide (TOPO) and oleic acid respectively as main surface coordinating ligands and used without further surface functionalization. Thus, all nanoparticles used in this study were terminated with hydrophobic alkyl molecules. Note that most literature procedures for organic phase synthesis of nanoparticles use surfactants terminated with a long alkyl chain as surface coordinating molecules.[35]

We have previously shown that TOPO-stabilized CdSe@ZnS nanoparticles and PAA-*b*-PS can self-assemble into well-defined spherical assemblies where nanoparticles form an unusual cavity-like structure as described in Figure 2.2 A.[26] In this body of work, the phenomenon was generalized for a range of different sized CdSe@ZnS nanoparticles emitting green, yellow, and red light (Figure 2.2 B,C). Fe_3O_4 nanoparticles also formed the cavity-like structure inside block copolymer assemblies as shown in Figure 2.2 D,E.[36] In all cases, block copolymers and nanoparticles self-assembled into a three layered structure that is composed of a polymer core, a polymer shell, and nanoparticles arranged at the interface between the polymer core and the polymer shell. The polymer structure of the radial assemblies bear a strong resemblance to the large compound micelles reported by Eisenberg and coworkers, which consist of one or more inverse micelles surrounded by a layer of PAA-*b*-PS.[26, 37]

2.3.2 Mechanism of Interfacial Assembly.

The radial co-assembly process was monitored by taking TEM images at a series of different water contents. As shown in the TEM image presented in Figure 2.3 A, TOPO-stabilized CdSe@ZnS nanoparticles are associated with block copolymers even before adding water due to the poor solubility of

CdSe@ZnS nanoparticles in DMF. In the absence of block copolymers, CdSe@ZnS nanoparticles in a DMF solution will precipitate out of solution and quickly lose their fluorescence. However, when a certain amount of amphiphilic block copolymer is present in a DMF solution, the system initially lowers the free energy by incorporating CdSe@ZnS nanoparticles in the PS domain of block copolymer aggregates because the TOPO/PS interaction is less unfavorable than TOPO/DMF interactions. The Flory-Huggins parameter for TOPO/PS (octane/PS = 9.0 MPa) is significantly smaller than all other interaction pairs (e.g., octane/PAA = 81.0 MPa, octane/DMF = 84.6), which means that the TOPO/PS interaction is the least repulsive (most favorable) when compared with the other possible interactions. At this stage, CdSe@ZnS nanoparticles are incorporated into the swollen polymer aggregates without any particular order. As a small amount of water is added to the system, larger micellar structures start to form (Figure 2.3 B). These structures are composed of a core of multiple reverse micelles surrounded by a shell of block copolymer with hydrophilic PAA at the exterior. At this small amount of water addition, the CdSe@ZnS nanoparticles begin to preferentially revert to the PS-PS interface between the core and the shell.

With further addition of water, a selective solvent for the PAA block, the aggregation number of polymers becomes larger to avoid the contact between PS and water, the PS block becomes less swollen, and the mobility of the polymer chains decreases.[12] As the polymer strands pack more densely, nanoparticles and polymers reorganize to adopt the radial assembly structure (Figure 2.3 C). This observation supports our hypothesis that the unusual radial co-assembly structure is the result of relatively unfavorable interactions between the nanoparticles and the polymer.

The TOPO-stabilized CdSe@ZnS nanoparticles are located in their preferred domain (PS) because this leads to an enthalpic gain in free energy. The CdSe@ZnS nanoparticles preferentially revert to the PS-PS interface because this minimizes the entropic cost associated with the polymers wrapping around the nanoparticles. This result is consistent with theoretical calculations that predict that particles that are selective towards just one block copolymer component would localize at the center of their preferred phase in order to minimize the free energy of the system.[11] After dialysis of the solutions into water, the mobility of the polymer chains is decreased to such a high extent that the micelles essentially become “frozen” and no further change in structure is evident (Figure 2.3 D). The final interfacial assembly structure is very stable and retains the optical properties of the incorporated CdSe@ZnS nanoparticles.

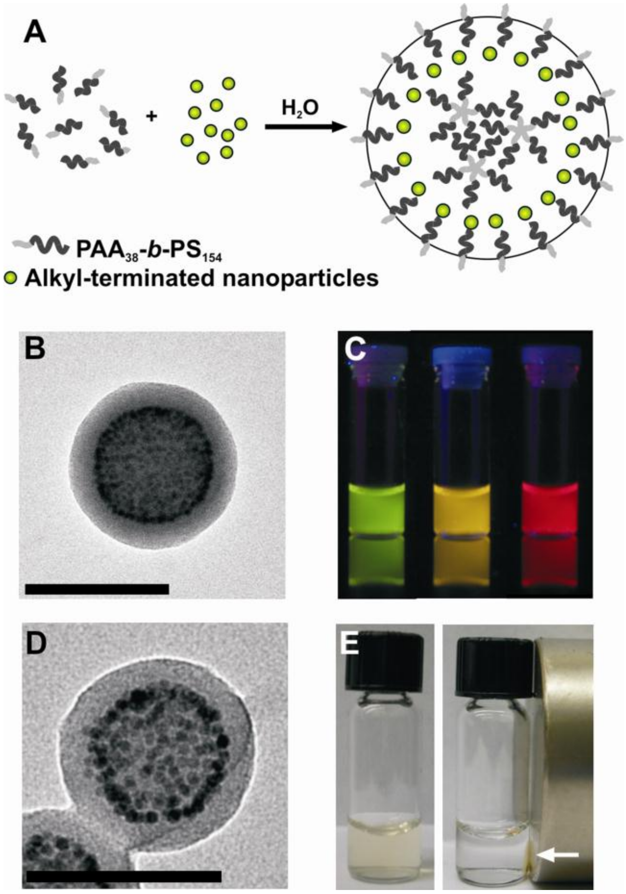

Figure 2.2. (A) Schematic depiction of the self-assembly of nanoparticles and block copolymers. (B) A TEM image of CdSe@ZnS nanoparticles (4.1 ± 0.4 nm) forming a cavity like structure in block copolymer assemblies. (C) Aqueous solutions of block copolymer assemblies incorporated with CdSe@ZnS nanoparticles of different sizes under UV illumination. (D) A TEM image of Fe_3O_4 (6.4 nm ± 0.5 nm) forming a cavity like structure in block copolymer assemblies. (E) An aqueous solution of block copolymer assemblies containing Fe_3O_4 nanoparticles. The picture on the right shows assemblies attracted to a magnet. Scale bar is 100 nm.

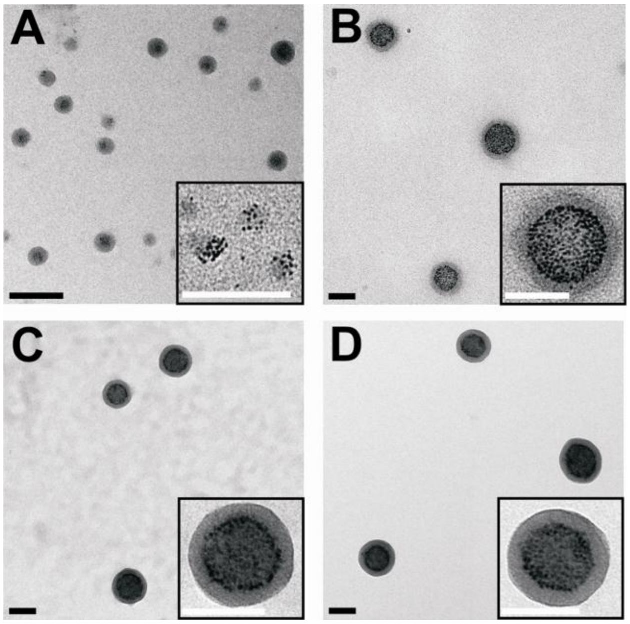

Figure 2.3. Co-assemblies of CdSe@ZnS nanoparticles (4.1 ± 0.4 nm) and block copolymers formed at a series of different water content, 0 % (A), 6 % (B), 17 % (C), and 100 % (D). Scale bar is 100 nm.

2.4 Contributing Factors for Radial Self-Assembly

2.4.1 Effect of Nanoparticle-Surface Coordinating Molecule. To examine the role of surface coordinating molecules on the formation of the radial assemblies, PS-modified Fe_3O_4 nanoparticles were prepared by ligand exchange and self-assembled with block copolymers by following the same procedure. As shown in Figure 2.4 A, the PS-modified nanoparticles were incorporated into block copolymer assemblies without any particular order. This is in contrast to the radial assembly formed with alkyl-terminated nanoparticles presented in Figure 2.4 B. This result confirms that the relatively unfavorable interaction between alkyl-terminated nanoparticles and PS is responsible for the formation of the unusual radial co-assemblies. Although alkyl-terminated nanoparticles and PS are both hydrophobic, the nanoparticle/PS interaction is unfavorable enough to cause the segregation of nanoparticles to the spherical PS/PS interface instead of being randomly incorporated throughout the polymer matrix. The incorporation of nanoparticles at the interface can also reduce the stretching penalty that would be incurred by incorporating them within the polymer core or in the shell. The distinct self-assembly behavior can be used to compartmentalize different types of nanoparticles within individual block copolymer assemblies. When PS-modified Fe_3O_4 nanoparticles and alkyl-terminated CdSe@ZnS nanoparticles were simultaneously incorporated into block copolymer assemblies, alkyl-terminated CdSe@ZnS nanoparticles were localized at the spherical interface while PS-terminated Fe_3O_4 nanoparticles were found throughout the assembly (Figure 2.4 C) as confirmed by the energy dispersive x-ray spectroscopy (EDS) (Figure 2.5).

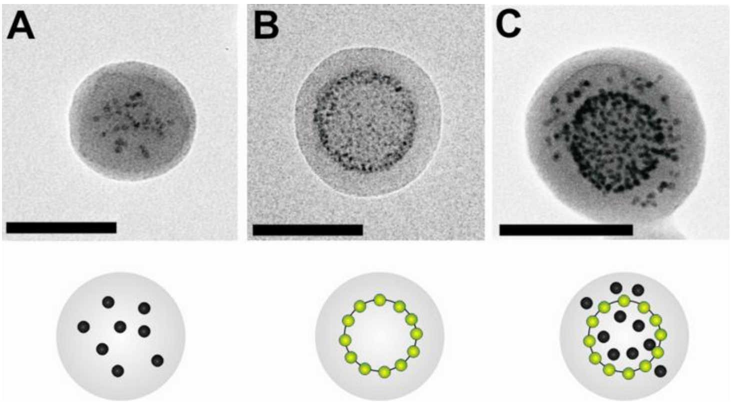

Figure 2.4. TEM images of block copolymer assemblies containing (A) PS-terminated Fe_3O_4 nanoparticles (4.1 nm ± 0.5 nm), (B) alkyl-terminated CdSe@ZnS nanoparticles (4.6 nm ± 0.4 nm), and (C) both PS-terminated Fe_3O_4 nanoparticles and alkyl-terminated CdSe@ZnS nanoparticles. The drawings showing the location of nanoparticles in the polymer matrix are given below the TEM images. Scale bar is 100 nm.

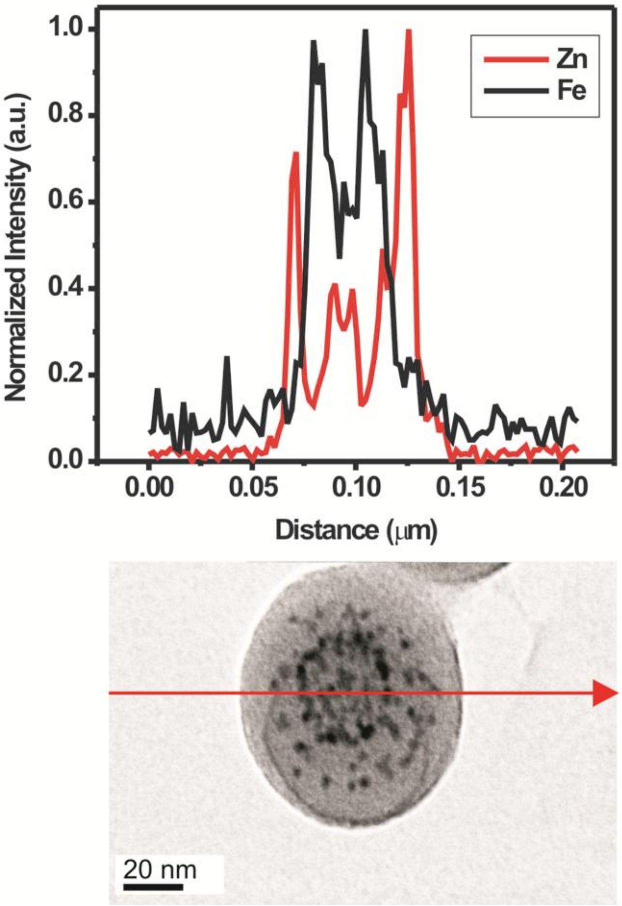

Figure 2.5. EDX of assembly containing PS-modified iron oxide nanoparticles and alkyl-terminated CdSe/ZnS nanoparticles which were simultaneously incorporated into block-copolymer micelles. Alkyl-terminated CdSe/ZnS nanoparticles (Zn) were localized at the spherical interface while PS-terminated iron oxide nanoparticles (Fe) were found throughout the assembly.

2.4.2 Effect of Nanoparticle Volume Fraction. The volume fraction of nanoparticles (Φ_{np}) was found to be a critical factor in stabilizing the co-assemblies, and the radial co-assembly structure was formed for only a limited range of nanoparticle volume fractions (Figure 2.6). When the nanoparticle volume fraction is larger than a threshold volume fraction ($\Phi_{np\text{-}max}$), nanoparticles and block copolymers macroscopically precipitate out of solution when dispersed in water. Figure 2.6 C presents the assemblies formed at Φ_{np} slightly larger than $\Phi_{np\text{-}max}$, which shows broken irregular assemblies. When Φ_{np} becomes even larger, massive aggregation and precipitation of nanoparticles and block copolymers occurs (Figure 2.6 C). When Φ_{np} was too low, asymmetric assemblies with one or multiple nanoparticle cavities (Figure 2.6 A) were formed instead of the well-defined symmetric radial assemblies shown in Figure 2.6 B. While the asymmetric assemblies have broad size distributions with different numbers of nanoparticle cavities, symmetric radial assemblies shown in Figure 2.6 B were quite uniform with an average diameter of 130 nm and a size distribution of 9 % by TEM, which suggest that the resulting assembly is a thermodynamic structure. Consistent with this notion, a slower addition of water (10 μL per 900 s) did not change the assembly structure.

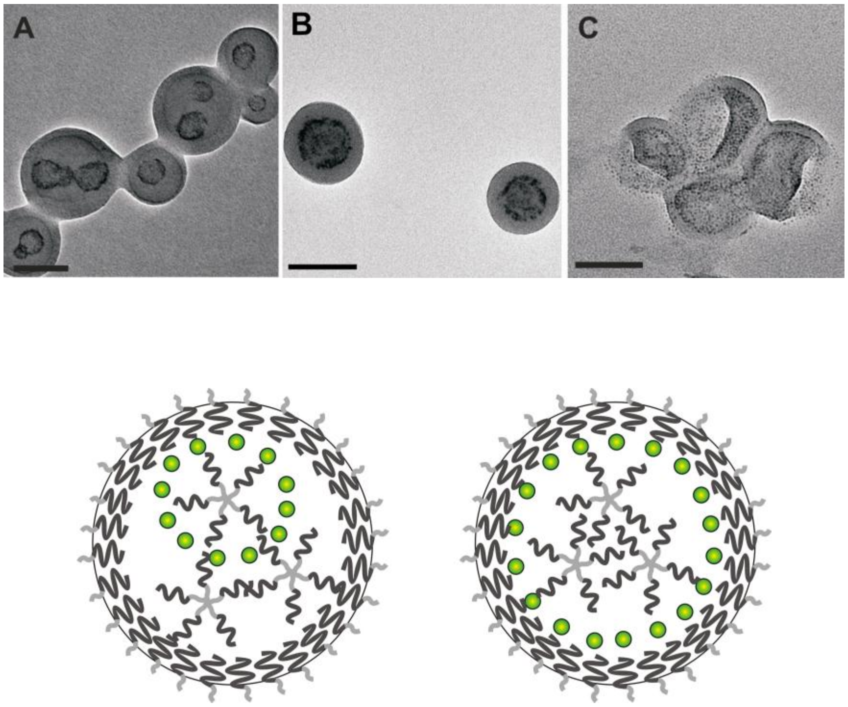

Figure 2.6. (A) Co-assemblies of CdSe@ZnS nanoparticles (4.1 nm ± 0.4 nm) and block copolymers formed at different nanoparticle volume fractions, 0.012 (A), 0.035 (B), and 0.068 (C), representing the asymmetric assembly range (A), radial assembly range (B), and phase separation range (C), respectively. Scale bar is 100 nm. Below the respective TEM images is a schematic depiction of co-assemblies with one or multiple reverse micelles in the core

2.4.3 Effect of Nanoparticle Size. The Φ_{np} ranges that yields well-defined symmetric radial co-assemblies were identified for three different sized CdSe@ZnS nanoparticles which emit green, yellow, and red light, respectively (Figure 2.7). The diameters of the inorganic part of the nanoparticles were determined to be 3.0 ± 0.4 nm, 4.1 ± 0.4 nm, and 6.9 ± 0.7 nm by TEM. The nanoparticle diameters plotted in Figure 5 include the TOPO layer and were estimated by adding the TOPO layer thickness (2 x 0.7 nm)[38] to the diameters determined by TEM. As shown in Figure 2.7, the volume fraction range that yields well-defined symmetric radial co-assemblies (radial assembly range) varied with the size of nanoparticles. Larger nanoparticles required a higher nanoparticle volume fraction to form stable co-assemblies, and have a wider range of volume fractions that yield well-defined radial assemblies. In fact, it was difficult to form stable co-assemblies with CdSe@ZnS nanoparticles smaller than 3.0 nm, as the radial assembly range becomes too narrow. When the nanoparticle volume fraction is larger than the threshold value ($\Phi_{QD\text{-}max}$), nanoparticles cannot effectively reduce the polymer stretching energy, which results in the phase separation of the two components with water addition (*vide infra*). The phase separation volume fraction range is indicated in grey in the phase map (Figure 2.7). Note that when the water content is low, co-assemblies with well-defined layered structures are formed even at a nanoparticle volume fraction larger than $\Phi_{np\text{-}max}$ (Figure 2.8 B). As the water content is increased, however, nanoparticles and block copolymers were eventually aggregated and precipitated out due to the destabilization of the core region (Figure 2.8 C). These observations imply that the polymer stretching is important in stabilizing the layered structure, which is supported by the theoretical study described below. Note that for homogeneous encapsulations, smaller nanoparticles are more readily incorporated because they have a less negative impact on the polymer conformation.[39]

Stable interfacial assemblies were formed for different sized CdSe@ZnS nanoparticles, but the $\Phi_{\text{QD-max}}$ increased with the size of nanoparticles. Co-assemblies formed with different sized CdSe@ZnS nanoparticles at their $\Phi_{\text{QD-max}}$ are shown in Figure 2.9 A-C. The structural parameters of the co-assemblies formed at their corresponding $\Phi_{\text{QD-max}}$ are shown in Figure 2.9 D. It is apparent from this data that the core radius increases with the radius of nanoparticles while the shell thickness remains constant. This behavior is most likely caused by the stretching of shell polymers. Incorporated nanoparticles create valleys that needed to be filled by polymers. Larger nanoparticles create deeper valleys in the shell and induce higher polymer stretching. For a given nanoparticle size, the extra volume in the shell relative to the total shell volume becomes smaller with increasing core size. Thus, the assemblies with bigger nanoparticles adopt a larger core in order to reduce the extra polymer stretching and keep the minimum shell thickness.

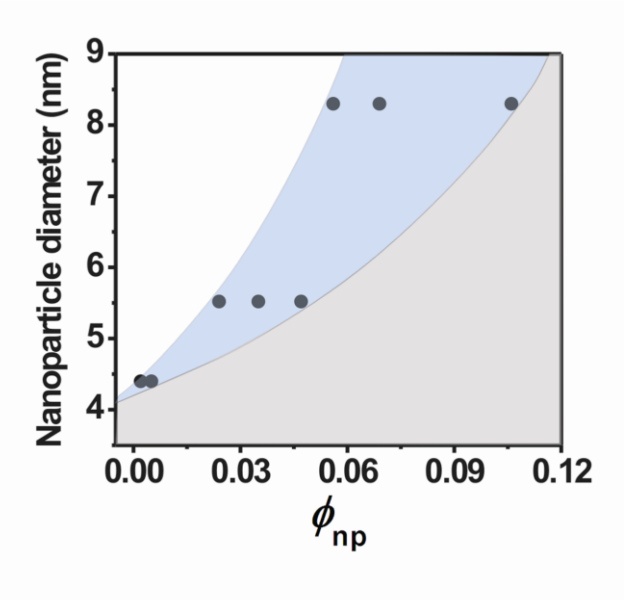

Figure 2.7. Nanoparticle volume fraction ranges yielding stable interfacial assemblies for different sized CdSe@ZnS nanoparticles (blue section). Experimentally determined data points are indicated with dots. The white section represents the asymmetric assembly range shown in Figure 2.6 A, and the grey section represents the phase separation range.

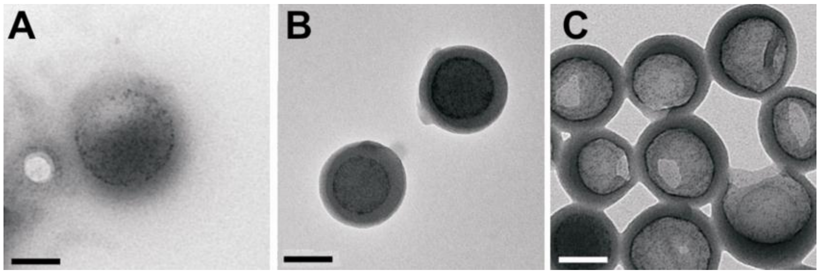

Figure 2.8. Co-assemblies of CdSe@ZnS nanoparticles (3.0 nm ± 0.4 nm) and block-copolymers in DMF/water mixtures at $\Phi_{\text{np}} = 0.024$, which is larger than $\Phi_{\text{np-max}}$ (0.01). The water contents are 12 % (A), 17 % (B), and 29 % (C). The assemblies were macroscopically aggregated and precipitated out of solution when the water content was higher than 29 %. Scale bar is 100 nm.

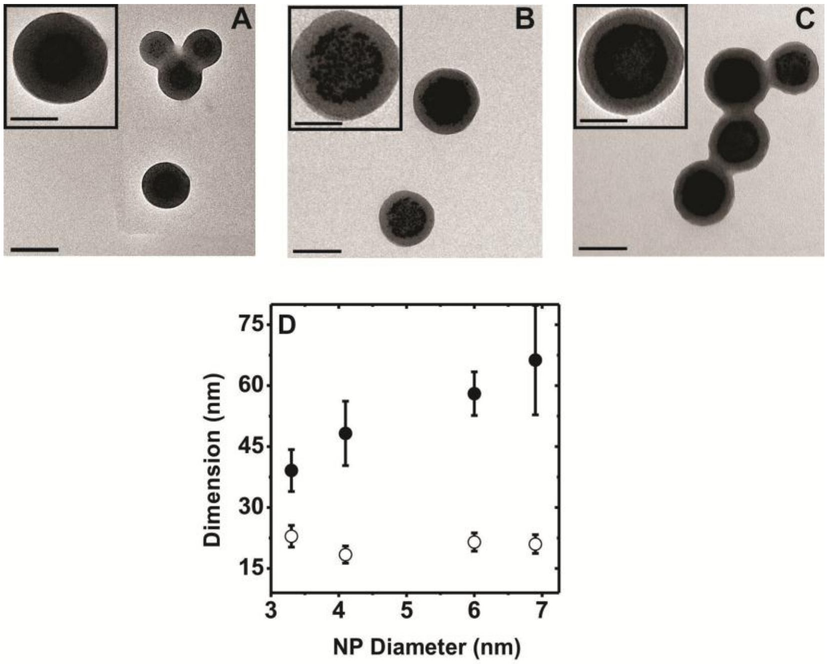

Figure 2.9. TEM images of co-assemblies formed with different sized CdSe@ZnS nanoparticles at their $\Phi_{\text{QD-max}}$, (A) 3.0 ± 0.4 nm, (B) 4.1 ± 0.4 nm, and (C) 6.9 ± 0.7 nm. (D) Plot of shell thicknesses (open circle) and radius (solid circle) of QD/BCP assemblies formed with different sized nanoparticles at their $\Phi_{\text{QD-max}}$. Scale bar is 100 nm. Inset scale bar is 50 nm.

2.5 Theoretical Modeling of Co-Assembly Structure

2.5.1 Strong Segregation Theory Calculations. To understand the formation of radial assemblies and the phase behavior further, we used a simple extension to the strong segregation theory of Olmsted and Milner[33] and calculated a phase map identifying nanoparticle volume fraction ranges where the core-shell structure with an interfacial nanoparticle layer has a lower free energy than such a structure without a nanoparticle layer. In the model, the only contributions to the free energy arise from chain stretching and the interfacial energy. Although a complete understanding of the physical processes may require calculations based on the self-consistent field theory, the strong segregation theory has the advantage of permitting further analytical progress, which enables a qualitative understanding of the dominant processes governing structure formation in the complex systems considered here. In the calculation, it is assumed that the core is composed of a single spherical block copolymer reverse micelle, with the PAA on the inside of the sphere and PS on the outside (Figure 2.10). We expect that the core structure can be actually more complex and comprised of more than one reverse micelle. We describe the nanoparticles as occupying a flat layer with thickness corresponding to that of the diameter of the nanoparticles, d_{np}; thus, we neglect the possibility of partial packing of the layer and the impact that the curvature of the nanoparticles might have on the chain configurations at the copolymer/nanoparticle interface. Despite these simplifications, this model qualitatively reproduces the observed conditions required to stabilize the core-shell structure with a nanoparticle layer.

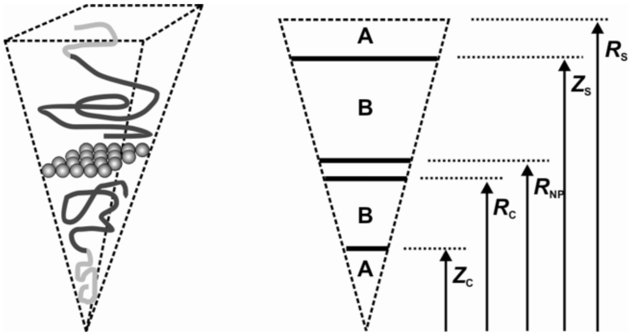

Figure 2.10. Schematic illustration of the wedge used to approximate a segment of the spherical core-shell structure with a nanoparticle layer at the interface. The dimensions used in the calculation are shown on the right. The radii, Z_c and Z_s correspond to the distance from the centre to the interfaces between the A and B blocks in the core and the shell, respectively. The R_c and R_s are the radii of the core and shell, and R_{np} is the radius of the inner surface of the shell, such that $R_{np} = R_c + d_{np}$, where d_{np} is the diameter of the nanoparticles.

2.5.2 Relating the Theoretical Phase Map to the Experimental Phase Map. The calculated phase map is presented in Figure 2.11 where the blue shaded area represents the conditions where the radial co-assemblies are stable. As mentioned above, the theoretical map reveals the same general trend observed in the experimental data in Figure 2.5. Firstly, it indicates that radial co-assemblies are stable for a limited range of nanoparticle volume fractions. When the nanoparticle volume fraction is too low, in the left side of the blue shaded region of the phase map, the inclusion of the nanoparticle layer destabilizes the assembly structure by increasing the stretching energy of the shell. Experimentally, the destabilization caused by the shell stretching is manifested by adopting the asymmetric structures shown in Figure 2.6 A. When the nanoparticle volume fraction is larger than the radial co-assembly range, right side of the blue shaded region of the phase map, the inclusion of the nanoparticle layer destabilizes the assembly structure by increasing the stretching of the core. Experimentally, the nanoparticle-induced strain on the core stretching results in the phase separation of the nanoparticles and block copolymer with the addition of water (Figure 2.6 C). In the blue shaded region, the nanoparticle layer has minimal impact on the dimensions of the polymer core and the shell. Furthermore, nanoparticles even relieve chain stretching, particularly in the shell, by reducing the curvature of the inner surface of the shell, stabilizing the co-assembly structure. Secondly, the range of volume fractions over which the co-assemblies are stable becomes broader as nanoparticle size increases because the stretching energy is relieved more significantly by incorporating larger nanoparticles.

The calculated phase map along with the experimental data provides an essential guideline for the cooperative self-assembly of nanoparticles and block copolymers, from which one can determine the self-assembly conditions for encapsulating nanoparticles into discrete block copolymer assemblies.

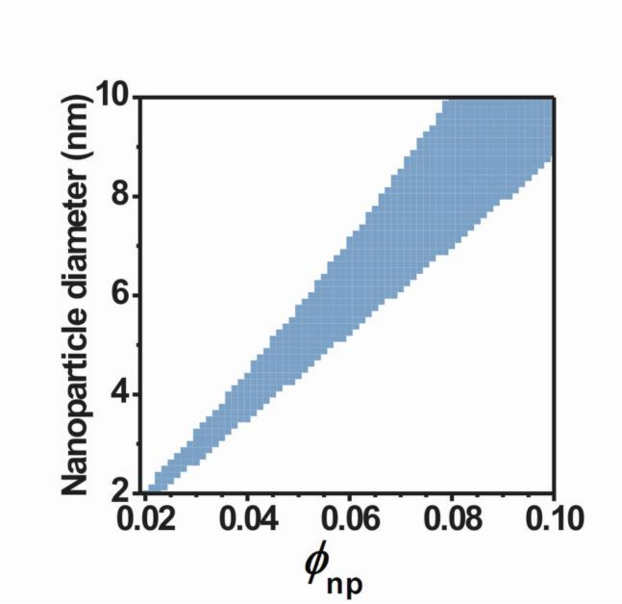

Figure 2.11. Calculated phase map in which the blue shaded region indicates the volume fraction ranges where the core-shell structure with a nanoparticle layer has a lower energy than the assemblies without the nanoparticle layer. The kappa value of 10^{-4} was used for the calculation.

2.6 Conclusions

Nanoparticles can self-assemble into unique cavity-like structures in core-shell type assemblies of PAA-*b*-PS amphiphilic block copolymers. Initially, nanoparticles are randomly incorporated into the swollen aggregates of block copolymers in DMF. As polymers pack more densely with the addition of water, nanoparticles phase segregate to the spherical interface between the polymer core and the shell, forming a submicrometer nanoparticle cavity inside the polymer matrix. It was found that both the enthalpic interaction and the polymer stretching energy are important factors in the formation of radial co-assemblies. The slightly unfavorable interaction between alkyl-terminated nanoparticles and the hydrophobic segment of polymers (*i.e.*, PS) causes the segregation of nanoparticles to the interface between the polymer core and the shell. PS-modified nanoparticles, on the contrary, were randomly incorporated into block copolymer micelles without a particular order because of the favorable interaction between nanoparticles and polymers. Strong segregation theory calculations along with corresponding experimental data revealed that the polymer stretching is also important in forming the layered structure. Due to the polymer stretching energy, co-assemblies were stabilized for limited nanoparticle volume fractions where the inclusion of nanoparticle layers reduces the polymer stretching and lowers the free energy of co-assemblies. In addition, the range of volume fractions required for the co-assembly varied sensitively with nanoparticle size. Because bigger nanoparticles can relieve stretching energy more effectively, the working volume fraction range became broader with increasing the nanoparticle size. The experimentally determined phase map along with the theoretical calculation provides the self-assembly conditions required to stabilize the co-assembly structure of as-synthesized alkyl-terminated nanoparticles and block copolymers.

2.7 References

1. Balazs, A. C.; Emrick, T.; Russell, T. P., Nanoparticle Polymer Composites: Where Two Small Worlds Meet. *Science* 2006, 314, 1107-1110.
2. Saunders, B. R.; Turner, M. L., Nanoparticle-Polymer Photovoltaic Cells. *Adv. Colloid Interface Sci.* 2008, 138, 1-23.
3. Yang, J.; Dave, S. R.; Gao, X. H., Quantum Dot Nanobarcodes: Epitaxial Assembly of Nanoparticle-Polymer Complexes in Homogeneous Solution. *J. Am. Chem. Soc.* 2008, 130, 5286-5292.
4. Ofir, Y.; Samanta, B.; Rotello, V. M., Polymer and Biopolymer Mediated Self-Assembly of Gold Nanoparticles. *Chem. Soc. Rev.* 2008, 37, 1814-1823.
5. Vaia, R. A.; Maguire, J. F., Polymer Nanocomposites with Prescribed Morphology: Going Beyond Nanoparticle-Filled Polymers. *Chem. Mater.* 2007, 19, 2736-2751.
6. Kang, Y. J.; Erickson, K. J.; Taton, T. A., Plasmonic Nanoparticle Chains Via a Morphological, Sphere-to-String Transition. *J. Am. Chem. Soc.* 2005, 127, 13800-13801.
7. Kinge, S.; Crego-Calama, M.; Reinhoudt, D. N., Self-Assembling Nanoparticles at Surfaces and Interfaces. *ChemPhysChem* 2008, 9, 20-42.
8. Shenhar, R.; Norsten, T. B.; Rotello, V. M., Polymer-Mediated Nanoparticle Assembly: Structural Control and Applications. *Adv. Mater.* 2005, 17, 657-669.
9. Yeh, S. W.; Wei, K. H.; Sun, Y. S.; Jeng, U. S.; Liang, K. S., Cds Nanoparticles Induce a Morphological Transformation of Poly(Styrene-B-4-Vinylpyridine) from Hexagonally Packed Cylinders to a Lamellar Structure. *Macromolecules* 2005, 38, 6559-6565.
10. Li, Q. F.; He, J. B.; Glogowski, E.; Li, X. F.; Wang, J.; Emrick, T.; Russell, T. P., Responsive Assemblies: Gold Nanoparticles with Mixed Ligands in Microphase

Separated Block Copolymers. *Adv. Mater.* 2008, 20, 1462-1466.

11. Chiu, J. J.; Kim, B. J.; Kramer, E. J.; Pine, D. J., Control of Nanoparticle Location in Block Copolymers. *J. Am. Chem. Soc.* 2005, 127, 5036-5037.

12. Chung, H.; Ohno, K.; Fukuda, T.; Composto, R. J., Self-Regulated Structures in Nanocomposites by Directed Nanoparticle Assembly. *Nano Lett.* 2005, 5, 1878-1882.

13. Hong, L.; Jin, F.; Li, J.; Lu, Y.; Wu, C., How Are Insoluble Blocks Interacted with and Packed inside a Micelle Made of Block Copolymers in a Selective Solvent? *Macromolecules* 2008, 41, 8220-8224.

14. Zhang, L. F.; Eisenberg, A., Formation of Crew-Cut Aggregates of Various Morphologies from Amphiphilic Block Copolymers in Solution. *Polym. Adv. Technol.* 1998, 9, 677-699.

15. Kim, B. J.; Chiu, J. J.; Yi, G. R. R.; Pine, D. J.; Kramer, E. J., Nanoparticle-Induced Phase Transitions in Diblock-Copolymer Films. *Adv. Mater.* 2005, 17, 2618-2622.

16. He, G.; Ginzburg, V. V.; Balazs, A. C., Determining the Phase Behavior of Nanoparticle-Filled Binary Blends. *J. Polym. Sci., Part B: Polym. Phys.* 2006, 44, 2389-2403.

17. Huang, C.-M.; Wei, K.-H., Pseudo-Single-Crystalline Self-Assembled Structure Formed from Hydrophilic Cdse and Hydrophobic an Nanoparticles in the Polystyrene and Poly(4-Vinylpyridine) Blocks, Respectively, of a Polystyrene-B-Poly(4-Vinylpyridine) Diblock Copolymer. *Macromolecules* 2008, 41, 6876-6879.

18. Gao, X. H.; Cui, Y. Y.; Levenson, R. M.; Chung, L. W. K.; Nie, S. M., In Vivo Cancer Targeting and Imaging with Semiconductor Quantum Dots. *Nat. Biotechnol.* 2004, 22, 969-976.

19. Euliss, L. E.; Grancharov, S. G.; O'Brien, S.; Deming, T. J.; Stucky, G. D.; Murray, C. B.; Held, G. A., Cooperative Assembly of Magnetic Nanoparticles and Block Copolypeptides in Aqueous Media. *Nano Lett.* 2003, 3, 1489-1493.

20. Kim, B. S.; Qiu, J. M.; Wang, J. P.; Taton, T. A., Magnetomicelles: Composite Nanostructures from Magnetic Nanoparticles and Cross-Linked Amphiphilic Block Copolymers. *Nano Lett.* 2005, 5, 1987-1991.

21. Kim, B. S.; Taton, T. A., Multicomponent Nanoparticles Via Self-Assembly with Cross-Linked Block Copolymer Surfactants. *Langmuir* 2007, 23, 2198-2202.

22. Zhu, J. T.; Hayward, R. C., Spontaneous Generation of Amphiphilic Block Copolymer Micelles with Multiple Morphologies through Interfacial Instabilities. *J. Am. Chem. Soc.* 2008, 130, 7496-7502.

23. Kang, Y. J.; Taton, T. A., Core/Shell Gold Nanoparticles by Self-Assembly and Crosslinking of Micellar, Block-Copolymer Shells. *Angew. Chem. Int. Ed.* 2005, 44, 409-412.

24. Jeon, S. J.; Yang, S. M.; Kim, B. J.; Petrie, J. D.; Jang, S. G.; Kramer, E. J.; Pine, D. J.; Yi, G. R., Hierarchically Structured Colloids of Diblock Copolymers and Au Nanoparticles. *Chem. Mater.* 2009, 21, 3739-3741.

25. Yusuf, H.; Kim, W. G.; Lee, D. H.; Guo, Y. Y.; Moffitt, M. G., Size Control of Mesoscale Aqueous Assemblies of Quantum Dots and Block Copolymers. *Langmuir* 2007, 23, 868-878.

26. Sanchez-Gaytan, B. L.; Cui, W. H.; Kim, Y. J.; Mendez-Polanco, M. A.; Duncan, T. V.; Fryd, M.; Wayland, B. B.; Park, S. J., Interfacial Assembly of Nanoparticles in Discrete Block-Copolymer Aggregates. *Angew. Chem. Int. Ed.* 2007, 46, 9235-9238.

27. Mayadunne, R. T. A.; Rizzardo, E.; Chiefari, J.; Krstina, J.; Moad, G.; Postma, A.; Thang, S. H., Living Polymers by the Use of Trithiocarbonates as Reversible Addition-Fragmentation Chain Transfer (Raft) Agents: Aba Triblock Copolymers by Radical Polymerization in Two Steps. *Macromolecules* 2000, 33, 243-245.

28. Davis, K. A.; Charleux, B.; Matyjaszewski, K., Preparation of Block Copolymers of Polystyrene and Poly (T-Butyl Acrylate) of Various Molecular Weights and Architectures by Atom Transfer Radical Polymerization. *J. Polym. Sci., Part A: Polym. Chem.* 2000, 38, 2274-2283.

29. Peng, Z. A.; Peng, X. G., Formation of High-Quality Cdte, Cdse, and Cds Nanocrystals Using Cdo as Precursor. *J. Am. Chem. Soc.* 2001, 123, 183-184.

30. Dabbousi, B. O.; RodriguezViejo, J.; Mikulec, F. V.; Heine, J. R.; Mattoussi, H.; Ober, R.; Jensen, K. F.; Bawendi, M. G., (Cdse)Zns Core-Shell Quantum Dots: Synthesis and Characterization of a Size Series of Highly Luminescent Nanocrystallites. *J. Phys.*

Chem. B 1997, 101, 9463-9475.

31. Sun, S. H.; Zeng, H., Size-Controlled Synthesis of Magnetite Nanoparticies. *J. Am. Chem. Soc.* 2002, 124, 8204-8205.

32. Yan, F.; Li, J.; Zhang, J.; Liu, F.; Yang, W., Preparation of Fe3o4/Polystyrene Composite Particles from Monolayer Oleic Acid Modified Fe3o4 Nanoparticles Via Miniemulsion Polymerization. *J. Nanopart. Res.* 2008, 11, 289-296.

33. Olmsted, P. D.; Milner, S. T., Strong Segregation Theory of Bicontinuous Phases in Block Copolymers. *Macromolecules* 1998, 31, 4011-4022.

34. Helfand, E.; Tagami, Y., Theory of Interface between Immiscible Polymers. *J. Poly. Sci., Part A: Poly. Chem. Lett.* 1971, 9, 741.

35. Murray, C. B.; Kagan, C. R.; Bawendi, M. G., Synthesis and Characterization of Monodisperse Nanocrystals and Close-Packed Nanocrystal Assemblies. *Annu. Rev. Mater. Sci.* 2000, 30, 545-610.

36. Hickey, R. J.; Sanchez-Gaytan, B. L.; Cui, W. H.; Composto, R. J.; Fryd, M.; Wayland, B. B.; Park, S. J., Morphological Transitions of Block-Copolymer Bilayers Via Nanoparticle Clustering. *Small* 2009, 6, 48-51.

37. Zhang, L. F.; Eisenberg, A., Multiple Morphologies and Characteristics of "Crew-Cut" Micelle-Like Aggregates of Polystyrene-B-Poly(Acrylic Acid) Diblock Copolymers in Aqueous Solutions. *J. Am. Chem. Soc.* 1996, 118, 3168-3181.

38. Jiang, J.; Krauss, T. D.; Brus, L. E., Electrostatic Force Microscopy Characterization of Trioctylphosphine Oxide Self-Assembled Monolayers on Graphite. *J. Phys. Chem. B* 2000, 104, 11936-11941.

39. Thompson, R. B.; Ginzburg, V. V.; Matsen, M. W.; Balazs, A. C., Predicting the Mesophases of Copolymer-Nanoparticle Composites. *Science* 2001, 292, 2469-2472.

Chapter 3: Hierarchical Self-Assembly of Amphiphilic Conjugated Polymers into Isolated, Bundled, and Branched Nanofibers[1,2]

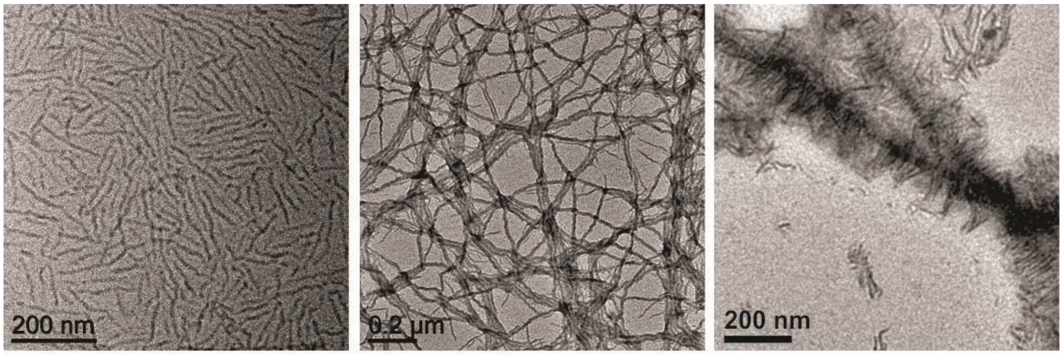

Nanofibers Bundled Nanofibers Branched Nanofibers

Herein, we provide fundamental studies that provide a better understanding of the solution phase nanoscale organization of a series of amphiphilic conjugated rod-coil block copolymers (PHT_m*-b-*PEG_n*) with well-defined relative block lengths. We also demonstrate that an amphiphilic conjugated block copolymer can act as an efficient encapsulation agent for semiconducting homopolymers with a unique solvent induced control over the supramolecular self-assembly structure and the formation of encapsulated nanofiber bundles and branched nanofiber structures. The crystallization and encapsulation strategy towards controlled supramolecular structures that is presented herein provides a new toolbox towards the formation of novel conjugated nanostructures.*

---

[1] Reproduced in part with permission from Kamps, A. C., Fryd, M., and Park, S.-J. (2012) Hierarchical Self-Assembly of Amphiphilic Conjugated Polymers into Isolated, Bundled, and Branched Nanofibers, *ACS Nano* 6, 2844-2852. Copyright 2012 American Chemical Society.

[2] Reproduced in part with permission from Gao, J.; Kamps, A.C.; Park; S.-J.; Grey, J.K. (2012) Encapsulation of Poly(3-hexylthiophene) J-Aggregate Nanofibers with an Amphiphilic Block Copolymer, *Langmuir*, submitted. Copyright 2012 American Chemical Society.

3.1 Introduction

Conjugated polymers have received a great deal of attention in recent years as an alternative to inorganic single crystalline semiconductors due to their excellent optoelectronic properties and solution-processability.[1] Among various conjugated polymers, poly(3-hexylthiophene) (PHT) has been one of the most widely studied semiconducting polymers in photovoltaic devices and field effect transistors owing to its high hole mobility.[2, 3] Unlike single crystalline semiconductors, however, thin films of conjugated polymers possess many defects and impurities, and the device performance depends highly on the molecular packing of the polymers and on the nanometer scale film morphology.[4] In fact, the high mobility of PHT originates partly from its tendency to form well-packed crystalline domains.[5] However, typical thin films of conjugated polymers including PHT contain many grain boundaries and defects, which impede efficient charge transport.[6, 7] Thus, the ability to control the polymer morphology is of paramount importance to fully exploit the potential of conjugated polymers in low-cost, flexible device fabrication.[8]

Block copolymers have been actively studied as tools for nanoscale device fabrication and new materials syntheses based on their ability to form well-ordered nanostructures by microphase segregation. For the past two decades, there have been numerous studies aimed at optimizing bulk block copolymer thin film morphologies by employing various thin film processing techniques such as thermal or solvent vapor annealing.[9-11] In recent years, there has been an increased interest in introducing conjugated polymers into block copolymer designs, as it provides an efficient way to organize technologically important semiconducting polymers into useful device architectures.[12-14] Solution phase self-assembly of conjugated amphiphilic polymers offers a powerful alternative to the thin film techniques.[15-18] In this approach, conjugated polymers are organized into technologically relevant building blocks such as nanowires via the nature of amphiphilic polymers to self-assemble into various nanostructures. However, solution phase self-assembly of conjugated amphiphilic polymers is not yet well understood, and the supramolecular self-assembly of such preformed building blocks into extended arrays by the bottom-up approach remains largely unexplored.

Among various conjugated polymers, poly(alkylthiophenes) are one of the most widely studied organic materials owing to their excellent optoelectronic properties, which make them suitable candidates for applications in optoelectronic devices including organic photovoltaic cells, light emitting diodes, and field effect transistors.[2] Conjugated block copolymers have been synthesized by many research groups via the macroinitiation approach, where the second polymer block is grown off of the end-functionalized conjugated polymer. McCullough and coworkers pioneered the synthesis of regioregular polythiophene (PHT) and PHT-containing block copolymers, and reported several different PHT-containing block copolymers including PHT-*b*-poly(styrene)[19] and PHT-*b*-poly(acrylates)[20, 21]. Recently, it has been shown that PHT thin films with a long range order can be generated by the self-assembly of PHT-*b*-poly(2-vinyl pyridine) with relatively long coil blocks.[13] Amphiphilic conjugated block copolymers have also been synthesized for solution phase assembly using the macroinitiation approach, including POT-*b*-poly(ethylene oxide)[22] and PHT-*b*-poly(2-ethyl-2-oxazoline)[23].

In order to create uniform nanostructures in a predictable fashion, it is critical to synthesize conjugated block copolymers with well-defined molecular weights and low polydispersity. While the macroinitiation approach described above has been successfully used to yield conjugated block copolymers of various polymer combinations, a precise control of the length of a growing polymer block can be challenging. Furthermore, it is often difficult to determine the molecular weight of synthesized polymers by conventional characterization techniques such as gel permeation chromatography (GPC) due to the rigid nature of conjugated polymers.[24]

Here, we report the high yield synthesis and self-assembly of a conjugated amphiphilic polymer composed of PHT and poly(ethylene glycols) (PEG) with well-controlled molecular weights. A series of different length polymers were synthesized in high yields by the copper catalyzed Huisgen's 1,3-dipolar cycloaddition between azido and alkynyl functionalized polymer end-groups. This click chemistry reaction has become rather ubiquitous in recent literature in topics ranging from small molecules[25] to polymeric nanomaterials[26,27, 28] and bioconjugates[29] due to its high yield, mild reaction conditions, and tolerance for various functional groups. The click chemistry coupling reaction was recently applied to synthesize conjugated block copolymers of PHT-*b*-PS[30], PHT-*b*-PAA[31], and a donor-accepter system[32]. However, these examples are mainly synthetic examples and do not give clear insights into how having a well-defined polymer coupling reaction can lead to well-defined self-assembly structures.

Here, we report the high yield click-coupling synthesis and self-assembly of conjugated amphiphilic block copolymers composed of PHT and poly(ethylene glycol)

(PEG) and their superstructures with preformed PHT assemblies. The PEG block was chosen for its solubility in various solvents ranging from polar organic solvents to water, which makes it an excellent system for studying solution phase self-assembly. A series of different length PHT-*b*-PEG were synthesized with precisely controlled molecular weights via the copper-catalyzed click reaction,[33] which enabled an accurate determination of the block-lengths and the systematic correlation of the block ratio and the self-assembly structure. A recent work by Manners and coworkers has shown that cylindrical micelles of PHT-*b*-poly(dimethylsiloxane) with controlled lengths can be formed by crystallization-driven self-assembly.[34] Here, we show that the length of PHT-*b*-PEG self-assembled nanofibers can be controlled by varying the weight fraction of PHT (f_{PHT}) from 0.41 to 0.82. Furthermore, we demonstrate that the self-assembly of PHT-*b*-PEG and preformed PHT nanofibers can lead to interesting superstructures such as closely packed nanofiber bundles and branched structures. The supramolecular self-assembly of PHT nanofibers presented here provides a new toolbox for the formation of novel organic nanostructures.

3.2 Experimental Section

3.2.1 Synthesis and Characterization of Ethynyl-PHT. Monoethynyl-terminated PHT (Ethynyl-PHT) was synthesized using the living Grignard metathesis (GRIM) polymerization and the end-functionalizaton method following a previously published procedure developed by McCullough.[35, 36] The regioregularity (>95% HT) and the monoethynyl-end group functionality of ethynyl-PHT was confirmed by ^{1}H-NMR spectroscopy (Figure 3.1 C). The molecular weight and polydispersity of the ethynyl-PHT were determined to be 3428 g/mol and 1.16 respectively by MALDI (Figure 3.1 A,B).

In a typical experiment, 2,5-dibromohexylthiophene (1.8 g, 5.6 mmol) and 10 mL of freshly distilled THF are added to a 100 mL round bottom flask and the system was purged with nitrogen. A 1.0 M solution of *tert*-butylmagnesium chloride in THF (5.6 mL, 5.6 mmol) was then added and the mixture was stirred for 3 hours at room temperature under nitrogen. During this time the solution changed from a yellow color to a green color. The mixture was then diluted with 30 mL of THF followed by addition of Ni(dppp)Cl_2 (70 mg, 0.1 mmol). The reaction proceeded under nitrogen flow for an additional 20 minutes and then a 0.5 M solution of ethynyl magnesium bromide in THF (2.8 mL, 1.4 mmol) was added and reacted for an additional 20 minutes. At this time, the reaction was quenched by adding methanol and then the product was purified by subsequent soxhlet extractions with methanol and hexanes. The final product was then collected by a final soxhlet extraction with chloroform. The ethynyl-PHT solid product (purple solid) was dried to a constant weight under vacuum (372 mg, 0.12 mmol) and then stored under inert atmosphere.

^{1}H NMR (500 MHz, CDCl3): δ_H 0.89 (t, 3H), 1.32-1.42 (m, 6H), 1.68 (t, 2H), 2.78 (t, 2H), 3.51 (s), 6.98 (s, 1H) ; GPC: M_n = 6562, PDI = 1.17; MALDI-MS: m/z = 3428.87 [M+] (calculated: 3428 , degree of polymerization (DP) of 20, ethynyl/Br end groups), PDI = 1.16.

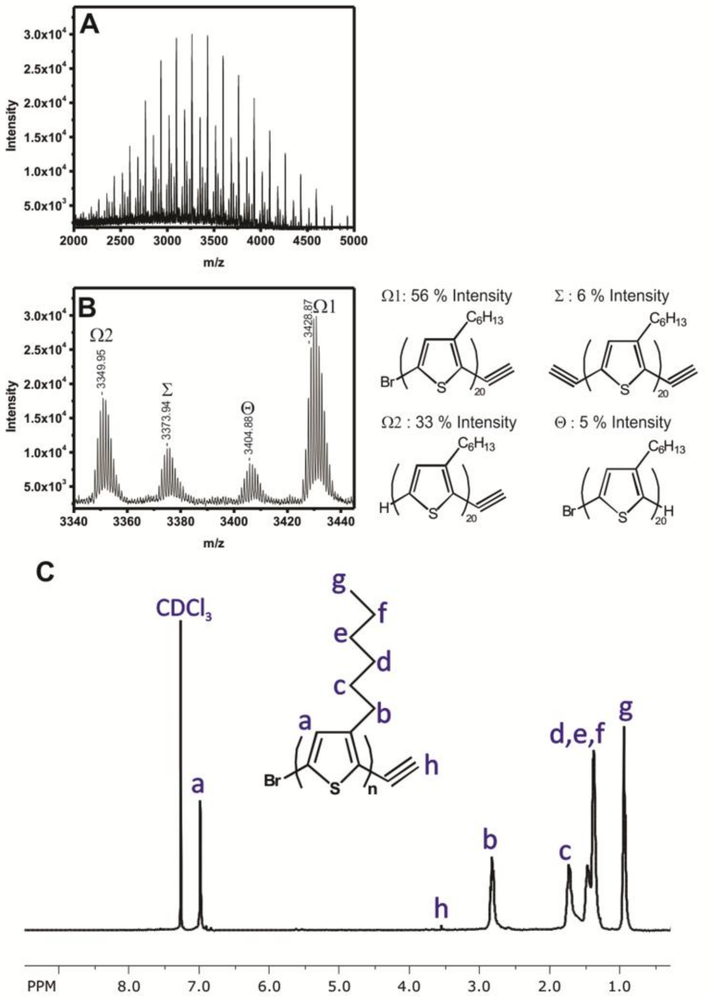

Figure 3.1. (A) MALDI-TOF of ethynyl-PHT and (B) end-group analysis. (C) ^{1}H-NMR spectra of PHT$_{20}$-ethynyl.

3.2.2 Synthesis and Characterization of Azide-PEG. Monoazide-terminated PEG (azide-PEG) was synthesized by the mesylation of the hydroxyl terminus of commercial methoxy PEG followed by sodium azide substitution.[37, 38] The presence of the azide-end group was confirmed by FT-IR spectroscopy (appearance of azide peak at 2101 cm^{-1}) (Figure 3.2 C) and by the end-group analysis of MALDI spectra (Figure 3.2 A,B). A series of different length methoxy-PEG was purchased and used to synthesize PHT-*b*-PEG with varying f_{PHT}.

Typically, a solution of methoxy-PEG (4.4 g, 0.92 mmol), triethylamine (0.51 mL, 3.7 mmol), and 50 mL of freshly distilled THF were added to a 3-neck roundbottom flask and the system was purged with nitrogen. Methanesulfonyl chloride (0.32 mL, 4.1 mmol) was then added to the flask and the solution was stirred at room temperature for 10 hours. The reaction product was then dried down using rotary evaporation, redissolved into minimal amount of deionized water (~ 1-2 mL), and then extracted into DCM (150 mL x 2). After drying the organic product layer with sodium sulfate, the product was filtered, concentrated and then precipitated from minimal DCM into cold diethyl ether. The off-white/yellow precipitate was then filtered, washed with cold diethyl ether, and then dried under vacuum to a constant weight (3.9 g, 88 %). The mesylated PEG (3.9 g, 0.81 mmol) was added to a roundbottom flask with 50 mL DMF and a reflux condenser. Sodium azide (4.3 g, 65 mmol) was then added to the flask and the solution is heated at 60 °C for 24 hours. The reaction product was then dried down using rotary evaporation. The product was then redissolved into DCM and the excess sodium azide was removed by filtration. The product in DCM was further cleaned by extraction with brine solution (100 mL x 4). After drying the organic layer with sodium sulfate, the product was filtered, concentrated and then precipitated from minimal DCM into cold diethyl ether. The azide-PEG product (white solid) was then filtered, washed with cold diethyl ether, and then dried under vacuum to a constant weight (2.2 g, 57 %).

Characterization of azide-PEG$_{108}$. IR: (KBr, cm^{-1}): 2101 (azide), 529, 842, 963, 1108, 1237, 1282, 1343, 1468. MALDI-MS: m/z = 4896.35 [M+] (calculated: 4896, DP of 108, N_3/CH_3 end groups), PDI = 1.21.

Characterization of azide-PEG$_{48}$. IR: (KBr, cm^{-1}): 2100 (azide), 529, 842, 963, 1108, 1237, 1282, 1343, 1468. MALDI-MS: m/z = 2167.1 [M+] (calculated: 2169.02, DP of 48, N_3/CH_3 end groups), PDI = 1.18.

Characterization of azide-PEG$_{16}$. IR: (KBr, cm^{-1}): 2100 (azide), 529, 842, 963, 1108, 1237, 1282, 1343, 1468. MALDI-MS: m/z = 759.5 [M+] (calculated: 761.02, DP of 16, N_3/CH_3 end groups), PDI = 1.22.

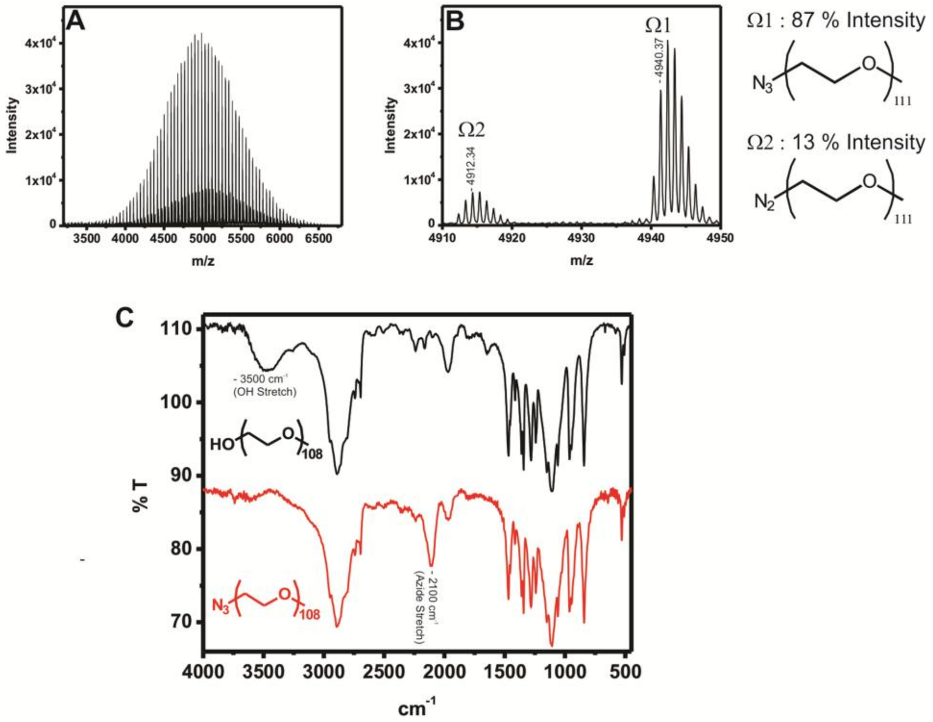

Figure 3.2. (A) MALDI-TOF of azide-PEG and (B) end-group analysis. (C) Representative FT-IR of azide-PEG (red) and methoxy-PEG (black).

3.2.3 Synthesis of PHT-*b*-PEG).

3.2.3 Synthesis of PHT-*b*-PEG). PHT-*b*-PEG was synthesized by the copper(I)-catalyzed click reaction between azide-PEG and ethynyl-PHT (Scheme 4). Typically, ethynyl-PHT (100 mg, 0.0266 mmol), azide-terminated PEG (257 mg, 0.0532 mmol) and 10 mL freshly distilled THF were added to a 25 mL Schlenk flask. A solution of 1,8-diazabicyclo[5.4.0]undec-7-ene (DBU) (152.2 mg, 1.0 mmol) and copper(I) iodide (1.9 mg, 0.010 mmol) was then degassed and then introduced into the schlenk flask. The mixture was then degassed with three freeze pump thaw cycles and subsequently refilled with nitrogen. The solution reacted at 40°C for 4 days. The excess copper salt and excess PEG homopolymer was removed by passing the product through a neutral alumina column. After the removal of THF by rotary evaporation, the product was precipitated into methanol and then filtered to remove any excess PHT homopolymer. The final product was washed with hexanes and then dried under vacuum and collected as a purple solid (229 mg, 92% Yield).

^{1}H NMR (500 MHz, CDCl3): δ_H 0.89 (t, 3H), 1.32-1.42 (m, 6H), 1.68 (t, 2H), 2.78 (t, 2H), 3.61 (s), 6.95 (s).

3.2.4 Preparation of J and H Aggregate PHT Nanofibers

3.2.4.1 Preparation of PHT$_{200}$ H-Aggregate Nanofibers. The commercial PHT (regioregular (> 95% HT) with a number average molecular weight of 33405 g mol^{-1}) was purified by sequential soxhlet extractions with hexanes, DCM and THF to remove lower molecular weight fractions (< 22000 g/mol). The purified higher molecular weight product (PHT$_{200}$) was then collected by a final soxhlet extraction with chloroform and used for subsequent experiments. In order to prepare the PHT_{200} nanofibers, the purified PHT_{200} was dissolved in anisole at a concentration of 1 mg/mL. This solution was heated to 70 °C in a hot water bath for 1 hour yielding a clear orange solution. The hot solution was then cooled to room temperature by placing in a drawer overnight to allow for complete crystallization as evidenced by the color change of the solution from orange to purple. The aged solution was then centrifuged at 5000 rpm for 30 minutes (x2) to isolate PHT_{200} crystallized nanofibers.

3.2.4.2 Preparation of PHT_{350} J-Aggregate Nanofibers. Commercial PHT (regioregular (> 95% HT) with a number average molecular weight of 50,000 – 65,000 g mol^{-1}) was obtained from Plextronics and used as received. This higher molecular weight polymer (PHT_{350}) was dissolved in toluene at a concentration of 2 mg/mL. This solution was heated in a 2 mL glass vial to 85 °C in a hot water bath for 1 hour yielding a clear orange solution. The hot solution was then cooled to room temperature by placing in a drawer overnight to allow for complete crystallization as evidenced by the color change of the solution from orange to purple. The aged solution was then centrifuged at 3500 rpm for 30 minutes (x2) to isolate PHT_{350} crystallized nanofibers.

3.2.5 Preparation of PHT Nanofibers Encapsulated in PHT_{20}-*b*-PEG_{108}. In a typical encapsulation experiment with a molar ratio of PHT_{20}-*b*-PEG_{108}:PHT_{200} of 173:1, 800 μL of a 5.12×10^{-5} M stock solution of PHT_{20}-*b*-PEG_{108} in chloroform (concentration determined from UV-vis with an extinction coefficient of 4.3×10^{4} M^{-1} cm^{-1}) was first dried down under nitrogen. Then, a 10 μL aliquot of a 2.37 x 10^{-5} M stock solution of PHT_{200} nanofibers in anisole (concentration determined from UV-Vis with an extinction coefficient of 1 x 10^{6} M^{-1} cm^{-1}) was added to the dried block copolymer. After 20 minutes of mixing, either 1000 μL of water or 1000 μL of methanol were added to the solution. The assemblies were mixed for 15 hours at 200 rpm on a shaker and then a low flow of nitrogen was used to dissipate anisole in the solution. Harsher mixing procedures such as vortexing or sonication were avoided because they caused significant entangling of PHT superstructures. After dissipation of any residual anisole, either methanol or water was added to the solution until a final volume of 1 mL of solution was reached. In some cases, the superstructures were purified and concentrated by the centrifugation at 2000 rpm for 45 minutes.

3.2.6 Materials and Instrumentation. Methanol, hexane, and chloroform were purchased from Fisher Scientific. Regioregular (> 95% HT) PHT with a number average molecular weight of 33405 g mol^{-1} was purchased from Sigma Aldrich. All other reagents were also purchased from Sigma Aldrich. THF was freshly distilled prior to use from sodium/benzophenone under nitrogen and all other reagents were used without further purification. All reactions were performed in oven-dried glassware under pre-purified nitrogen.

Electronic absorption spectra were acquired on an Agilent 8453 spectrophotometer. Emission spectra were acquired on a Spex Fluorolog 3 utilizing a R928 PMT detector. Proton NMR spectra were obtained on a Bruker-DMX500 interfaced to an Aspect 3000 computer in $CDCl_3$ at ambient temperature. IR spectra were obtained on a Perkin-Elmer system 2000 FTIR spectrometer. TEM was performed on a JEOL 1400 electron microscope operating at 120 kV accelerating voltage. GPC measurements were carried out at room temperature at a flow rate of 1.0 mL/min on a Shimadzu LC-10AT liquid chromatography system equipped with a series of two PLgel 10µm 10E6A columns, an SPD-10AVvp absorbance UV/VIS detector, and a refractive index detector (RID-10A) calibrated against linear polystyrene standards in THF. DLS measurements were taken on a Malvern Zetasizer Nano Series. Matrix assisted laser desorption ionization time-of-flight mass spectrometry (MALDI-TOF/TOF MS) spectra were obtained on a Bruker Flex Series MALDI-TOF/TOF MS. Spectra were recorded in the positive-ion reflectron mode with an accelerating voltage of 20 kV. The MALDI samples were prepared by mixing a THF solution of PHT (10 mg/mL) and a THF solution of 2,2':5,2"-terthiophene matrix solution (0.25 M). For PEG samples, a THF solution of 4'hydroxyazobenzene-2-carboxylic acid (HABA) (0.25 M) was used as a matrix and was mixed with a THF solution of PEG (10 mg/mL). The MALDI sample was prepared by depositing 1 µL of a (1 matrix:1 sample) solution on the stainless steel sample target and then letting the sample air dry.

3.3 Synthesis and Characterization of PHT-*b*-PEG

A series of different length PHT-*b*-PEG was synthesized via the copper(I)-catalyzed click-coupling reaction of azide-PEG and ethynyl-PHT (Scheme 4) to generate PHT_{20}-*b*-

PEG_n (n = 16, 48, 108) (Table 1). The chemical structure of the synthesized PHT-*b*-PEG was confirmed by ^{1}H-NMR (Figure 3.3 B). The GPC data shows a reduction of the retention time with the increasing of the molecular weight of PEG, which confirms that ethynyl-PHT and azide-PEG are indeed coupled to yield PHT-*b*-PEG (Figure 3.3 A). The reaction yields were calculated to be over 70 % for all synthesized polymers (Table 1). This result contradicts the previous observation that a spacer was needed to prevent steric hindrance from the bulky alkyl side chains for the click syntheses of PHT-*b*-PS.[30] However, a more recent report on the click synthesis of P3HT-*b*-PAA indicated that ethynyl homocoupling could be the main factor that led to the low yield observed in the previous synthesis of PHT-*b*-PS.[31] Therefore, in our system, to avoid homocoupling and increase the reaction yield of our synthesis, end-functionalized homopolymers were kept under inert conditions and used shortly after the synthesis (< ~ 1 week). In the synthesis of PHT-*b*-PEG presented herein, the length of PEG and alkyl side chains did not significantly affect the coupling efficiency, and all of the products were synthesized in high yields (>70%).

Molecular weights of PHT-*b*-PEG were obtained by combining the predetermined molecular weights of PEG and PHT homopolymers (Table 1). An important advantage of the click chemistry coupling reaction is that the relative block-length can be readily controlled by the choice of parent homopolymers. In contrast, in the macroinitiation approach, the second polymer length and f_{PHT} are controlled by adjusting reaction conditions such as time, temperature, and the monomer concentration,[39] and it can be challenging to precisely and reproducibly control the polymer lengths.[40] Furthermore, due to the rigid nature of conjugated polymers, it is difficult to accurately determine the molecular weight of conjugated block copolymers by common techniques such as gel permeation chromatography (GPC).[24] In our synthesis of PHT-*b*-PEG, both PHT and PEG parent homopolymers were fully characterized by GPC, FTIR, NMR, and MALDI prior to the coupling reaction, which allowed for an accurate determination of the molecular weights of the resultant block-copolymers and straightforward control of relative block lengths. As presented in Table 1, f_{PHT} was varied from 0.41 to 0.82 by changing the molecular weight of the PEG block while keeping the length of PHT constant. For comparison, molecular weights estimated using GPC with polystyrene standards are also given in Table 1. Note that many previous works on conjugated block copolymers reported the molecular weights determined by GPC despite the common knowledge that GPC overestimates the MW of rod-like polymers. The two sets of molecular weights presented in Table 1 clearly show that GPC significantly overestimates the molecular weights of PHT-*b*-PEG even for the polymers with small f_{PHT}, demonstrating an important advantage of click syntheses.

Scheme 4. The synthetic scheme for the click chemistry of PHT-*b*-PEG.

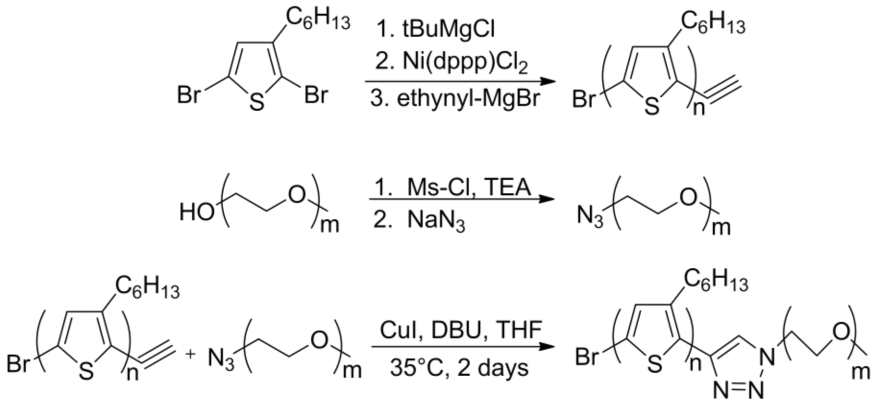

Table 1. Molecular weights and molecular weight distributions of synthesized PHT-*b*-PEG and parent PHT and PEG homopolymers.

Polymer	$M_{n,\,MALDI,\,PEG}{}^{a}$ (g mol^{-1})	$M_w/M_n{}^{a}$	$M_{n,\,MALDI,\,PHT\text{-}b\text{-}PEG}{}^{b}$ (g mol^{-1})	$M_{n,\,GPC}{}^{c}$ (g/mol^{-1})	$M_w/M_{n,\,GPC}{}^{c}$	f_{PHT}
PHT_{20}	--	1.16	--	6562	1.17	1.00
PHT_{20}-*b*- PEG_{16}	761	1.04	4189	8489	1.21	0.82
PHT_{20}-*b*- PEG_{48}	2169	1.05	5597	11710	1.22	0.61
PHT_{20}-*b*- PEG_{108}	4896	1.04	8324	18200	1.21	0.41

[a] M_n and M_w/M_n were determined by MALDI-TOF analysis.

[b] M_n was determined by taking the sum of the homopolymer molecular weights as determined by MALDI-TOF analysis.

[c] M_n and M_w/M_n were determined by GPC and are reported as their polystyrene equivalents.

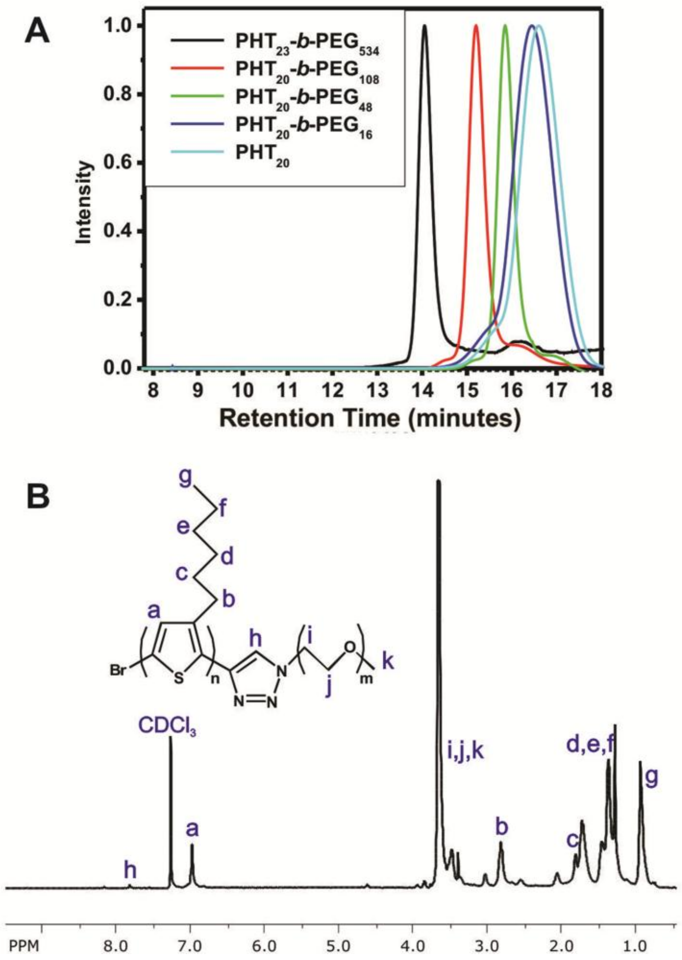

Figure 3.3. (A) GPC spectrum (RID trace) of PHT$_{20}$-*b*-PEG$_n$ in THF. (B) Representative ^{1}H-NMR spectra of PHT$_{20}$-*b*-PEG$_m$.

3.4 Self-Assembly in Selective Solvents

3.4.1 Morphology. Due to its amphiphilic nature, PHT-*b*-PEG can be dispersed in a wide range of solvents. The optical properties of the block copolymer in solution change depending on the selectivity of the solvent and can be correlated to the morphology of the self-assembled block copolymers in solution. In polar organic solvents such as tetrahydrofuran (THF) and dichloromethane (DCM) where both polymer blocks are soluble, PHT-*b*-PEG exists as isolated chains and shows UV-vis and photoluminescence (PL) spectra that are characteristic of PHT homopolymers in good solvents (Figure 3.4 A-B); the π-π* absorption peak at ~450 nm and a high intensity PL at ~576 nm observed for PHT-*b*-PEG in DCM are characteristic of regioregular PHT in the same solvent.[41] This result indicates that the attachment of PEG does not significantly affect the conformation of PHT in good solvents. When PHT_{20}-*b*-PEG_{108} is dispersed in a selective solvent for PEG such as water and methanol, the block copolymer organizes into supermolecular assemblies as evidenced by the red shift and the appearance of the vibronic structure in the UV-vis spectra (Figure 3.4 A). The red-shifted absorption is a result of the increased effective conjugation length due to the induced planarity of the closely packed PHT chains in polymer assemblies. The vibronic structures with peak positions at 503 nm, 541 nm, and 590 nm arise from a combination of π-π* electronic transition and the strong lattice vibrations in PHT crystalline domains.[42] The efficient PL quenching of PHT_{20}-*b*-PEG_{108} in selective solvents is also indicative of tightly packed PHT and strong interchain coupling of the PHT block in the polymer assemblies (Figure 3.4 B).[15, 43]

The transmission electron microscopy (TEM) images in Figure 3.4 C-D show that PHT_{20}-b-PEG_{108} self- assembles into one-dimensional fiber-like structures in selective solvents, with the darker contrast arising from the electron-dense PHT block. The PEG block was selectively stained with a phosphotungstic acid solution in Figure 3.4 D, revealing the hydrophilic PEG block surrounding the PHT nanofiber core. The width of the PHT domain was measured to be 8.1 ± 1.1 nm, which corresponds to the length of one PHT_{20} chain calculated with the monomer length of 0.4 nm.[43] This indicates that the nanofiber is composed of interdigitated PHT chains surrounded by hydrophilic PEG chains as depicted in Figure 3.4 E. The height of the nanofibers was determined to be 5 ± 1.5 nm by AFM, which is approximately 2-3 times the vertical lattice dimension of a P3HT unit cell which is reported to be 1.68 nm.[44-46] This data indicates that the PHT-*b*-PEG nanofibers are composed of 1-3 vertical stacks of PHT-*b*-PEG. These one-dimensional wire-like assemblies of semiconducting polymers are highly desirable for device applications as they can support high carrier mobility.[45] While the insulating block of semiconducting-insulating block copolymers can reduce the overall device performance, this effect can be overcome with highly ordered self-assembled systems.[20, 47, 48]

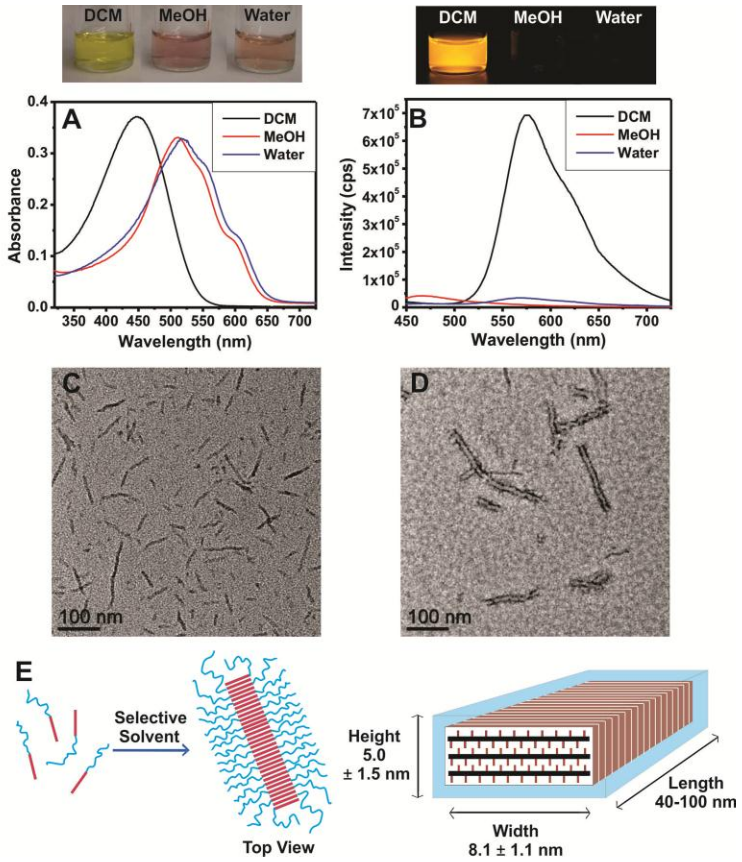

Figure 3.4. (A) Absorbance and (B) PL spectra of PHT$_{20}$-*b*-PEG$_{108}$ dissolved in dichloromethane, methanol, and water at a concentration of 0.1 mg/mL. Pictures of PHT$_{20}$-*b*-PEG$_{108}$ (0.1 mg/mL) solutions under ambient light (top-left) and under UV light (top-right) are given above the spectra. PL spectra were collected using an excitation wavelength of 380 nm. (C) TEM image of PHT$_{20}$-*b*-PEG$_{108}$ assemblies formed in water. (D) TEM image of PHT$_{20}$-*b*-PEG$_{108}$ assemblies stained with phosphotungstic acid solution. (E) Schematic depiction of the nanofiber morphology formed from the self-assembly of amphiphilic PHT$_{20}$-*b*-PEG$_{108}$ in a selective solvent.

3.4.2 Solvatochromism. It is well known that thiophene homopolymers have a tendency towards crystallization and under certain conditions thiophene homopolymers have been found to crystallize into similar nanofiber structures.[49, 50] In order to confirm that the nanofiber formation in polar solvents was a result of the self-assembly of block copolymers, the aggregation behavior of PHT-*b*-PEG was compared with that of PHT homopolymers in a methanol/DCM mixture and presented in Figure 3.5. As the methanol content was increased from 0% to 90%, the absorption spectrum of PHT-*b*-PEG was red-shifted, resulting in a visible color change of the solution from yellow to orange to red (Figure 3.5 B-C). The isosbestic point at ~480 nm indicates the coexistence of two distinct conformations of the block copolymer: an isolated form and a coplanar aggregated form. The PL intensity of the block copolymer also decreased with an increasing amount of methanol content as expected (Figure 3.5 D). The mixture of PHT and PEG homopolymers showed similar absorption red-shift and PL quenching with the introduction of methanol. However, when the percentage of methanol was increased to > 50 % the PHT homopolymer began to quickly precipitate out of solution. This observation confirms that the covalently attached PEG block of the conjugated block copolymer is necessary for making stable suspensions of PHT nanofibers in polar solvents.

The reversibility of the block copolymer assembly process was also demonstrated by drying repeatedly drying down samples and redissolving them into different solvents (either selective or non-selective solvents). Thus proving that the observed morphological and optical changes are not a result of heat induced crystallization or oxidation. The amphiphilic conjugated block copolymer, PHT-*b*-PEG, is soluble in a wide range of solvents with a wide range of polarity indexes (Figure 3.6) and can be used to critically tune the optical and morphological characteristics of the block copolymer.

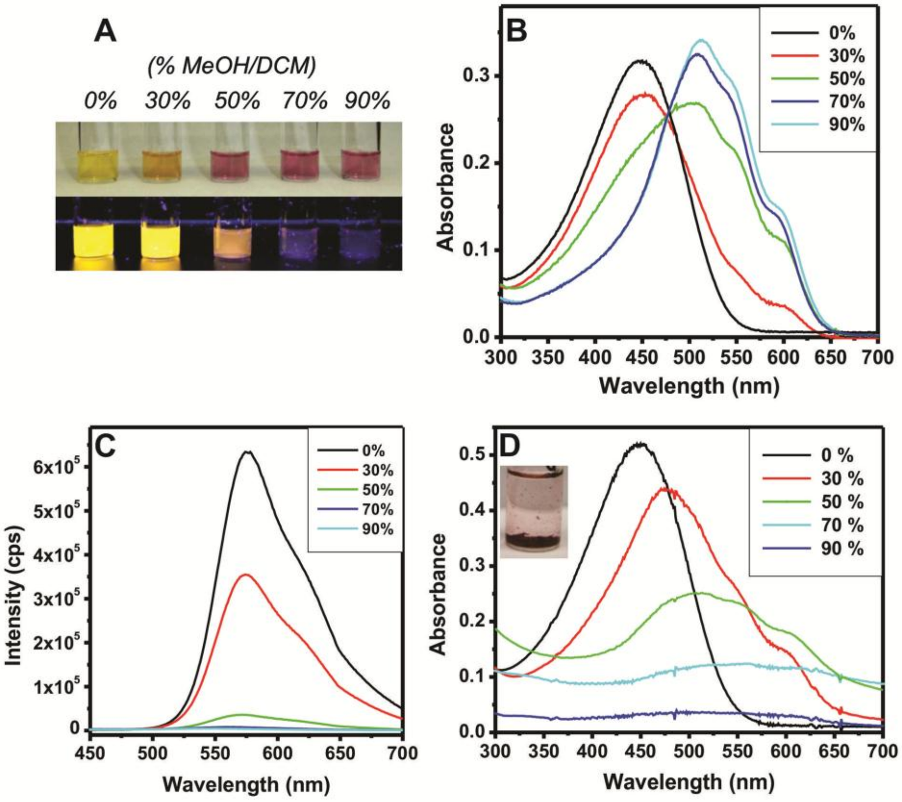

Figure 3.5. (A) Pictures of PHT$_{20}$-*b*-PEG$_{108}$ (0.1 mg/mL) with varying solvent compositions under ambient light (top) and under UV light (bottom). From left to right: 0 %, 30 %, 50 %, 70 %, 90 % methanol in DCM. (B) Absorption and (C) PL spectra of PHT$_{20}$-*b*-PEG$_{108}$ (0.1 mg/mL) with varying solvent composition in terms of % methanol (v/v). (D) Absorption spectra of mixtures of PHT$_{20}$ and PEG$_{108}$ homopolymers (0.1 mg/mL) with varying solvent composition in terms of % methanol (v/v). PL spectra were collected using an excitation wavelength of 380 nm.

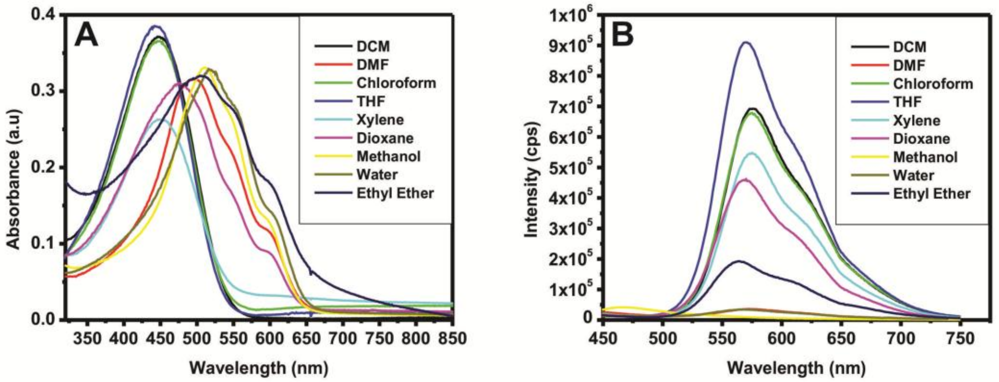

Figure 3.6. (A) Absorption and (B) PL spectra of PHT_{20}-*b*-PEG_{108} in different solvents at a concentration of 0.1 mg/mL. PL spectra were collected using an excitation wavelength of 380 nm.

3.4.3 Thermochromism. The PHT-*b*-PEG nanofibers are strongly held together by π-π interactions and they are not easily disrupted by external stimuli (i.e., ions, temperature) in highly selective solvents such as water and methanol (Figure 3.7). However, the unusual solubility of PEG in various solvents allows for fabricating responsive PHT-*b*-PEG nanofibers. The thermochromic behavior of PHT-*b*-PEG in ethyl acetate was not found in any other solvents including methanol, water, THF, chloroform, and DCM. When PHT-b-PEG is heated in DCM and methanol, no spectroscopic changes occur, thus indicating no changes in optical or morphological properties. It is hypothesized that the unique thermochromic behavior of the block copolymer was found in ethyl acetate due to the intermediate polarity of the solvent index of ethyl acetate (4.4) relative to the more polar methanol (5.1) and less polar DCM (3.1). The higher polarity index of methanol means it is a much more selective solvent for the hydrophilic PEG block and thus the aggregated nanofiber micelle assembly is the most stable conformation even upon heating the sample. On the other hand, the less polar DCM is a non-selective solvent for both blocks and thus the non-aggregated single molecule of the block copolymer is the most stable conformation. However, in ethyl acetate upon heating the sample, the solvent becomes less selective towards the PEG block and thus acts more as a non-selective solvent in which the non-aggregated single molecule conformation of the block copolymer is the most stable conformation. UV-vis absorption and PL measurements indicate that PHT-*b*-PEG self-assembles when dispersed in ethyl acetate. However, with increasing temperature, PHT-*b*-PEG aggregates disassembled into isolated polymer chains which resulted in a red to yellow color change and recovery of the PL intensity. Poly(alkylthiophenes) are known to show thermochromic behavior due to the changes in polymer conformation with temperature, which occurs at a fairly high temperature (~150 °C).[51, 52] The temperature-dependent optical properties of PHT shown here are induced by a different origin (i.e., assembly-disassembly) and results in a greater spectral shift at a lower temperature range.

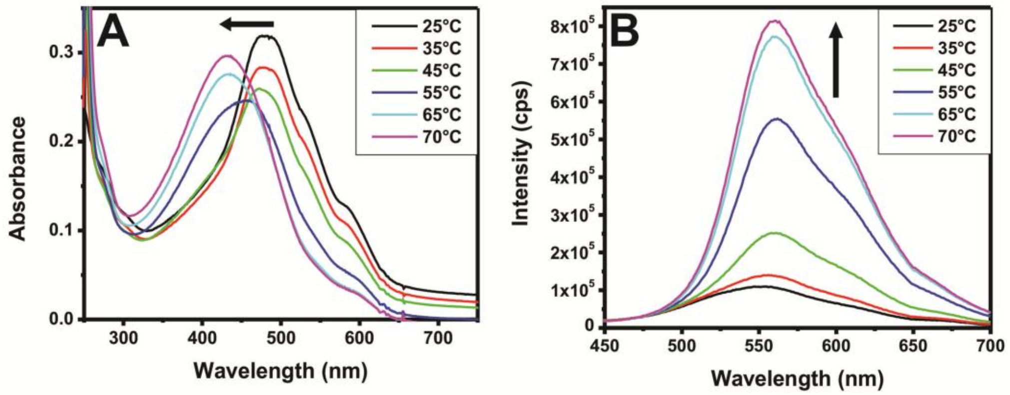

Figure 3.7. (A) Absorbance and (B) PL spectra of PHT_{20}-*b*-PEG_{108} (0.1 mg/mL) in ethyl acetate plotted as a function of increasing temperature. PL spectra were collected using an excitation wavelength of 380 nm.

3.5 Effect of Relative Block Lengths on the Self-Assembly Structure of PHT-*b*-PEG

3.5.1 Assembly Structure. In order to examine the effect of block lengths on the self-assembly of PHT-*b*-PEG, the molecular weight of the PEG block was varied from 761 g/mol to 4896 g/mol while keeping the length of PHT constant, which yielded block copolymers with $f_{\mathrm{PHT}} = 0.41$, 0.61, and 0.82 (Table 1). For all polymers examined in this study, PHT-*b*-PEG self-assembled into the same morphology of nanofibers in selective solvents (Figure 3.8). In general, coil-coil block copolymers self-assemble into various assembly structures such as simple micelles, cylindrical micelles, and vesicles depending on the relative block lengths and the Flory-Huggins parameters of the two polymers.[53] Rod-coil block copolymers have additional factors contributing to the self-assembly structure such as the large dissimilarity of the conformationally distinct two blocks and the π-π interaction between rigid conjugated blocks.[54, 55] The nanofiber morphology has been seen in other rod-coil block copolymer systems,[56, 57] and is typically driven by the packing of the conjugated block.[58] However, previous studies on amphiphilic molecules containing different types of conjugated oligomers (*e.g.*, tetra-p-phenylene, isocyano-(l-alanyl-amino-ethyl)-thiophene) have shown that various types of self-assembly structures such as spherical micelles and vesicles can be formed in addition to one-dimensional rods and wires by varying the relative rod to coil lengths.[59, 60] On the contrary, the study presented herein on PHT-*b*-PEG shows that the nanofiber structure is prevalent for a broad range of f_{PHT} ($f_{\mathrm{PHT}} = 0.41$, 0.61, and 0.82) due to the strong tendency of PHT to form well-packed quasi one-dimensional crystals.

A recent work by Manners and coworkers has shown that cylindrical micelles of PHT-*b*-poly(dimethylsiloxane) with controlled lengths can be formed by crystallization-driven self-assembly.[34] Here, we show that the length of PHT-*b*-PEG self-assembled nanofibers can be controlled by varying the weight fraction of PHT (f_{PHT}) from 0.41 to 0.82. The length of the nanofibers was found to gradually increase with decreasing PEG block lengths (Figure 3.8 A-C). At f_{PHT} of 0.41 and 0.60, the lengths of nanofibers were ~40-100 nm (Figure 3.8A) and ~150 - 400 nm (Figure 3.8 B), respectively. At the largest f_{PHT} of 0.82, longer nanofibers with a length of >1000 nm were commonly observed (Figure 3.8 C). The increase of the aggregation number with the increase of f_{PHT} was also confirmed by dynamic light scattering (DLS) analysis (Figure 3.9 B). The relative hydrodynamic diameters determined by DLS were 78.0 ± 7.0, 126.4 ± 8.6, and 172.2 ± 8.1, for f_{PHT} = 0.40, 0.60, and 0.80 respectively. Although the DLS data does not take into account the anisotropy of the nanofiber micelle structure, it does show increased aggregation numbers with shorter PEG chains, providing corroborative evidence that the TEM images reflect the solution phase assembly structures.

The self-assembled structure of rod-coil amphiphilic species into distinct microdomains is dependent on the π-π stacking of the aromatic rod, the relative volume ratio of the two dissimilar blocks, the interaction parameter between the two blocks, and the molecular architecture or shape of the molecule.[61] In our system, we kept all of the aforementioned parameters constant and focused solely on changing the length of the hydrophilic PEG block. Interestingly, the smallest length of nanofiber micelles was found for the longest hydrophilic chain lengths. We hypothesize that this conformation is more stable because it acts to reduce the stretching energy of long PEG chains through adopting shorter fibers. Similar behavior was found in studies of pyrene-*b*-tetra-*p*-phenylene-b-PEG [62] and oligo-(p-phenylenevinylene)-*b*-PEG [63] where polymers with longer PEG chains were found to form shorter cylinders in solution.

The schemes below the TEM images in Figure 3.8 show the likely packing arrangement of the nanofiber micelles. Analysis of TEM images resulted in measured widths of 8.15 ± 1.09, 8.06 ± 1.06, and 7.80 ± 1.06 for f_{PHT} = 0.41, 0.61, and 0.82, respectively (Figure 3.9 A). This indicates that the nanofiber morphology for each block length is most likely composed of interdigitated polythiophene chains as shown schematically under the TEM images in Figure 3.8. This result indicates that the packing of PHT is the dominating factor for the solution phase morphology for a wide range of f_{PHT}, and that the packing structure of PHT in the fiber, which is closely related to transport properties, does not significantly change with the length of the PEG block and the length of nanofibers. Note that the formation of uniform assemblies of PHT-*b*-PEG in this study is in part a result of the low polydispersity of PHT-*b*-PEG synthesized by click chemistry. When the assemblies were formed from polymer mixtures, resulting nanofibers had a broad range of lengths as expected (Figure 3.10).

Fiber like micelles with nanometer sized cross-sections are currently under investigation for drug delivery applications, as templates for the deposition of metal nanoparticles and as nanoscopic etch resists.[64] Recent publications have also demonstrated that PHT nanofibers exhibit higher organic photovoltaic devices performance than amorphous PHT due to the higher carrier mobility and more efficient charge separation of the confined nanofiber structure.[65] The efficient formation of different length nanofibers via tuning the block length of our amphiphilic block copolymer may offer even more control and enhanced device characteristics.

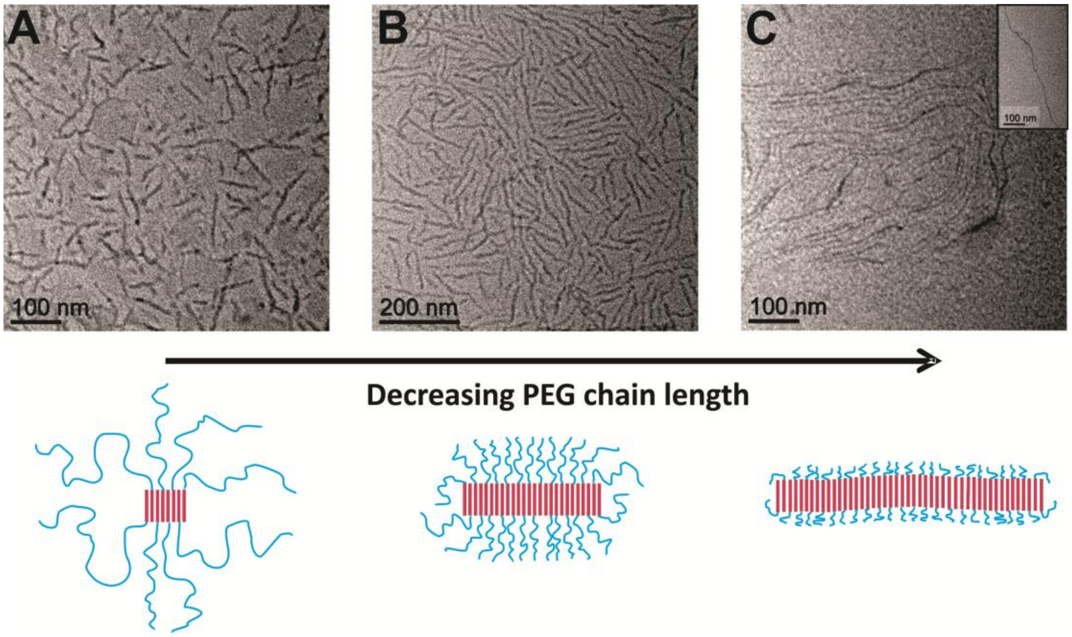

Figure 3.8. TEM images of PHT_{20}-*b*-PEG_n (n = 108, 48, 16) in water with varying f_{PHT}; (A) f_{PHT} = 0.41 (B) f_{PHT} = 0.61, and (C) f_{PHT} = 0.82. Below the respective TEM images is a schematic depiction of the effect of relative block lengths on the self-assembly structure.

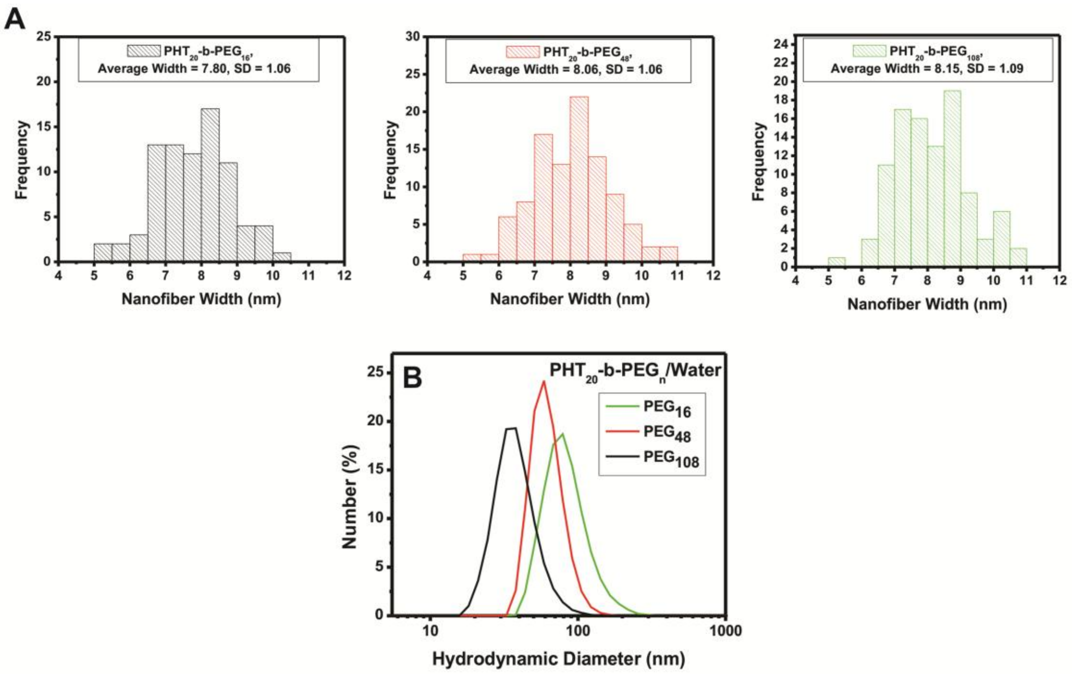

Figure 3.9. (A) Histogram of cylindrical micelle widths measures from TEM images of PHT$_{20}$-*b*-PEG$_{16}$ (black) PHT$_{20}$-*b*-PEG$_{48}$ (red), and PHT$_{20}$-*b*-PEG$_{108}$ (green) in aqueous solutions at concentrations of ~0.1 mg/mL. (B) DLS data showing the hydrodynamic diameter of PHT$_{20}$-*b*-PEG$_{n}$ aggregates in water with varying $f_{\text{PHT};}$ f_{PHT} = 0.41 (green), f_{PHT} = 0.61 (red), and f_{PHT} = 0.82 (black).

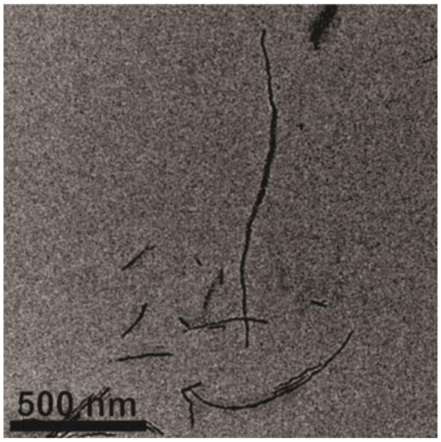

Figure 3.10. TEM image of assemblies formed from a mixture of PHT$_{20}$-*b*-PEG$_{16}$, PHT$_{20}$-*b*-PEG$_{48}$, and PHT$_{20}$-*b*-PEG$_{108}$ in a ratio of 1:1:1. The self-assembly was induced by the slow addition of water to a 0.1 mg/mL polymer solution (THF) and subsequent dialysis into water.

3.5.2 Optical Properties. As was described earlier, the morphology of the block copolymer is very dependent on the block length, with longer nanofibers being formed from PHT-*b*-PEG with shorter PEG lengths. However, the optical properties of the PHT-*b*-PEG block copolymer were not nearly as sensitive to the PEG block length. In "good" solvents such as THF and DCM, all synthesized amphiphilic polymers show UV-vis and PL spectra identical to that of homopolymers with the absorbance maxima at 450 nm and the emission maxima at 576 nm (Figure 3.11 A-B). This again indicates that the attachment of PEG does not affect the conformation of PHT in good solvents. The same behavior was observed for assemblies formed in selective solvents (Figures 3.11 C-F); the polymers dispersed in selective solvents showed essentially the same UV-vis and PL spectra regardless of the PEG chain length. The optical properties of PHT-b-PEG arise solely from the conjugated PHT block. Therefore, although the lengths of the nanofiber micelles are changing with changing f_{PHT}, the conformation and packing of the conjugated PHT block remains the same and therefore there is no significant change in the optical properties. As is shown schematically in Figure 3.8, the interdigitated packing arrangement of the polythiophene block remains the same for the different length nanofiber micelles, thus yielding similar red-shifted absorbance spectra and fluorescence quenching characteristics. These results indicate that the conformation and packing of the conjugated PHT block remains the same in different length nanofibers. Therefore, the lengths of nanofibers can be controlled by changing the relative block length of polymers without changing the packing structure and properties (optical, transport) of the PHT-*b*-PEG block copolymer nanofibers.

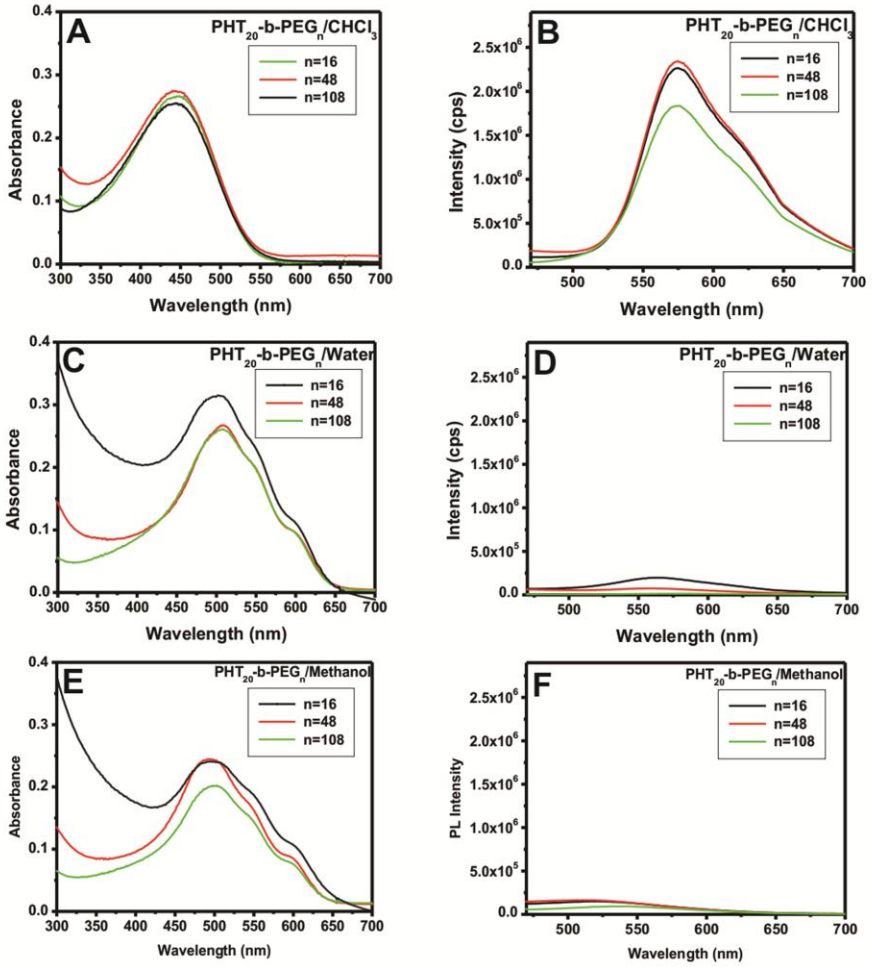

Figure 3.11. Absorption spectra of PHT_{20}-*b*-PEG_n directly dissolved in (A) chloroform, (C) water, (E) methanol at a concentration of 0.1 mg/mL. PL spectra of PHT_{20}-b-PEG_n directly dissolved in (B) chloroform, (D) water, (F) methanol at a concentration of 0.1 mg/mL. Photoluminescence spectra were collected using an excitation wavelength of 380 nm.

3.5.3 Comparison with POT-*b*-PEG. The optical and structural characteristics of the series of PHT-*b*-PEG block copolymer prepared by click chemistry (click-PHT-*b*-PEG) were studies for a wide range of f_{PHT} (0.41 to 0.82). However, these optical and morphological characteristics are very different than those found from a very similar polymer, POT-*b*-PEG prepared by anionic polymerization (anionic-POT-*b*-PEG).[16] Compared to click-PHT-b-PEG, anionic-POT-*b*-PEG is not quenched in selective solvents, but instead emits a bright blue color in methanol and a red color in water. Furthermore, the absorption spectra in methanol and water are blue-shifted and do not show the characteristic vibration spectra found in click-PHT-*b*-PEG (Figure 3.12 C-D)

It was hypothesized that the different optical and morphological structures could be a result of the different packing tendencies of PHT and POT. In order to test this hypothesis, a series of POT-*b*-PEG polymers were prepared by click-chemistry (click-POT-*b*-PEG) and the optical properties were compared with those of anionic-POT-*b*-PEG (Figure 3.12 A-D). It is evident from Figure 3.12 A-B that the optical properties, and therefore the packing structure, of click-POT-*b*-PEG is very similar to those seen in click-PHT-*b*-PEG. This means that the length of the alkyl side chain (ie. POT vs. PHT) does not account for the different morphologies and packing properties of the polymers.

The structures of click-POT-*b*-PEG and anionic-POT-*b*-PEG are almost identical except for the triazole linkage that connects the click product. One possibility is that the triazole linkage causes a critical role in the self-assembly of the click product and drives the dominant tightly interdigitated packing structure that results in the distinctive vibrational spectra and quenched emission spectra found in all the click products.

However, other reports such as the ATRP synthesis of PHT-*b*-PAA that do not have a triazole linker, also report similar red-shifted vibrational spectra and quenched emission in selective solvents.[66] Therefore, this is also an unlikely explanation for the observed differences presented in Figure 3.12.

Another possibility is that the synthetic conditions for anionic polymerization of POT-*b*-PEG[16] are harsher then the click reaction conditions and may have led to oxidizing of the anionic-POT-*b*-PEG and therefore resulted in defects that caused different self-assembled morphologies and different optical characteristics. In its pristine state click-PHT_{20}-*b*-PEG_{108} shows a high fluorescence emission when dissolved in a good solvent such as chloroform, but the fluorescence is highly quenched when dissolved in methanol. However, after oxidation with m-CPBA the fluorescence of the block copolymer decreases when dissolved in chloroform, but increases when dissolved in methanol as shown if Figure 3.13. The significant decrease in the extinction coefficient (100-fold) of the anionic polymerization POT-*b*-PEG product suggests that oxidation is the most likely cause of the unique fluorescence qualities reported for the anionic polymerization product.[16] The naphthalene radical present in solution after the anionic synthesis may have caused oxidation defects that resulted in a decreased extinction coefficient and a twisted morphology of anionic POT-*b*-PEG in solution.[67]

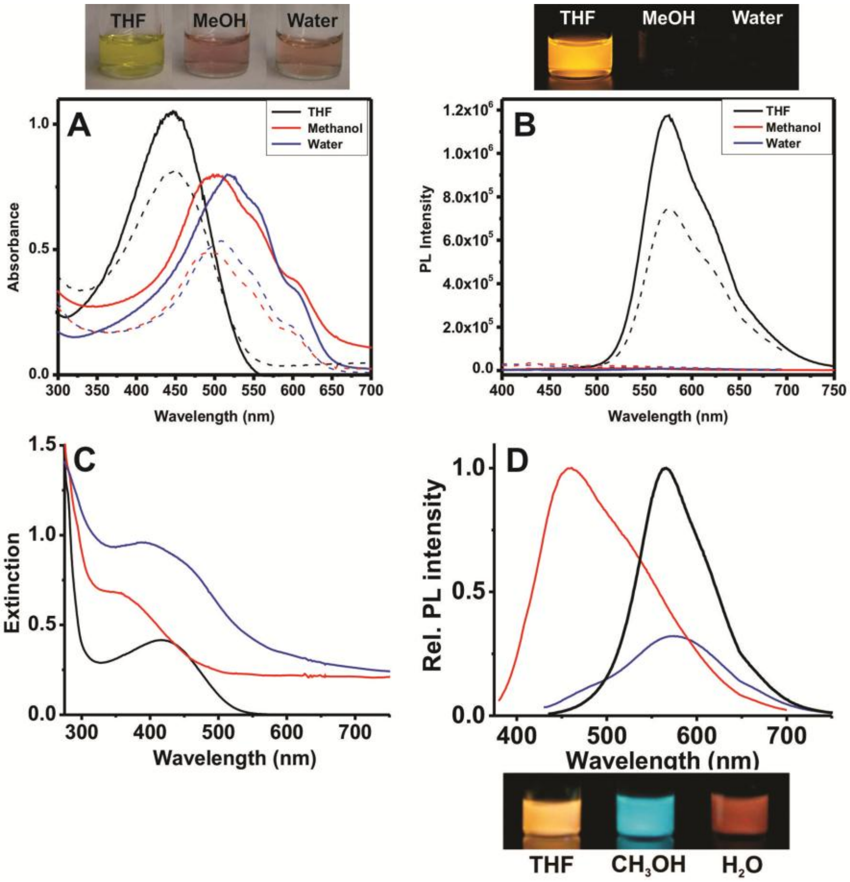

Figure 3.12. (A) Absorbance and (B) PL spectra of click-PHT$_{20}$-*b*-PEG$_{48}$ (dashed lines) and click-POT$_{15}$-*b*-PEG$_{48}$ (solid lines) synthesized by click chemistry and dissolved in different solvents at a concentration of 0.1 mg/mL. PL spectra were collected using an excitation wavelength of 380 nm. Pictures of click-POT$_{15}$-*b*-PEG$_{48}$ (0.1 mg/mL) solutions under ambient light (top-left) and under UV light (top-right) are given above the spectra. (C) Absorbance and (D) PL spectra of anionic-POT$_{15}$-*b*-PEG$_{38}$ (solid lines) synthesized by anionic polymerization at a concentration of 0.35 mg/mL and excited at their respective excitation maxima (THF (black, λ_{exc}= 419 nm), methanol (red, λ_{exc}= 364 nm), and water (blue, λ_{exc}= 396 nm). Pictures of anionic-POT$_{15}$-*b*-PEG$_{38}$ under UV light (bottom right) is shown below the emission spectra.

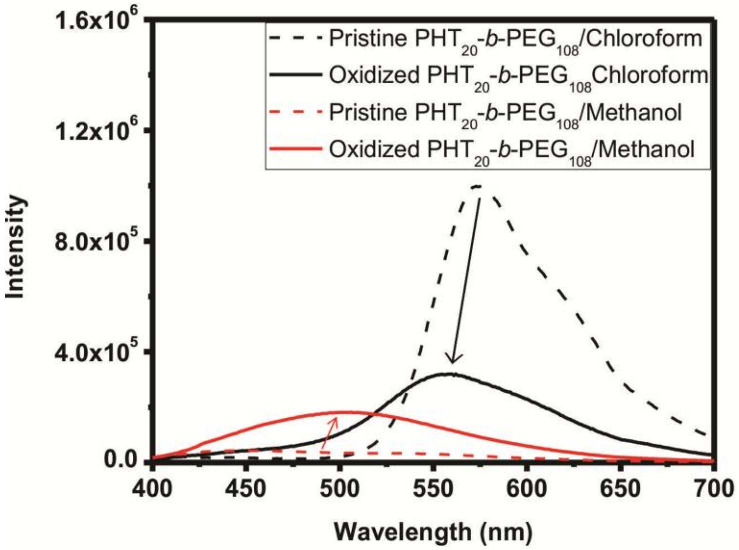

Figure 3.13. PL spectra of PHT$_{20}$-*b*-PEG$_{108}$ in its pristine state (dashed lines) and after 4 hours of oxidation with m-CPBA (solid lines) when dissolved in methanol (red) and chloroform (black). PL spectra were collected using an excitation wavelength of 380 nm.

3.6 Controlled Encapsulation of PHT Homopolymer within an Amphiphilic Block Copolymer Matrix.

Over the years, a rather thorough understanding of PHT homopolymer crystallization in marginal solvents has been reported.[68-70] The quasi-one dimensional crystallization of poly(alkylthiophene) is induced by an attractive π-π interaction between the polymer backbones and by the concurrent crystallization of the alkyl side chains.[50] The crystallization driven self-assembly of PHT has been used to form inorganic semiconducting nanowire-polymer hybrids for photovoltaic applications and has also been used to form hybrid nanowires through the co-crystallization of semiconducting nanorods and PHT.[71] In another recent example, 2D functional conductive supramolecular structures were assembled using a carbon nanotube induced PHT crystallization strategy.[72, 73] In the work presented herein, we utilize the PHT homopolymer crystallization strategy and further demonstrate that an amphiphilic conjugated block copolymer can act as an efficient encapsulation agent for semiconducting homopolymers. Furthermore, unique solvent induced control over the supramolecular self-assembly structure is demonstrated with the formation of encapsulated nanofiber bundles and branched nanofiber structures. It is well-known that the morphology and crystalline structure of poly(thiophenes) have a critical effect on thin film charge transport and are therefore critical to the enhancement of device performances. The crystallization and encapsulation strategy towards controlled supramolecular structures that is presented herein provides a new toolbox towards the formation of novel conjugated structures.

3.6.1 Self-Assembly of PHT Nanofibers into Bundled and Branched Superstructures. The self-assembly of PHT-*b*-PEG was utilized to organize, solubilize, and stabilize preformed nanofibers of PHT homopolymer. It is well known that high molecular weight homopolymers of PHT tend to crystallize into long fibers in marginal solvents.[69, 74, 75] Typically, high aspect ratio nanofibers of PHT were prepared by slowly cooling a hot (70 °C) anisole solution of commercial PHT_{200} (1 mg/mL), following a modified literature procedure[43] (Figure 3.14 A-B). The dimensions of the PHT_{200} nanofibers was similar to those reported in the literature;[76] the PHT_{200} nanofibers had an average width of 15.2 ± 1.7 nm (which corresponds to a folded backbone structure calculated with a monomer length of 0.4 nm)[50] and a very high aspect ratio with a length of 1-10 μm measured by TEM and an average height of 5.0 ± 1.2 nm measured by AFM. The high aspect ratio anisole nanofibers are relatively stable in the marginal anisole solvent, but are not soluble in, or transferrable to, more polar solvents such as methanol and water. Towards this end, the mutual interaction between the PHT_{20}-*b*-PEG_{108} amphiphilic block copolymer and its homopolymer analogue was used to solubilize the high aspect ratio homopolymer structures and to form unique supramolecular structures in more selective polar solvents. The preformed PHT_{200} nanofibers were organized into fiber bundles or branched fibers by the self-assembly with PHT-*b*-PEG. The controlled encapsulation of PHT_{200} homopolymer was achieved by adding dry PHT_{20}-*b*-PEG_{108} to the PHT_{200} high aspect ratio nanofibers in anisole followed by addition of either excess water or excess methanol to the solution. After mixing overnight, the residual anisole was dissipated under a low nitrogen flow.

When methanol was used to drive the self-assembly, PHT nanofibers were encapsulated in PHT_{20}-*b*-PEG_{108} as fiber bundles (Figure 3.14 C-D). The width of the bundles were about 26-80 nm, corresponding to 2-6 fibers, and the length of the bundles was typically 1-10 μm, as determined by TEM. A critical amount of PHT_{20}-*b*-PEG_{108} was necessary to encapsulate the preformed homopolymer structure and form the hierarchical bundled structure. At low PHT_{20}-*b*-PEG_{108} concentrations, PHT_{200} nanofibers precipitated out of solution upon the addition of methanol (Figure 3.14 E). However, as shown in Figure 3.14 E, when a critical molar ratio of block copolymer is present in the anisole homopolymer solution, the solution turns a red color when methanol is added to the system, thus indicating that a stable encapsulated assembly has been formed. Adding an excess amount of PHT_{20}-*b*-PEG_{108} did not notably change the structure of the encapsulated PHT_{200} nanofibers, but instead resulted in isolated PHT_{20}-*b*-PEG_{108} nanofibers (Figure 3.4 C) coexisting with bundled PHT_{200} nanofibers. These isolated nanofibers could be removed via a series of centrifugations, thereby leaving just the bundled PHT_{200} nanofibers in solution.

A distinct type of superstructure of branched fibers was formed when water was used to induce the self-assembly process instead of methanol (Figure 3.15A). The resulting superstructure was composed of PHT_{20}-*b*-PEG_{108} fibers perpendicularly grown off of PHT_{200} nanofibers. This branched structure is reminiscent of the crystallization of PHT homopolymers on PHT nanofibers[77, 78] and carbon nanotubes.[79] The width of the PHT_{20}-*b*-PEG_{108} nanofiber branches was 7.9 ± 1.2 nm which is similar to the dimension of isolated PHT_{20}-*b*-PEG_{108} nanofibers shown in Figure 3.4 C. The origin of the lateral growth of PHT_{20}-*b*-PEG_{108} nanofibers is believed to be associated with the immiscibility of water and anisole. Upon the addition of water, PHT_{20}-*b*-PEG_{108} nanofibers are likely to be formed in water while PHT_{200} nanofibers remain in anisole. When the anisole is dissipated under nitrogen flow, the highest energy tip of the preformed PHT_{20}-*b*-PEG_{108} fibers stack onto PHT_{200} nanofibers, thereby forming the distinctive supramolecular structure and bringing PHT_{200} nanofibers into water. As in the methanol case, a critical amount of PHT_{20}-*b*-PEG_{108} was needed to disperse the PHT_{200} nanofibers in water.

Further control over the dimensions of the branched assembly structure was obtained by varying the composition and concentration of the block copolymer. Increasing the concentration of PHT_{20}-*b*-PEG_{108} relative to the PHT_{200} nanofibers resulted in a higher density of lateral PHT_{20}-*b*-PEG_{108} as shown in Figure 3.15 B. When PHT_{20}-*b*-PEG_{48} is used to encapsulate PHT_{200} nanofibers in water, a similar branched structure is obtained, but longer branches are formed. Overall, the shape, length and density of the hierarchical assembly structures were efficiently controlled by varying the solvent quality, polymer lengths, and block-copolymer/homopolymer ratio. The pre-formed homopolymer structure is only transiently stable in anisole solution and starts degrading after about a week. In direct contrast, the encapsulated structures are very stable and retain the bundled or branched structures for at least four months which offers a significant advantage for use in device applications.

Interestingly, it was found that the preformed high aspect ratio PHT_{200} nanofibers are necessary to obtain distinct encapsulated supramolecular structures. When self-assembly of PHT_{200} and block copolymers is induced by slow addition of water to a non-selective solvent such as THF, a non-specific block copolymer encapsulation occurs (Figure 3.16 A). In contrast, when a shorter PHT_{20} block is encapsulated in PHT-*b*-PEG block copolymers utilizing the same methodology, a different ribbon-like encapsulated structure is formed in solution (Figure 3.16 B). This data demonstrates that the preformed PHT_{200} nanofibers are necessary to obtain distinct encapsulated superstructures.

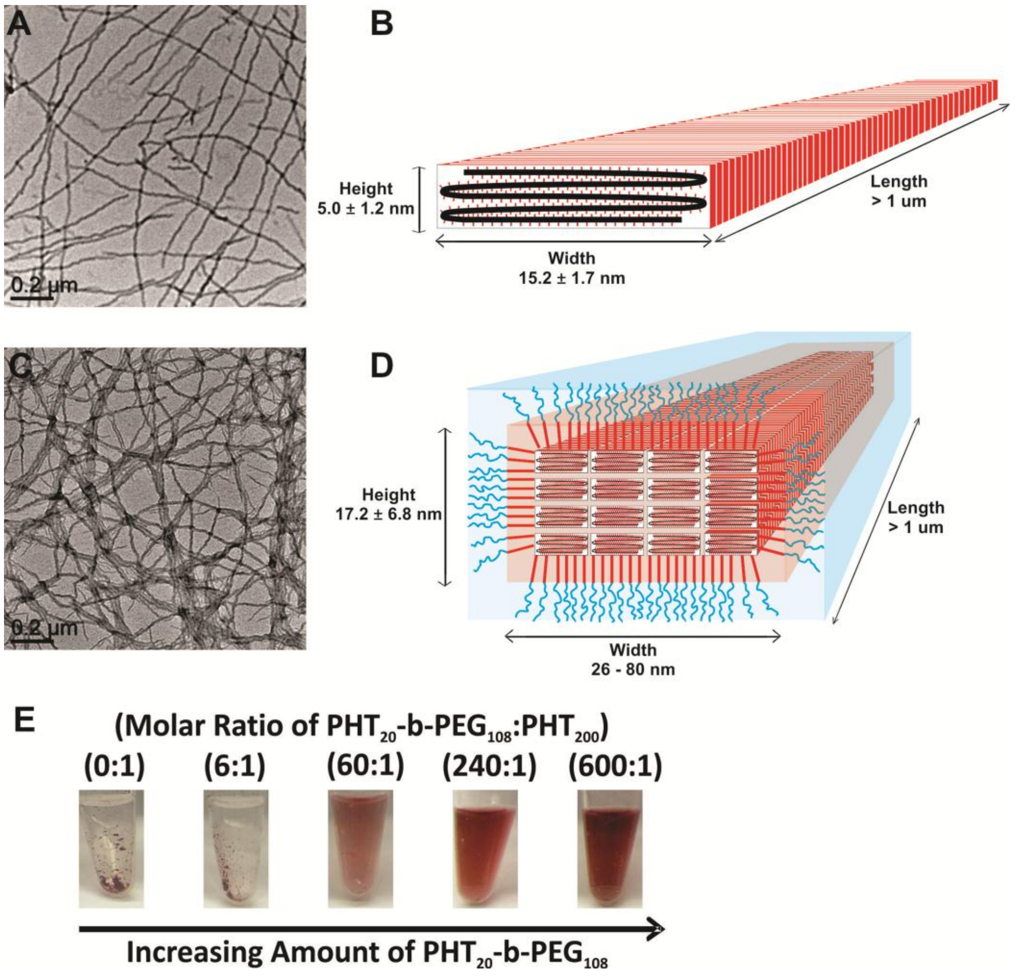

Figure 3.14. (A) TEM image of PHT$_{200}$ nanofibers in anisole. (B) Pictorial depiction of PHT$_{200}$ nanofibers. (C) TEM image of PHT$_{200}$ nanofiber bundles encapsulated in PHT$_{20}$-*b*-PEG$_{108}$ in methanol. (D) Pictorial description of superstructure (fiber bundles) formed in methanol. (E) Pictures of PHT$_{200}$ nanofibers in 99% methanol:1% anisole with increasing amounts of PHT$_{20}$-*b*-PEG$_{108}$.

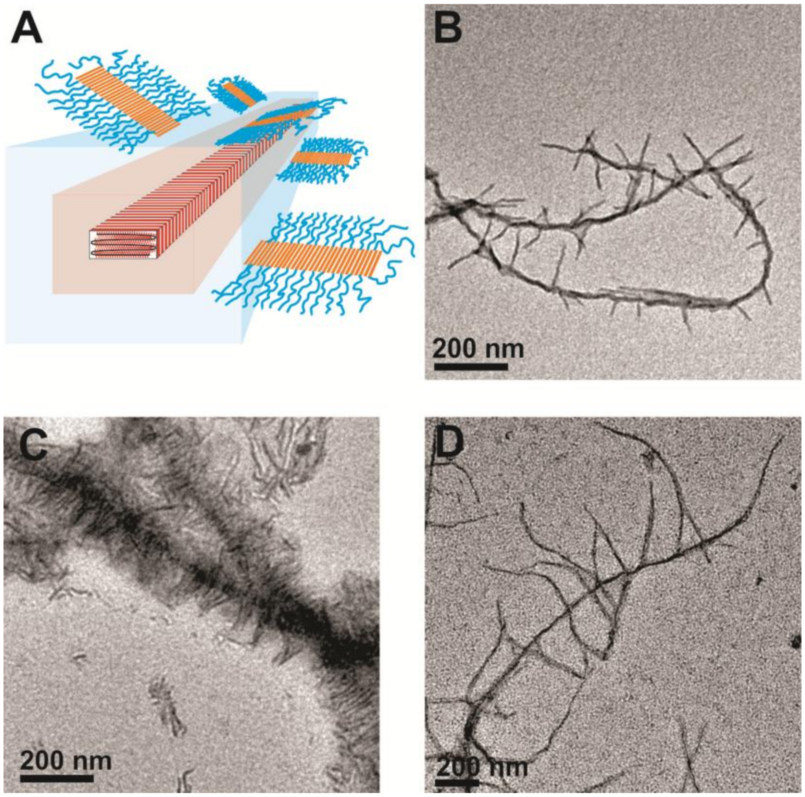

Figure 3.15. (A) Pictorial depiction of the branched superstructure composed of PHT_{200} nanofibers and PHT_{20}-*b*-PEG_{108}. TEM images of (B) a branched structure composed of PHT_{200} nanofibers decorated with low density PHT_{20}-*b*-PEG_{108} nanofibers formed at a molar ratio of 60:1 (PHT_{20}-*b*-$PEG_{108:}PHT_{200}$), (C) a high density branched structure composed of PHT_{200} nanofibers decorated with PHT_{20}-*b*-PEG_{108} nanofibers at a molar ratio of 480:1 (PHT_{20}-*b*-$PEG_{108:}PHT_{200}$), and (D) a branched structure composed of PHT_{200} nanofibers decorated with longer PHT_{20}-*b*-PEG_{48} nanofibers formed at a molar ratio of 250:1 (PHT_{20}-*b*-$PEG_{48:}PHT_{200}$).

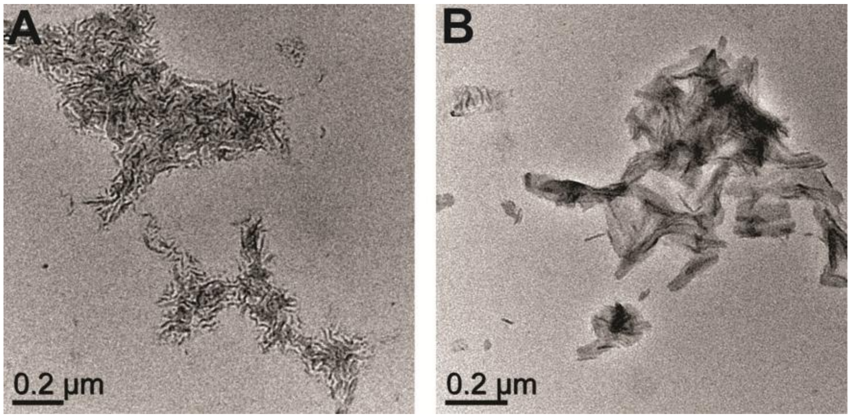

Figure 3.16. TEM images of polymer aggregates formed by the self-assembly of (A) PHT_{200} homopolymers and PHT_{20}-*b*-PEG_{108} block copolymers and (B) PHT_{20} homopolymers and PHT_{20}-*b*-PEG_{108} block copolymers. The molar ratio between PHT_{20}-*b*-PEG_{108} and PHT_{200} was 46:1 with a PHT_{200} concentration of 0.1 mg/mL. The molar ratio between PHT_{20}-*b*-PEG_{108} and PHT_{20} was 10:1 with a PHT_{20}-*b*-PEG_{108} concentration of 0.1 mg/mL.

3.6.2 Optical Properties of Encapsulated Structures. A variety of different nanostructures were formed from the hierarchical self-assembly of PHT homopolymers and PHT-*b*-PEG block copolymers. Interestingly, the dominant packing structures of all these very different self-assembled structures are very similar as is evident by the optical absorption characteristics in Figure 3.17. The line shapes of the respective self-assembled morphologies and the relative ratios of the 0-2 transition (510 nm), 0-1 transition (540 nm) and 0-0 transition (610 nm) are very similar for all the self-assembled structures and are all characteristic of H-aggregate behavior with weak interchain coupling.

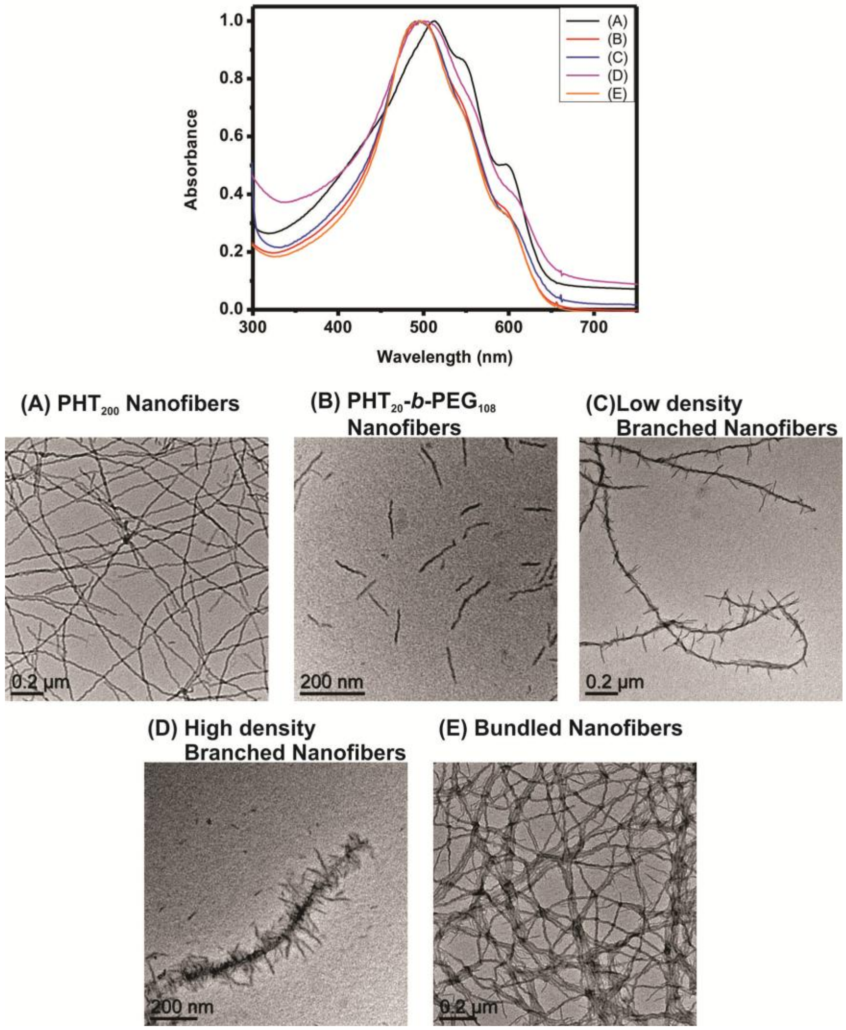

Figure 3.17. Absorption spectra of PHT_{20}-*b*-PEG_{108}, PHT_{200}, and their superstructures along with the corresponding TEM images. (A) PHT_{200} nanofibers in anisole (10 mg/mL). (B) PHT_{20}-*b*-PEG_{108} in methanol (0.1 mg/mL). (C) Low density branched nanofibers composed of PHT_{200} nanofibers decorated with PHT_{20}-*b*-PEG_{108} nanofibers at a molar ratio of 60:1 (PHT_{20}-*b*-PEG_{108}:PHT_{200}) in water. (D) High density branched nanofibers composed of PHT_{200} nanofibers decorated with PHT_{20}-*b*-PEG_{108} nanofibers at a molar ratio of 360:1 (PHT_{20}-*b*-PEG_{108}:PHT_{200}) in water. (E) PHT_{200} nanofiber bundles encapsulated in PHT_{20}-*b*-PEG_{108} in methanol.

3.7 Encapsulation of J-Aggregate Nanofibers with a Conjugated Block Copolymer

3.7.1 Properties of J-Aggregates. It is well known that the intrachain and interchain order and defect density have a large effect on the optical and transport properties of PHT films. The absorbance spectrum of PHT thin films has been used as a measure to probe exciton coupling, intrachain order and the fraction of crystalline regions within thin films.[80] The interplay between processing, order, and device performance are dependent on the interchain and intrachain effects in PHT thin films and can be correlated to the absorption and emission spectra of PHT thin films.[81, 82]

The emission from PHT thin films arises from weakly coupled H-aggregates with face-to-face oriented chains that exhibit weak exciton coupling, but have no significant contributions from intrachain excitons. A recent theoretical model based on weakly interacting H-aggregate states was proposed and was further found to comprehensively describe the photophysics of PHT thin films. [83] Within this model, the magnitude of the interchain coupling is estimated via the ratio (A_{0-0}/ A_{0-1}) of the lowest energy peak (A_{0-0}) and the next vibrational peak (A_{0-1}) absorbance peaks. An increase in the A_{0-0}/ A_{0-1} ratio represents an increase in conjugation length and intrachain order, and a decrease in excitonic coupling.

The self-assembled structures of PHT-*b*-PEG, the crystallized PHT_{200} homopolymer nanofibers and the block copolymer encapsulated structures that are described in more detail in section 3.6.2 all have similar absorption spectra line shapes and the relative ratios of the 0-2 transition (510 nm), 0-1 transition (540 nm) and 0-0 transition (610 nm) are very similar to each other and to that of typical PHT thin films[82, 84-86]. The emission of these structures are all quenched and the photophysical properties are characteristic of typical H-aggregate behavior with predominant interchain interactions. The electronic 0-0 transition in these structures is attenuated because of its forbidden nature [87] and the overall interchain interactions dominate because of the presence of amorphous chains that reduce the overall intrachain order and planarity of the aggregate.[83]

Recently, Dr. John Grey's group reported the formation of PHT nanofibers that exhibit single-chain J-aggregate character. The absorption, emission, and raman spectroscopy of these crystallized homopolymer nanofibers suggested that these J-aggregates nanofibers possess long-range intrachain ordering that suppresses the interchain exciton coupling found in other systems of PHT.[88] Furthermore, Niles *et al.* performed pressure dependent photoluminescent studies that showed a distinct shift from J to H aggregates over the pressure range studied.[88] This pressure dependent effect was attributed to minor deformations of PHT chain planarity which led to an increased interchain exciton coupling. It was also hypothesized that dangling segments of the PHT nanofiber structure acted as levers that transmitted small perturbations to chain segments within the PHT nanofiber. The encapsulation of J-aggregates in PHT-*b*-PEG block copolymer offers another approach to develop a better understanding of how intrachain order and interchain exciton coupling will be affected by mechanical perturbations of the nanofiber structure. Encapsulation induces formation of hierarchal superstructures and represents a mild chemical pressure on the periphery of the NF structure, which can be used to further study the delicate interplay between intra-chain order and inter-chain exciton coupling that exists in these structures. The encapsulation approach presented herein also offers a potential means to disperse these exciting new nanomaterials into non-organic media making them attractive for biological applications.

3.7.2 Block Copolymer Encapsulation of J-Aggregates. The self-assembly of PHT-*b*-PEG was utilized to organize, solubilize, and stabilize preformed J-aggregate nanofibers of PHT_{350} homopolymer. The J-aggregate nanofibers were prepared by slowly cooling a hot (80 °C) toluene solution of commercial PHT_{350} (2 mg/mL), following a modified literature procedure.[43] In comparison, the H-aggregate nanofibers were prepared by the slow cooling of a hot anisole solution of commercial PHT_{200} as described in more detail in Section 3.6.1. The J-aggregates are formed because of the fractionation of polymer chains, solvent interactions that cause chain conformational differences, and because of the kinetics of the crystallization process.[89] In other words, the fractionation of the higher molecular weight PHT_{350} in a good solvent (toluene) results in J-aggregate nanofibers that have less defect sites and a more linear and planar conformation. A representative TEM image of the J-aggregate nanofibers is shown in Figure 3.18 A. When compared to the TEM image of a typical H-aggregate structure (15.2 ± 1.8 nm) shown in Figure 3.18 B, it is clear that the J-aggregates are less electron dense and have a larger nanofiber width (38.2 ± 4.9 nm). Interestingly the J-aggregates character of the J-aggregate nanofibers can be altered to more closely resemble that of H-aggregate nanofibers by simply sonicating the J-aggregates. After sonication, the J-aggregates break apart and become shorter in length as shown in Figure 3.19 B, but also become more electron dense and have a more compact width of 21.2 ± 2.6 nm compared with pristine J-aggregates which have a width of (38.2 ± 4.9 nm). The decrease in the 0-0 peak shown in Figure 3.19 after sonication indicates that the sonicated J-aggregates became more H-like after sonication. These results support the previously proposition that the increase in the intrachain order for J-aggregates arises from their elongation.

The J-aggregate nanofibers are highly unstable and tend to gel and precipitate out of solution after a few days. Towards this end, the mutual interaction between the PHT_{20}-*b*-PEG_{108} amphiphilic block copolymer and the J-aggregate nanofibers was used to solubilize and stabilize the J-aggregate nanofibers and to form unique supramolecular structures in more selective polar solvents. J-aggregate nanofiber bundles or branched nanofibers were formed when methanol or water, respectively, were used to drive the self-assembly. The TEM images of J-aggregate bundled and branched encapsulated structures are shown in Figure 3.18 C-D. The corresponding absorption spectra of the bundled and branched encapsulated J-aggregate samples presented in Figure 3.18 reveals a large decrease in the relative intensity of the 0-0/0-1 bands which indicates an increase in the H-aggregates character and a decrease in the intrachain ordering of the encapsulated samples. The increase in H-aggregates character of the encapsulated J-aggregates could be due to encapsulation induced deformations of the PHT planarity. However, it is difficult to quantify the excitonic coupling based solely on the absorption characteristics because the block copolymer spectra also overlaps with the PHT nanofiber spectra.

Although, the TEM images, sonication studies, and optical absorptions do give a basic understanding of basic arrangements, structure, and packing characteristics of encapsulated J-aggregates, further resolution of vibronic transitions and the nature of electronic coupling in the encapsulated J-aggregate samples was achieved using PL and raman spectroscopy. The combined PL and Raman studies can be used to separately evaluate vibronic and excitonic coupling contributions to optical lineshapes. This work was done in collaboration with J.K. Grey and further details on this aspect of the work will be presented elsewhere.

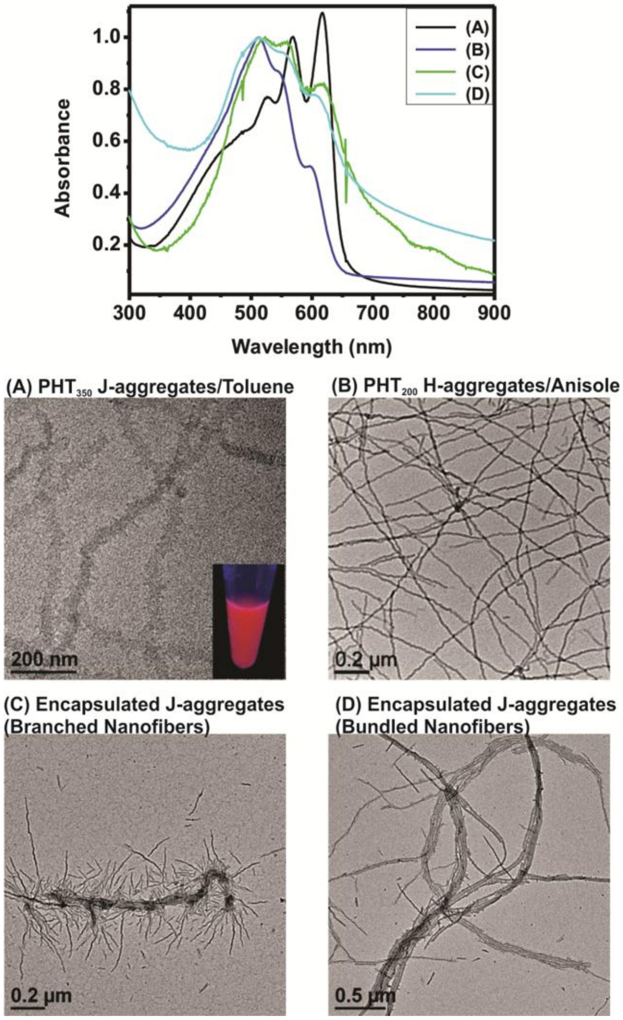

Figure 3.18. Absorption spectra of PHT_{350} J-aggregates, PHT_{200} H-aggregates and their encapsulated superstructures along with the corresponding TEM images. (A) PHT_{350} nanofibers in toluene (2 mg/mL). (B) PHT_{200} nanofibers in anisole (10 mg/mL). (C) Branched nanofibers composed of PHT_{350} J-aggregate nanofibers decorated with PHT_{20}-*b*-PEG_{108} nanofibers at a molar ratio of 120:1 (PHT_{20}-*b*-PEG_{108}:PHT_{350}) in water. (D) PHT_{350} J-aggregate nanofiber bundles encapsulated in PHT_{20}-*b*-PEG_{108} at a molar ratio of 120:1 (PHT_{20}-*b*-PEG_{108}:PHT_{350}) in methanol.

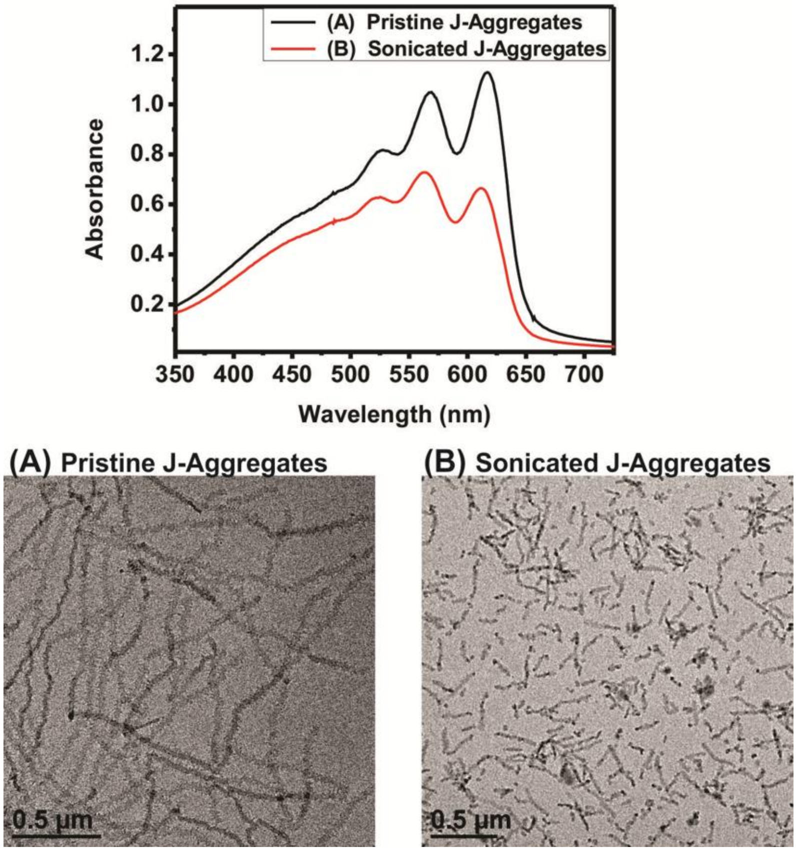

Figure 3.19. Absorption spectra of PHT_{350} J-aggregates before and after sonication along with the corresponding TEM images. (A) Pristine PHT_{350} J-aggregates. (B) PHT_{350} J-aggregates after 2 minutes of sonication.

3.8 Conclusions

A series of different length PHT_m-*b*-PEG_n (m = 20, n = 16, 48, 108) was synthesized in high yields (> 70%) by copper-catalyzed click chemistry. The molecular weight and relative block lengths of the synthesized polymers were determined by thoroughly characterizing each block prior to coupling, which allowed for a systematic study of the block length effect on the self-assembly structure. In selective solvents such as water and methanol, PHT_m-*b*-PEG_n self-assembled into interdigitated one-dimensional assemblies (nanofibers). The self-assembly of PHT_m-*b*-PEG_n accompanied an efficient PL quenching and red-shift of absorption spectra, indicating a tight packing of PHT in the assembly structure. The length of nanofibers was increased with decreasing PEG lengths due to the reduced stretching energy, and a large f_{PHT} of 0.82 led to the formation of micrometer-long nanofibers. The wire-like morphology was maintained for a wide range of relative polymer lengths with weight factions of PHT (f_{PHT}) varying from 0.41 to 0.82, indicating that the packing of PHT is the main factor that controls the self-assembly structure. In addition, the width and optical properties of PHT_m-*b*-PEG_n nanofibers did not change significantly with the relative PEG block length, which shows that the lengths of nanofibers can be controlled without changing the packing structure and properties (optical, transport) of PHT in the nanofibers. The PHT_m-*b*-PEG_n nanofibers were further used as building blocks to form hierarchical assemblies of nanofibers. The self-assembly of PHT_m-*b*-PEG_n and preformed nanofibers of high molecular weight PHT (PHT_{200}) in methanol led to the formation of bundled nanofibers encapsulated in PHT_m-*b*-PEG_n. In addition, unique superstructures of branched nanofibers were formed when water was used for the self-assembly instead of methanol. The density and the length of nanofiber branches in the superstructure could be controlled by varying the concentration and the length of PEG, respectively. The controlled self-assembly and encapsulation strategy presented here provides a new toolbox towards the fabrication of novel organic semiconducting nanostructures.

3.9 References

1. Schenning, A.; Meijer, E. W., Supramolecular Electronics; Nanowires from Self-Assembled Pi-Conjugated Systems. *Chem. Commun.* 2005, 3245-3258.
2. Moliton, A.; Hiorns, R. C., Review of Electronic and Optical Properties of Semiconducting Pi-Conjugated Polymers: Applications in Optoelectronics. *Polym. Int.* 2004, 53, 1397-1412.
3. Pal, T.; Arif, M.; Khondaker, S. I., High Performance Organic Phototransistor Based on Regioregular Poly(3-Hexylthiophene). *Nanotechnology* 2010, 21, 1-5.
4. Wu, Z.; Petzold, A.; Henze, T.; Thurn-Albrecht, T.; Lohwasser, R. H.; Sommer, M.; Thelakkat, M., Temperature and Molecular Weight Dependent Hierarchical Equilibrium Structures in Semiconducting Poly(3-Hexylthiophene). *Macromolecules* 2010, 43, 4646-4653.
5. Schwartz, B. J., Conjugated Polymers as Molecular Materials : How Chain Conformation and Film Morphology Influence Energy Transfer and Interchain Interactions. *Annu. Rev. Phys. Chem.* 2003, 54, 141-172.
6. Yang, H.; Shin, T. J.; Bao, Z.; Ryu, C. Y., Structural Transitions of Nanocrystalline Domains in Regioregular Poly(3-Hexyl Thiophene) Thin Films. *J. Polym. Sci., Part B: Polym. Phys.* 2007, 45, 1303-1312.
7. Lee, S. S.; Kim, C. S.; Gomez, E. D.; Purushothaman, B.; Toney, M. F.; Wang, C.; Hexemer, A.; Anthony, J. E.; Loo, Y.-L., Controlling Nucleation and Crystallization

in Solution-Processed Organic Semiconductors for Thin-Film Transistors. *Adv. Mater.* 2009, 21, 3605-3609.

8. Gao, Y.; Martin, T. P.; Niles, E. T.; Wise, A. J.; Thomas, A. K.; Grey, J. K., Understanding Morphology-Dependent Polymer Aggregation Properties and Photocurrent Generation in Polythiophene/Fullerene Solar Cells of Variable Compositions. *J. Phys. Chem. C* 2010, 114, 15121-15128.

9. Olsen, B. D.; Li, X.; Wang, J.; Segalman, R. A., Thin Film Structure of Symmetric Rod-Coil Block Copolymers. *Macromolecules* 2007, 40, 3287-3295.

10. Hamley, I. W., Ordering in Thin Films of Block Copolymers: Fundamentals to Potential Applications. *Prog. Polym. Sci.* 2009, 34, 1161-1210.

11. Hlaing, H.; Lu, X.; Hofmann, T.; Yager, K. G.; Black, C. T.; Ocko, B. M., Nanoimprint-Induced Molecular Orientation in Semiconducting Polymer Nanostructures. *ACS Nano* 2011, 5, 7532-7538.

12. Ho, V.; Boudouris, B. W.; McCulloch, B. L.; Shuttle, C. G.; Burkhardt, M.; Chabinyc, M. L.; Segalman, R. A., Poly(3-Alkylthiophene) Diblock Copolymers with Ordered Microstructures and Continuous Semiconducting Pathways. *J. Am. Chem. Soc.* 2011, 133, 9270-9273.

13. Dai, C.-A.; Yen, W.-C.; Lee, Y.-H.; Ho, C.-C.; Su, W.-F., Facile Synthesis of Well-Defined Block Copolymers Containing Regioregular Poly(3-Hexyl Thiophene) Via Anionic Macroinitiation Method and Their Self-Assembly Behavior. *J. Am. Chem. Soc.* 2007, 129, 11036-11038.

14. Iovu, M. C.; Jeffries-El, M.; Zhang, R.; Kowalewski, T.; McCullough, R. D., Conducting Block Copolymer Nanowires Containing Regioregular Poly(3-Hexylthiophene) and Polystyrene. *J. Macromol. Sci., Pure Appl. Chem.* 2006, 43, 1991-2000.

15. Tu, G. L.; Li, H. B.; Forster, M.; Heiderhoff, R.; Balk, L. J.; Sigel, R.; Scherf, U., Amphiphilic Conjugated Block Copolymers: Synthesis and Solvent-Selective Photoluminescence Quenching. *Small* 2007, 3, 1001-1006.

16. Park, S. J.; Kang, S. G.; Fryd, M.; Saven, J. G.; Park, S. J., Highly Tunable Photoluminescent Properties of Amphiphilic Conjugated Block Copolymers. *J. Am. Chem. Soc.* 2010, 132, 9931-9933.

17. Lee, E.; Hammer, B.; Kim, J.-K.; Page, Z.; Emrick, T.; Hayward, R. C., Hierarchical Helical Assembly of Conjugated Poly(3-Hexylthiophene)-Block-Poly(3-Triethylene Glycol Thiophene) Diblock Copolymers. *J. Am. Chem. Soc.* 2011, 133, 10390-10393.

18. Gaedt, T.; Ieong, N. S.; Cambridge, G.; Winnik, M. A.; Manners, I., Complex and Hierarchical Micelle Architectures from Diblock Copolymers Using Living, Crystallization-Driven Polymerizations. *Nature Mater.* 2009, 8, 144-150.

19. Iovu, M. C.; Craley, C. R.; Jeffries-El, M.; Krankowski, A. B.; Zhang, R.; Kowalewski, T.; McCullough, R. D., Conducting Regioregular Polythiophene Block Copolymer Nanofibrils Synthesized by Reversible Addition Fragmentation Chain Transfer Polymerization (Raft) and Nitroxide Mediated Polymerization (Nmp). *Macromolecules* 2007, 40, 4733-4735.

20. Iovu, M. C.; Zhang, R.; Cooper, J. R.; Smilgies, D. M.; Javier, A. E.; Sheina, E. E.; Kowalewski, T.; McCullough, R. D., Conducting Block Copolymers of Regioregular Poly(3-Hexylthiophene) and Poly(Methacrylates): Electronic Materials with Variable Conductivities and Degrees of Interfibrillar Order. *Macromolecular Rapid Communications* 2007, 28, 1816-1824.

21. Liu, J.; Sheina, E.; Kowalewski, T.; McCullough, R. D., Tuning the Electrical Conductivity and Self-Assembly of Regioregular Polythiophene by Block Copolymerization: Nanowire Morphologies in New Di- and Triblock Copolymers. *Angew. Chem. Int. Ed.* 2002, 41, 329-332.

22. Park, S.-J.; Kang, S.-G.; Fryd, M.; Saven, J. G.; Park, S.-J., Highly Tunable Photoluminescent Properties of Amphiphilic Conjugated Block Copolymers. *J. Am. Chem. Soc.* 2010, 132, 9931-9933.

23. Alemseghed, M. G.; Servello, J.; Hundt, N.; Sista, P.; Biewer, M. C.; Stefan, M. C., Amphiphilic Block Copolymers Containing Regioregular Poly(3-Hexylthiophene)

and Poly(2-Ethyl-2-Oxazoline). *Macromolecular Chemistry and Physics* 2010, 211, 1291-1297.

24. Holdcroft, S., Determination of Molecular-Weights and Mark-Houwink Constants for Soluble Electronically Conducting Polymers. *J. Polym. Sci., Part B: Polym. Phys.* 1991, 29, 1585-1588.

25. Binder, W. H.; Kluger, C., Azide/Alkyne-"Click" Reactions: Applications in Material Science and Organic Synthesis. *Current Organic Chemistry* 2006, 10, 1791-1815.

26. Fu, R.; Fu, G. D., Polymeric Nanomaterials from Combined Click Chemistry and Controlled Radical Polymerization. *Polymer Chemistry* 2011, 2, 465-475.

27. Sumerlin, B. S.; Vogt, A. P., Macromolecular Engineering through Click Chemistry and Other Efficient Transformations. *Macromolecules* 2010, 43, 1-13.

28. Golas, P. L.; Matyjaszewski, K., Marrying Click Chemistry with Polymerization: Expanding the Scope of Polymeric Materials. *Chemical Society Reviews* 2010, 39, 1338-1354.

29. El-Sagheer, A. H.; Brown, T., Click Chemistry with DNA. *Chemical Society Reviews* 2010, 39, 1388-1405.

30. Urien, M.; Erothu, H.; Cloutet, E.; Hiorns, R. C.; Vignau, L.; Cramail, H., Poly(3-Hexylthiophene) Based Block Copolymers Prepared by "Click" Chemistry. *Macromolecules* 2008, 41, 7033-7040.

31. Li, Z. C.; Ono, R. J.; Wu, Z. Q.; Bielawski, C. W., Synthesis and Self-Assembly of Poly(3-Hexylthiophene)-Block-Poly(Acrylic Acid). *Chemical Communications* 2011, 47, 197-199.

32. Bolognesi, A.; Galeotti, F.; Mroz, W.; Gancheva, V.; Terlemezyan, L., Towards Semiconducting Graft Copolymers: Switching from Atrp to "Click" Approach. *Macromolecular Chemistry and Physics* 2010, 211, 1488-1495.

33. Bock, V. D.; Hiemstra, H.; van Maarseveen, J. H., Cu-I-Catalyzed Alkyne-Azide "Click" Cycloadditions from a Mechanistic and Synthetic Perspective. *Eur. J. Org. Chem.* 2005, 51-68.

34. Patra, S. K.; Ahmed, R.; Whittell, G. R.; Lunn, D. J.; Dunphy, E. L.; Winnik, M. a.; Manners, I., Cylindrical Micelles of Controlled Length with a Π-Conjugated Polythiophene Core Via Crystallization-Driven Self-Assembly. *J. Am. Chem. Soc.* 2011, 133, 8842-5.

35. Jeffries-El, M.; Sauve, G.; McCullough, R. D., Facile Synthesis of End-Functionalized Regioregular Poly(3-Alkylthiophene)S Via Modified Grignard Metathesis Reaction. *Macromolecules* 2005, 38, 10346-10352.

36. Iovu, M. C.; Jeffries-El, M.; Sheina, E. E.; Cooper, J. R.; McCullough, R. D., Regioregular Poly(3-Alkylthiophene) Conducting Block Copolymers. *Polymer* 2005, 46, 8582-8586.

37. Szwarc, M.; Levy, M.; Milkovich, R., Polymerization Initiated by Electron Transfer to Monomer - a New Method of Formation of Block Polymers. *J. Am. Chem. Soc.* 1956, 78, 2656-2657.

38. Hiki, S.; Kataoka, K., A Facile Synthesis of Azido-Terminated Heterobifunctional Poly(Ethylene Glycol)S for "Click" Conjugation. *Bioconjugate Chem.* 2007, 18, 2191-2196.

39. Wu, Z.-Q.; Ono, R. J.; Chen, Z.; Bielawski, C. W., Synthesis of Poly(3-Alkylthiophene)-Block-Poly(Arylisocyanide): Two Sequential, Mechanistically Distinct Polymerizations Using a Single Catalyst. *Journal of the American Chemical Society* 2010, 132, 14000-1.

40. Braunecker, W.; Matyjaszewski, K., Controlled/Living Radical Polymerization: Features, Developments, and Perspectives. *Progress in Polymer Science* 2007, 32, 93-146.

41. McCullough, R. D., The Chemistry of Conducting Polythiophenes. *Adv. Mater.* 1998, 10, 93-116.

42. Yamamoto, T.; Komarudin, D.; Arai, M.; Lee, B.-l.; Suganuma, H.; Asakawa, N.; Inoue, Y.; Kubota, K.; Sasaki, S., Extensive Studies on Π-Stacking of Poly (3-Alkylthiophene-2 , 5-Diyl) S and Poly (4-Alkylthiazole-2 , 5-Diyl) S by Optical

Spectroscopy , Nmr Analysis , Light Scattering Analysis , and X-Ray Crystallography. *Chart* 1998, 7863, 2047-2058.

43. Samitsu, S.; Shimomura, T.; Heike, S.; Hashizume, T.; Ito, K., Effective Production of Poly(3-Alkylthiophene) Nanofibers by Means of Whisker Method Using Anisole Solvent: Structural, Optical, and Electrical Properties. *Macromolecules* 2008, 41, 8000-8010.

44. Ihn, K. J.; Moulton, J.; Smith, P., Whiskers of Poly(3-Alkylthiophene)S. *J. Polym. Sci., Part B: Polym. Phys.* 1993, 31, 735-742.

45. Sun, S.; Salim, T.; Wong, L. H.; Foo, Y. L.; Boey, F.; Lam, Y. M., A New Insight into Controlling Poly(3-Hexylthiophene) Nanofiber Growth through a Mixed-Solvent Approach for Organic Photovoltaics Applications. *J. Mater. Chem.* 2011, 21, 377-386.

46. Brinkmann, M.; Rannou, P., Molecular Weight Dependence of Chain Packing and Semicrystalline Structure in Oriented Films of Regioregular Poly(3-Hexylthiophene) Revealed by High-Resolution Transmission Electron Microscopy. *Macromolecules* 2009, 42, 1125-1130.

47. Choi, S. Y.; Lee, J. U.; Lee, J. W.; Lee, S.; Song, Y. J.; Jo, W. H.; Kim, S. H., Highly Ordered Poly(3-Hexylthiophene) Rod Polymers Via Block Copolymer Self-Assembly. *Macromolecules* 2011, 44, 1771-1774.

48. Tao, Y.; McCulloch, B.; Kim, S.; Segalman, R. A., The Relationship between Morphology and Performance of Donor-Acceptor Rod-Coil Block Copolymer Solar Cells. *Soft Matter* 2009, 5, 4219-4230.

49. Oosterbaan, W. D., *et al.*, Efficient Formation, Isolation and Characterization of Poly(3-Alkylthiophene) Nanofibres: Probing Order as a Function of Side-Chain Length. *Journal of Materials Chemistry* 2009, 19, 5424-5435.

50. Samitsu, S.; Shimomura, T.; Heike, S.; Hashizume, T.; Ito, K., Effective Production of Poly(3-Alkylthiophene) Nanofibers by Means of Whisker Method Using Anisole Solvent: Structural, Optical, and Electrical Properties. *Macromolecules* 2008, 41, 8000-8010.

51. Faied, K.; Frechette, M.; Ranger, M.; Mazerolle, L.; Levesque, I.; Leclerc, M.; Chen, T.-A.; Rieke, R. D., Chromic Phenomena in Regioregular and Nonregioregular Polythiophene Derivatives. *Chem. Mater.* 1995, 7, 1390-1396.

52. Lévesque, I.; Leclerc, M., Ionochromic and Thermochromic Phenomena in a Regioregular Polythiophene Derivative Bearing Oligo(Oxyethylene) Side Chains. *Chem. Mater.* 1996, 8, 2843-2849.

53. Zhang, L. F.; Eisenberg, A., Formation of Crew-Cut Aggregates of Various Morphologies from Amphiphilic Block Copolymers in Solution. *Polym. Adv. Technol.* 1998, 9, 677-699.

54. Chou, S.-H.; Tsao, H.-K.; Sheng, Y.-J., Structural Aggregates of Rod-Coil Copolymer Solutions. *J. Chem. Phys.* 2011, 134.

55. Olsen, B. D.; Segalman, R. A., Self-Assembly of Rod-Coil Block Copolymers. *Mater. Sci. Eng., R* 2008, 62, 37-66.

56. Wang, H. B.; Wang, H. H.; Urban, V. S.; Littrell, K. C.; Thiyagarajan, P.; Yu, L. P., Syntheses of Amphiphilic Diblock Copolymers Containing a Conjugated Block and Their Self-Assembling Properties. *J. Am. Chem. Soc.* 2000, 122, 6855-6861.

57. de Cuendias, A.; Ibarboure, E.; Lecommandoux, S.; Cloutet, E.; Cramail, H., Synthesis and Self-Assembly in Water of Coil-Rod-Coil Amphiphilic Block Copolymers with Central Pi-Conjugated Sequence. *J. Polym. Sci., Part A: Polym. Chem.* 2008, 46, 4602-4616.

58. Lin, J.; Lin, S.; Zhang, L.; Nose, T., Microphase Separation of Rod-Coil Diblock Copolymer in Solution. *J. Chem. Phys.* 2009, 130.

59. Ryu, J.-H.; Hong, D.-J.; Lee, M., Aqueous Self-Assembly of Aromatic Rod Building Blocks. *Chem. Commun.* 2008, 1043-1054.

60. Vriezema, D. M.; Hoogboom, J.; Velonia, K.; Takazawa, K.; Christianen, P. C. M.; Maan, J. C.; Rowan, A. E.; Nolte, R. J. M., Vesicles and Polymerized Vesicles from Thiophene-Containing Rod-Coil Block Copolymers. *Angew. Chem.* 2003, 42, 772-776.

61. Ryu, J. H.; Hong, D. J.; Lee, M., Aqueous Self-Assembly of Aromatic Rod Building Blocks. *Chemical Communications* 2008, 1043-1054.

62. Han, K. H.; Lee, E.; Kim, J. S.; Cho, B. K., An Extraordinary Cylinder-to-Cylinder Transition in the Aqueous Assemblies of Fluorescently Labeled Rod-Coil Amphiphiles. *Journal of the American Chemical Society* 2008, 130, 13858-13859.

63. Mori, T.; Watanabe, T.; Minagawa, K.; Tanaka, M., Self-Assembly of Oligo(P-Phenylenevinylene)-Block-Poly(Ethylene Oxide) in Polar Media and Solubilization of an Oligo(P-Phenylenevinylene) Homooligomer inside the Assembly. *Journal of Polymer Science Part A: Polymer Chemistry* 2005, 43, 1569-1578.

64. Qian, J. S.; Zhang, M.; Manners, I.; Winnik, M. A., Nanofiber Micelles from the Self-Assembly of Block Copolymers. *Trends in Biotechnology* 2010, 28, 84-92.

65. Sun, S.; Salim, T.; Wong, L. H.; Foo, Y. L.; Boey, F.; Lam, Y. M., A New Insight into Controlling Poly(3-Hexylthiophene) Nanofiber Growth through a Mixed-Solvent Approach for Organic Photovoltaics Applications. *Journal of Materials Chemistry* 2011, 21, 377.

66. Craley, C. R.; Zhang, R.; Kowalewski, T.; McCullough, R. D.; Stefan, M. C., Regioregular Poly(3-Hexylthiophene) in a Novel Conducting Amphiphilic Block Copolymer. *Macromol. Rapid Commun.* 2009, 30, 11-16.

67. Henry Hsieh, R. P. Q., *Anionic Polymerization: Principles and Practical Applications*. CRC Press: 1996; p 744.

68. Ihn, K. J.; Moulton, J.; Smith, P., Whiskers of Poly(3-Alkylthiophene)S. *Journal of Polymer Science Part B: Polymer Physics* 1993, 31, 735-742.

69. Oosterbaan, W. D., *et al.*, Efficient Formation, Isolation and Characterization of Poly(3-Alkylthiophene) Nanofibres: Probing Order as a Function of Side-Chain Length. *J. Mater. Chem.* 2009, 19, 5424.

70. Liu, J.; Arif, M.; Zou, J.; Khondaker, S. I.; Zhai, L., Controlling Poly(3-Hexylthiophene) Crystal Dimension: Nanowhiskers and Nanoribbons. *Macromolecules* 2009, 42, 9390-9393.

71. Bokel, F. A.; Sudeep, P. K.; Pentzer, E.; Emrick, T.; Hayward, R. C., Assembly of Poly(3-Hexylthiophene)/Cdse Hybrid Nanowires by Cocrystallization. *Macromolecules* 2011, 18-20.

72. Liu, J.; Zou, J.; Zhai, L., Bottom-up Assembly of Poly(3-Hexylthiophene) on Carbon Nanotubes: 2d Building Blocks for Nanoscale Circuits. *Macromolecular Rapid Communications* 2009, 30, 1387-1391.

73. Sarker, B. K.; Liu, J.; Zhai, L.; Khondaker, S. I., Fabrication of Organic Field Effect Transistor by Directly Grown Poly(3 Hexylthiophene) Crystalline Nanowires on Carbon Nanotube Aligned Array Electrode. *ACS Appl. Mater. Interfaces* 2011, 3, 1180-5.

74. Berson, S.; De Bettignies, R.; Bailly, S.; Guillerez, S., Poly(3-Hexylthiophene) Fibers for Photovoltaic Applications. *Adv. Funct. Mater.* 2007, 17, 1377-1384.

75. Hammer, B. A. G.; Bokel, F. A.; Hayward, R. C.; Emrick, T., Cross-Linked Conjugated Polymer Fibrils: Robust Nanowires from Functional Polythiophene Diblock Copolymers. *Chem. Mater.* 2011, 23, 4250-4256.

76. Liu, J.; Arif, M.; Zou, J.; Khondaker, S. I.; Zhai, L., Controlling Poly(3-Hexylthiophene) Crystal Dimension: Nanowhiskers and Nanoribbons. *Macromolecules* 2009, 42, 9390-9393.

77. Brinkmann, M.; Chandezon, F.; Pansu, R. B.; Julien-Rabant, C., Epitaxial Growth of Highly Oriented Fibers of Semiconducting Polymers with a Shish-Kebab-Like Superstructure. *Adv. Funct. Mater.* 2009, 19, 2759-2766.

78. Yan, H.; Yan, Y.; Yu, Z.; Wei, Z., Self-Assembling Branched and Hyperbranched Nanostructures of Poly(3-Hexylthiophene) by a Solution Process. *J. Phys. Chem. C* 2011, 115, 3257-3262.

79. Liu, J.; Zou, J.; Zhai, L., Bottom-up Assembly of Poly(3-Hexylthiophene) on Carbon Nanotubes: 2d Building Blocks for Nanoscale Circuits. *Macromol. Rapid Commun.* 2009, 30, 1387-1391.

80. Clark, J.; Chang, J.-F.; Spano, F. C.; Friend, R. H.; Silva, C., Determining Exciton Bandwidth and Film Microstructure in Polythiophene Films Using Linear Absorption Spectroscopy. *Appl. Phys. Lett.* 2009, 94, 163306-163306.

81. Brown, P.; Thomas, D.; Köhler, A.; Wilson, J.; Kim, J.-S.; Ramsdale, C.; Sirringhaus, H.; Friend, R., Effect of Interchain Interactions on the Absorption and Emission of Poly(3-Hexylthiophene). *Physical Review B* 2003, 67, 1-16.

82. Spano, F., Absorption in Regio-Regular Poly(3-Hexyl)Thiophene Thin Films: Fermi Resonances, Interband Coupling and Disorder. *Chem. Phys.* 2006, 325, 22-35.

83. Clark, J.; Silva, C.; Friend, R.; Spano, F., Role of Intermolecular Coupling in the Photophysics of Disordered Organic Semiconductors: Aggregate Emission in Regioregular Polythiophene. *Phys. Rev. Lett.* 2007, 98, 1-4.

84. Brinkmann, M., Structure and Morphology Control in Thin Films of Regioregular Poly(3-Hexylthiophene). *J. Polym. Sci., Part B: Polym. Phys.* 2011, 49, 1218-1233.

85. Zhao, K.; Xue, L.; Liu, J.; Gao, X.; Wu, S.; Han, Y.; Geng, Y., A New Method to Improve Poly(3-Hexyl Thiophene) (P3ht) Crystalline Behavior: Decreasing Chains Entanglement to Promote Order-Disorder Transformation in Solution. *Langmuir* 2010, 26, 471-7.

86. Yang, H. H.; LeFevre, S. W.; Ryu, C. Y.; Bao, Z. N., Solubility-Driven Thin Film Structures of Regioregular Poly(3-Hexyl Thiophene) Using Volatile Solvents. *Appl. Phys. Lett.* 2007, 90.

87. Spano, F. C., The Spectral Signatures of Frenkel Polarons in H- and J-Aggregates. *Acc. Chem. Res.* 2009, 43, 429-439.

88. Niles, E. T.; Roehling, J. D.; Yamagata, H.; Wise, A. J.; Spano, F. C.; Moule, A. J.; Grey, J. K., J-Aggregate Behavior in Poly-3-Hexylthiophene Nanofibers. *J. Phys. Chem. Lett.* 2012, 3, 259-263.

89. Roehling, J. D.; Arslan, I.; Moule, A. J., Controlling Microstructure in Poly(3-Hexylthiophene) Nanofibers. *J. Mater. Chem.* 2012, 22, 2498-2506.

Chapter 4: Hydrogen Bonding Assisted Self-Assembly of Conjugated Brush Copolymers into Nanoribbons

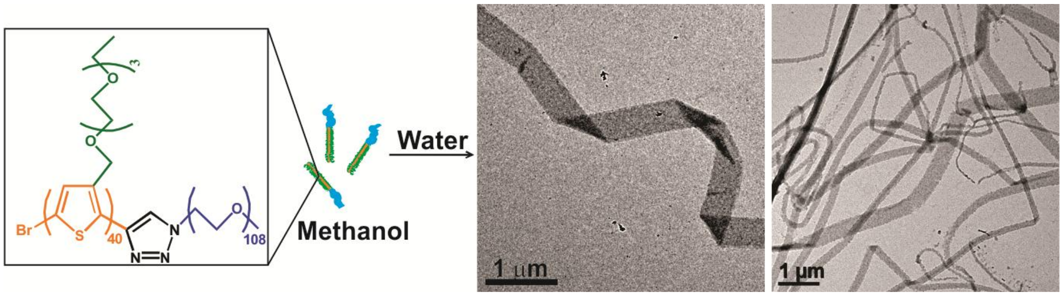

We report the hierarchical solution phase self-assembly of an amphiphilic conjugated brush copolymer, poly(tetra-oxo-tridecanyl-thiophene)-block-poly(ethylene glycol), into an elongated nanoribbon structure. The interaction of the polar substituents of the conjugated polymer with polar protic common solvents dominate the self-assembly process and provide a facile route to achieve stable conjugated polymer nanoribbons in aqueous solvents. The self-assembly structure of PTOTT-b-PEG varies sensitively with the solvent composition and polymer concentration, and the nanoribbon structure was formed only when polar protic solvents were used as an initial co-solvent. These results indicate that the nanoribbon structure is formed due to a delicate interplay between conjugated pi-pi stacking and hydrogen bonding interactions. This type of elongated nanoribbon structure has not been reported for amphiphilic conjugated block copolymers and could offer further insight into how internal packing structure affects the electronic properties of the conjugated block copolymer.

4.1 Introduction

The hierarchical assembly of conjugated polymers is important for organic optoelectronic device applications because intermolecular interactions and long-range ordering are critical in determining electronic properties.[1] This bottom-up self-assembly approach to device applications has been explored for conjugated small molecules[2-4] and conjugated polymers such as poly(alkylthiophenes) (PAT).[5, 6] Typically, the crystallization of the alkyl side chains into well-packed structures dominates the self-assembly process of PAT.[7, 8] Elongated nanowires have been synthesized via crystallization driven self-assembly of PAT block copolymers[5] and branched or bundled superstructures were formed through hierarchical self-assembly.[8] By introducing a tetraethylene glycol side chain into the conjugated polymer this affords new opportunities for achieving conjugated block copolymer assemblies with diverse morphologies and internal packing structures.

Herein, we present the solution phase self-assembly of an amphiphilic conjugated brush copolymer, poly(tetra-oxo-tridecanyl-thiophene)-*block*-poly(ethylene glycol) **(**PTOTT-*b*-PEG) into an extended nanoribbon structure. Derivations of the elongated nanoribbon structure have been reported by a number of research groups and are typically achieved via the self-assembly of small conjugated molecules[9-12], linear dendritic diblock copolymers[13-15], and metal metal phthalocyanines[16]. A recent report by Wudl *et al.* characterized the charge transport properties of a nanoribbon structure and showed that the supramolecular organization of the small molecule determined the inherent electronic properties.[11] The nanoribbon structure has not been reported for amphiphilic conjugated block copolymers and is achieved herein due to a delicate interplay between conjugated π-π stacking and hydrogen bonding interactions. The central driving forces for the supramolecular self-assembly of the block copolymer into this unique structure were identified by varying the solvent composition and polymer concentration.

4.2 Experimental Section

4.2.1 Synthesis of PTOTT-*b*-PEG. PTOTT$_{40}$-*b*-PEG$_{108}$ diblock copolymers were synthesized via the triazole cycloaddition click coupling reaction between ethynyl-PTOTT and azide-PEG (Scheme 5). The di-brominated TOTT monomer was synthesized using modified literature procedures[17, 18,19] and was polymerized into PTOTT-ethynyl block using the end-functionalization Grignard metathesis polymerization method.[20, 21]

Scheme 5. The synthetic scheme for the click chemistry of PTOTT-*b*-PEG.

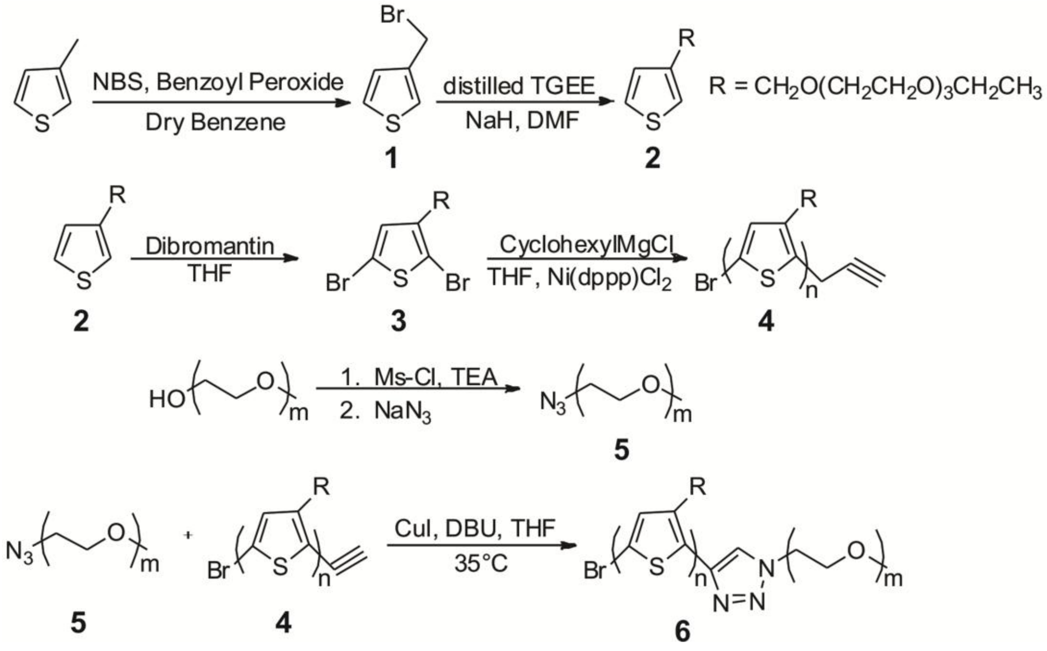

4.2.1.1 Synthesis of 3-Bromomethylthiophene (1). Synthesis of 3-bromomethylthiophene was based on a previously reported method.[17, 18] Typically, 3-methylthiophene (12 g, 122 mmol) was added to a dry three-neck round bottom flask equipped with two reflux condensers and a glass stopper. Benzene (200 mL) and 75 wt % benzoyl peroxide (184 mg, 0.61 mmol) were then added to the reaction flask and subsequently refluxed under air. While the reaction was refluxing a mixture of recrystallized *N*-bromosuccinimide (NBS) (10.9 g, 61 mmol) and 75 wt % benzoyl peroxide was slowly added to the reaction flask from a plastic addition funnel at the top of the reflux condenser and washed down with another 100 mL of benzene (Caution: reaction is highly exothermic and reacts violently). The solution was then refluxed for another four hours and then cooled to room temperature. The reaction was then cooled in an ice water bath and the solid succinimide by-product was removed by filtration. After the product was filtered, the solvent was removed by rotary evaporation. The crude product (10 g, 46% yield, 98% conversion) obtained from 3-methylthiophene was immediately used in the next synthesis without further purification.

^{1}H NMR (500 MHz, $CDCl_3$): δ_H 4.52 (s, 2H), 7.12 (dd, J_{AX} = 1.32 Hz, J_{AM} = 4.91 Hz, 1H), 7.28-7.33 (m, 2H)

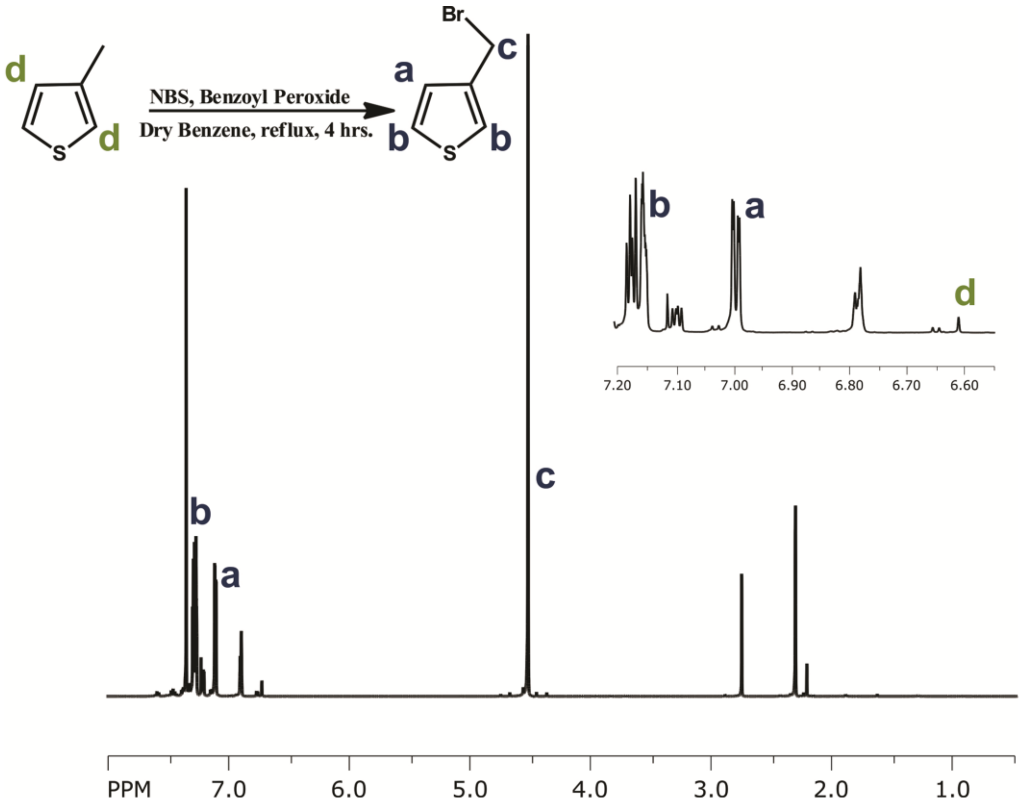

Figure 4.1. ^{1}H-NMR spectra of 3-bromomethylthiophene.

4.2.1.2 Synthesis of (tetra-oxo-tridecanyl-thiophene) (TOTT) (2). Sodium hydride (NaH) (3.2 g, 60% in mineral oil, 0.133 mol) was weighed into a dry 500-mL two-neck round bottom flask equipped with a condenser and was suspended in DMF (150 mL). The reaction set-up was flushed with N_2 and was cooled down to 0°C, after which TGEE (48 mL, 0.271 mol) was added dropwise over 30 minutes. To ensure complete consumption of NaH, the reaction was allowed to stir for an additional hour at 0°C. Crude 3-bromomethylthiophene (1) (10 g, 0.0565 mol) was then added into the reaction mixture and the solution was heated to reflux overnight (110°C). The reaction mixture was then allowed to cool to room temperature and was poured into 1M NH_4Cl (150 mL) and stirred for ten minutes. The organic phase was extracted with hexanes and dried over anhydrous $MgSO_4$. After the product was filtered, the solvent was removed by rotary evaporation. The crude product was purified using column chromatography on silica gel using 7:3 hexanes/ethyl acetate as the eluent to yield 6.99 g (37%) of a yellow oil of TOTT.

^1H NMR (500 MHz, $CDCl_3$): δ_H 1.19 (t, J = 7 Hz, 3H), 3.48-3.53 (m, 2H), 3.56 (m, 2H), 3.58-3.67 (m, 10H), 4.55 (s, 2H), 7.05 (m, 1H), 7.19 (m, 1H), 7.26 (dd, J_{MX} = 3 Hz, J_{AM} = 4.9 Hz, 1H)

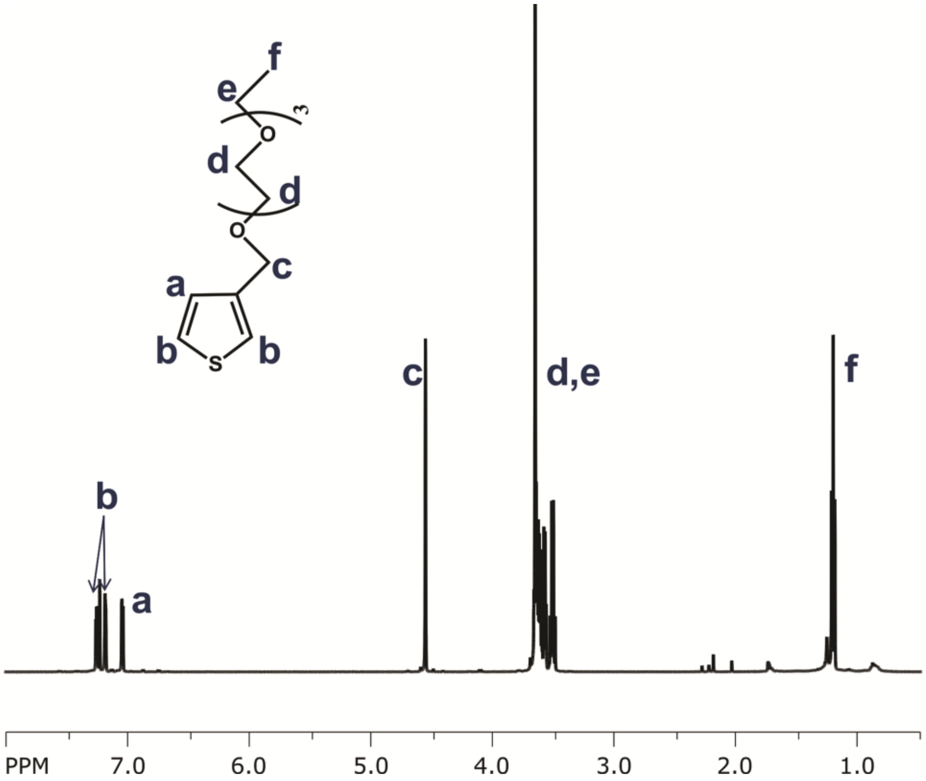

Figure 4.2. ^{1}H-NMR spectra of TOTT.

4.2.1.3 Synthesis of 2,5-dibromo-(tetra-oxo-tridecanyl-thiophene) (Br_2-TOTT) (3). TOTT (2) (12.9 g, 0.05 mol) was weighed into a dry 250-mL three-neck round bottom flask and was dissolved in THF (50-60 mL). The reaction set-up was flushed with N_2 and was cooled down to -78°C, after which dibromantin (8.03 g, 0.0281 mol) was added. The reaction mixture was stirred for 30 minutes at -78°C and was then allowed to slowly warm up to ambient temperature. The reaction was stirred for another two hours at room temperature and the color of the solution changes from yellow to brown. The solvent was then removed by rotary evaporation. The resulting residue was washed with hexanes, filtered to remove succinimide, dried over anhydrous $MgSO_4$ and purified using column chromatography on silica gel with 8:2 hexanes/ethyl acetate as the eluent to yield 6.5 g (59%) of an orange oil of 2,5-dibromo-3-TOTT.

^1H NMR (500 MHz, $CDCl_3$): δ_H 1.20 (t, J = 7 Hz, 3H), 3.49-3.53 (m, 2H), 3.57-3.61 (m, 4H), 3.63-3.67 (m, 8H), 4.42 (s, 2H), 7.00 (s, 1H)

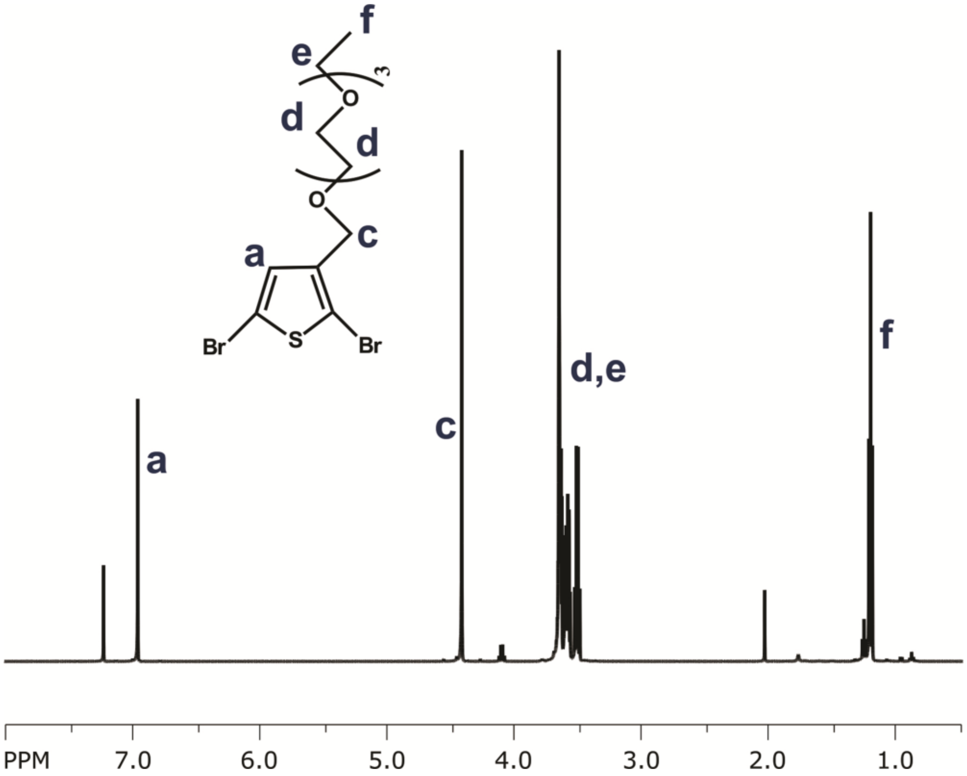

Figure 4.3. ^{1}H-NMR spectra of Br_2-TOTT.

4.2.1.4 Synthesis of ethynyl-terminated poly(tetra-oxo-tridecanyl-thiophene) (ethynyl-PTOTT) (4). 2,5-dibromo-TOTT (3) (1.93 g, 4.47 mmol) was weighed into a 250 mL 3-neck round bottom flask and was dissolved in freshly distilled THF (100 mL). The reaction set-up was flushed with argon. Cyclohexylmagnesium chloride (2.0 M / diethyl ether, 4.79 mL, 9.58 mmol) was added into the flask and the reaction was allowed to proceed for 30 minutes. Solid Ni(dppp)Cl_2 was then added under high argon flow, and the mixture was allowed to stir for another ten minutes. End-group termination was then achieved by adding ethynyl magnesium bromide (1.0 M/ THF, 2.40 mL, 2.40 mmol). The termination reaction was allowed to proceed for an additional 30 minutes before it was quenched with hexanes (20 mL). The reaction mixture was then concentrated using rotary evaporation and then the product was precipitated into hexanes, filtered, and purified by soxhlet extraction with hexanes and chloroform. The solvent was removed by rotary evaporation and the blood-red product was dried under vacuum overnight to yield 1.02 g (83%) of ethynyl-PTOTT.

^{1}H NMR (500 MHz, $CDCl_3$): δ_H 1.17 (t, J = 6.97 Hz, 3H), 3.49 (q, J = 6.92 Hz, 2H), 3.55 (t, J = 4.61 Hz, 2H), 3.61-3.68 (m, 8H), 3.72 (s, 2H), 4.65 (s, 2H), 7.24 (s, 1H); GPC: Mn = 22000, Mn(corrected[22]) = 11000, PDI = 1.17.

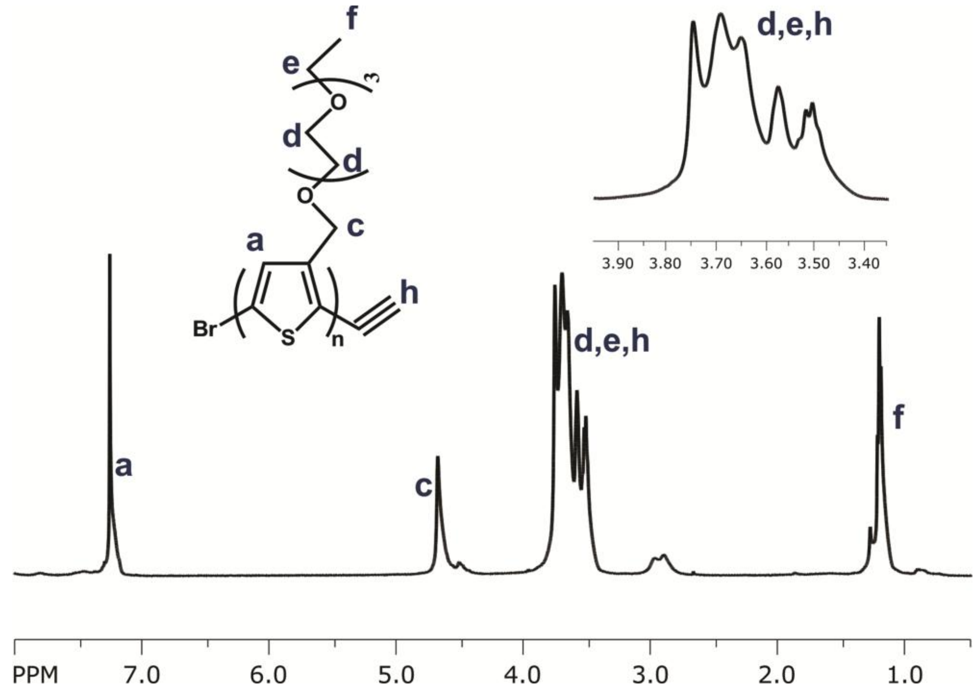

Figure 4.4. ^{1}H-NMR spectra of ethynyl-PTOTT$_{40}$.

4.2.1.5 Synthesis of azide-terminated poly(ethylene glycol) (Azide-PEG) (5).

The monoazide-terminated poly(ethylene glycol) (azide-PEG) was synthesized following a modified literature procedure.[23, 24] Azide-PEG was synthesized by mesylation of the hydroxyl terminus of commercial methoxy-PEG followed by sodium azide substitution. Typically, a solution of methoxy-PEG (4.4 g, 0.92 mmol), triethylamine (0.51 mL, 3.7 mmol), and 50 mL of freshly distilled THF were added to a 3-neck roundbottom flask and the system was purged with nitrogen. Methanesulfonyl chloride (0.32 mL, 4.1 mmol) was then added to the flask and the solution was stirred at room temperature for 10 hours. The reaction product was then dried down using rotary evaporation, redissolved into minimal amount of deionized water (~ 1-2 mL), and then extracted into DCM (150 mL x 2). After drying the organic product layer with sodium sulfate, the product was filtered, concentrated and then precipitated from minimal DCM into cold diethyl ether. The off-white/yellow precipitate was then filtered, washed with cold diethyl ether, and then dried under vacuum to a constant weight (3.9 g, 88 %). The mesylated PEG (3.9 g, 0.81 mmol) was added to a roundbottom flask with 50 mL DMF and a reflux condenser. Sodium azide (4.3 g, 65 mmol) was then added to the flask and the solution is heated at 60 °C for 24 hours. The reaction product was then dried down using rotary evaporation. The product was then redissolved into DCM and the excess sodium azide was removed by filtration. The product in DCM was further cleaned by extraction with brine solution (100 mL x 4). After drying the organic layer with sodium sulfate, the product was filtered, concentrated and then precipitated from minimal DCM into cold diethyl ether. The azide-PEG product (white solid) was then filtered, washed with cold diethyl ether, and then dried under vacuum to a constant weight (2.2 g, 57 %).

Characterization of azide-PEG$_{108}$. IR: (KBr, cm^{-1}): 2101 (azide), 529, 842, 963, 1108, 1237, 1282, 1343, 1468. MALDI-MS: m/z = 4896.35 [M+] (calculated: 4896, DP of 108, N_3/CH_3 end groups), PDI = 1.21.

4.2.1.6 Synthesis of poly(tetra-oxo-tridecanyl-thiophene)-*block*-poly(ethylene glycol) (PTOTT-*b*-PEG) (6). PTOTT-*b*-PEG was synthesized by the copper(I)-catalyzed click reaction between azide-PEG (5) and ethynyl-PTOTT (4) (Scheme 1). Typically, ethynyl-PTOTT (150 mg, 0.014 mmol), azide- PEG (67 mg, 0.014 mmol), 1,8-diazabicyclo[5.4.0]undec-7-ene (DBU) (1.0M/ THF, 0.56 mL, 0.56 mmol) and copper(I) iodide (1.9 mg, 0.010 mmol), and 10 mL freshly distilled THF were added to a 25 mL round bottom flask. Copper(I) iodide (1.9 mg, 0.010 mmol) was then added to a 50 mL schlenk flask in the glove box. The polymer solution was then added to the schlenk flask via a cannula transfer. The reactants in the schlenk flask were then degassed with three freeze pump thaw cycles and subsequently refilled with nitrogen. The solution reacted at 40°C for 2 days. The copper salt was then removed by passing the product through a neutral alumina column. After the removal of THF by rotary evaporation the product was dissolved into a minimal amount of chloroform and precipitated into ethyl ether to remove any excess PTOTT homopolymer which will come off in the filtrate. The ethyl ether precipitate was collected using gravity filtration and then dried to a constant weight under vacuum. The dry product was then washed with water (20 mL x 3) followed by centrifugation at 14K rpm to remove the aqueous supernatant which will contain any excess PEG homopolymer. The final orange-solid product was then dried to a constant weight under vacuum yielding 190 mg (86%) of PTOTT$_{40}$-*b*-PEG$_{108}$. The purity of the PTOTT-*b*-PEG block copolymer was confirmed by GPC and NMR analysis.

^{1}H NMR (500 MHz, CDCl$_3$): δ_H 1.17 (t, *J* = 6.97 Hz, 3H), 1.94 (m), 3.49 (q, *J* = 6.92 Hz, 2H), 3.55 (t, *J* = 4.61 Hz, 2H), 3.61-3.68 (m, 8H), 3.65 (s), 3.72 (s, 2H), 3.95 (t), 4.65 (s, 2H), 7.24 (s, 1H).

4.2.2 Preparation of PTOTT-*b*-PEG Assemblies. In a typical experiment, 50 μL of a PTOTT$_{40}$-*b*-PEG$_{108}$ solution (6.3 x 10^{-5} M) in chloroform was dried down under nitrogen and then redissolved in 1 mL of methanol (DMF, THF, acetonitrile were other common solvents that were used). A slow addition of 300 μL of water (18 MΩ-cm) was added to the block copolymer solution at a rate of 10 μL per 30 s while stirring. The mixture was kept under stirring for 12 h before adding an additional 1mL of water at a rate of 50 μL per 30 s. Then, the samples were dialyzed against water for 24 h and further concentrated by a series of centrifugations.

4.2.3 Materials, Measurements, and Instrumentation. All reactions were carried out using standard Schlenk techniques under an inert atmosphere of pre-purified nitrogen or argon, using oven-dried glassware. Commercial chemicals 3-methylthiophene, sodium hydride, 1,3-dibromo-5,5'-dimethylhydantoin(dibromantin), [1,3-bis(diphenylphosphino)propane] dichloronickel(II) (Ni(dppp)Cl$_2$), cyclohexylmagnesium chloride, vinylmagnesium bromide, benzene, and anhydrous *N*,*N*-dimethylformamide (DMF) were purchased from Aldrich and used without further purification. *N*-Bromosuccinimide (Aldrich, 99%) was recrystallized from water, dried under vacuum, and stored over Drierite. Triethylene glycol monoethyl ether (TGEE) (Aldrich, tech.) was dried and vacuum-distilled over phosphorus pentoxide. Tetrahydrofuran was freshly distilled from sodium/benzophenone to ensure anhydrous conditions, and all other reagents were used without further purification.

IR spectra were obtained on a Perkin-Elmer system 2000 FTIR spectrometer. Electronic absorption spectra were acquired on an Agilent 8453 spectrophotometer. Photoluminescence spectra were acquired on a Spex Fluorolog 3 utilizing a R928 PMT detector. TEM was performed on a JEOL 1400 electron microscope operating at 120 kV accelerating voltage. GPC measurements were carried out at room temperature at a flow rate of 1.0 mL/min on a Shimadzu LC-10AT liquid chromatography system equipped with a series of two PLgel 10μm 10E6A columns, an SPD-10AVvp absorbance UV/VIS detector, and a refractive index detector (RID-10A) calibrated against linear polystyrene standards in THF. Dynamic light scattering (DLS) measurements were taken on a Malvern Zetasizer Nano Series. Matrix assisted laser desorption ionization time-of-flight mass spectrometry (MALDI-TOF/TOF MS) spectra were obtained on a Bruker Flex Series MALDI-TOF/TOF MS. Spectra were recorded in the positive-ion reflectron mode with an accelerating voltage of 20 kV. The MALDI samples were prepared via the sandwich method by first depositing 1 μL of a 40 mg/mL DCTB matrix chloroform solution, followed by the deposition of 1 μL of a 1 mg/mL PTOTT chloroform solution on top of the matrix, and finally depositing another 1 μL of a 40 mg/mL *trans*-2-[3-(4-*tert*-Butylphenyl)-2-methyl-2-propenylidene]malononitrile (DCTB) matrix chloroform solution on top of the sample. After each of the solutions (1 μL) were deposited on the stainless steel sample target they were then air dried prior to the addition of the next solution.

4.3 Synthesis and Characterization of PTOTT-*b*-PEG. PTOTT$_{40}$-*b*-PEG$_{108}$ diblock copolymers were synthesized via the triazole cycloaddition click coupling reaction between ethynyl-PTOTT and azide-PEG (Scheme 5). The di-brominated TOTT monomer was synthesized using modified literature procedures[18,19, 25] and was polymerized into PTOTT-ethynyl block using the end-functionalization Grignard metathesis polymerization method.[20, 21] Azide-PEG was synthesized by the mesylation of the hydroxyl terminus of commercial methoxy PEG followed by sodium azide substitution.[23, 24] The click coupling product was purified by precipitation into diethyl ether and aqueous washing to remove excess ethynyl-PTOTT homopolymer and azide-PEG, respectively. The purity of the block copolymer was confirmed by ^{1}H NMR spectroscopy (Figure 4.5 A) and gel permeation chromatography (Figure 4.5 B).

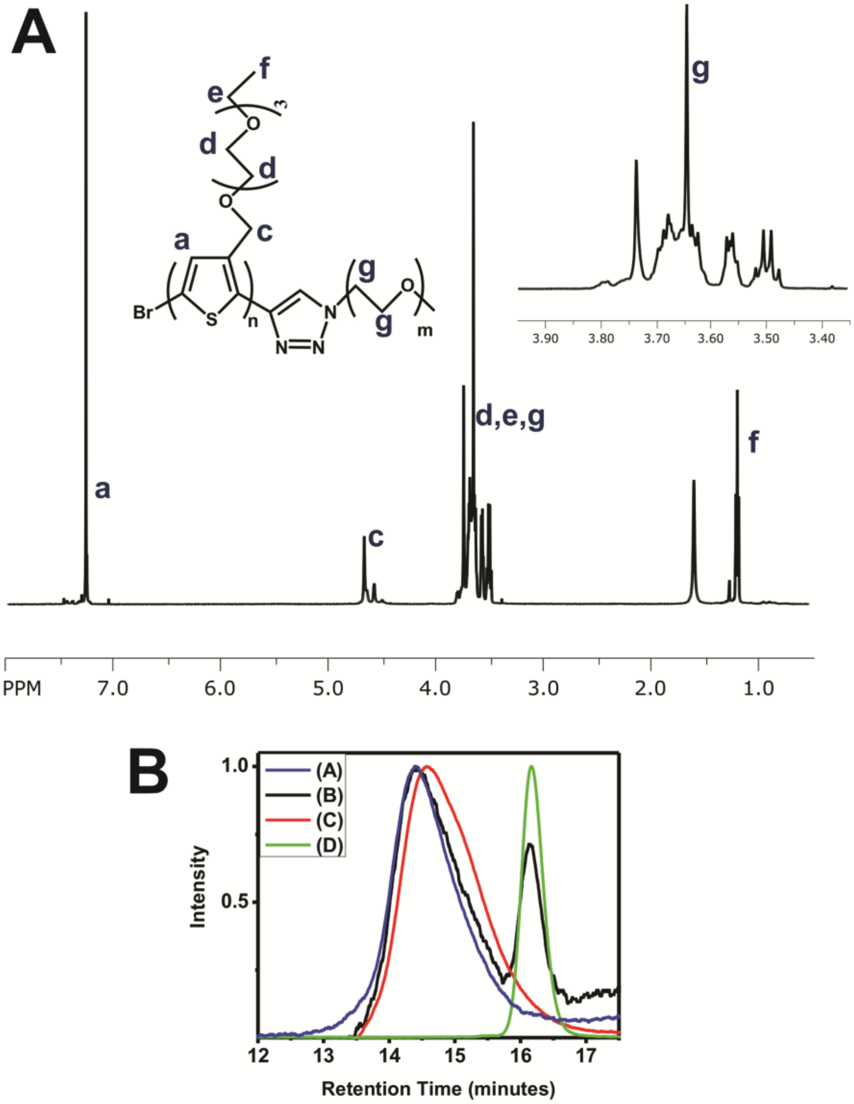

Figure 4.5. (A) ^{1}H-NMR spectra of PTOTT$_{40}$-*b*-PEG$_{108}$. (B) GPC spectrum (RID trace) of (A) purified PTOTT$_{40}$-*b*-PEG$_{108}$ (Blue), (B) crude PTOTT$_{40}$-*b*-PEG$_{108}$ (Black), (C) PTOTT$_{40}$ homopolymer (Red), and (D) PEG$_{108}$ homopolymer (Green).

4.4 Self-Assembly into Nanoribbon Structure

PTOTT-*b*-PEG is an interesting moiety that can be described as an amphiphilic conjugated brush copolymer because it possesses a conjugated thiophene backbone with hydrophilic oligomeric polar ethylene glycol side chains and is covalently attached to a hydrophilic poly(ethylene glycol) block. Despite the hydrophilic nature of the PEG block and the oligomeric tetraethylene glycol side-chains, the block copolymer will not directly dissolve or self-assemble into aqueous solutions. In order to induce self-assembly, the polymer is first dissolved in a common solvent followed by a slow addition of water and subsequent dialysis into water. When the common solvent used in this process is methanol, the block copolymer self-assembles into a unique nanoribbon structure in the final aqueous solution (Figure 4.6 A). The TEM images in Figure 4.6 B-C show the elongated structure of the nanoribbon. Dimensional analysis of the TEM images yields a width distribution of 250 ± 139 nm and a length distribution of 18.3 ± 5.8 μm. AFM images shown in Figure 4.6 D-E yield an average height of 38 ± 5 nm, which closely matches with the expected height (40.2 nm) of the interdigitated PTOTT-*b*-PEG bilayers depicted in Figure 4.6 A.

The two possible packing structures of PTOTT-*b*-PEG nanoribbons, interdigitated and parallel, are shown in Figure 4.7. It is hypothesized that the PTOTT chains are most likely packed in an interdigitated arrangement as shown schematically in Figure 4.7 A and not in an end to end or parallel arrangement as depicted in Figure 4.7 B. The theoretical heights shown next to the corresponding structures in Figure 4.7 are calculated based on the radius of gyration of PEG_{108} of 1.23 nm[26] and the length of one $PTOTT_{40}$

chain (15.2 nm)[27]. Overall, the theoretical height of the interdigitated packed structure (40.2 nm) correlates more closely with the experimentally determined height of 38 ± 5 nm and is therefore the more likely candidate. Furthermore, the experimental height might be a slight underestimation due to the possible deformation of the soft PEG block via the use of a hard tapping mode during AFM measurements. Although, the interdigitation model seems likely, it can be difficult to precisely determine the precise internal packing arrangement of rod-like polymers. Another group[28] analyzed the emission spectroscopy of a pyrenyl group attached to the polymer as a molecular probe to obtain insight into the precise internal packing arrangement of a rod-coil block copolymer while other groups[29] have assumed interdigitation models based on spectroscopic height measurements. The TEM images of broken PTOTT-*b*-PEG nanoribbons shown in Figure 4.7 C show the double layered nature of the nanoribbon, but does not necessarily discriminate between the two possible packing models.

Further confirmation that the self-assembled structure in solution is in fact anisotropically flattened and not just collapsed due to capillary forces[30] was confirmed via cryo-TEM images (Figure 4.8 A,B). The semiconducting nature along with the flatness of the nanoribbon structure could also be visualized using SEM as is shown in Figure 4.8 C,D. Overall, the term “nanoribbon” is aptly used to describe this self-assembled structure because the width of the ribbon is approximately 10 times its height and typically has extended lengths of > 10 μm.

The optical characteristics of conjugated polymers can be used to provide more information on their packing structure, conjugation length, and environment. The absorbance spectra of the nanoribbons are blue-shifted (428 nm) relative to both well-dissolved PTOTT-*b*-PEG in chloroform (440 nm) and to PTOTT-*b*-PEG self-assembled into quasi-spherical micelle-like aggregates (455-485 nm). The emission of the PTOTT-*b*-PEG nanoribbons is also efficiently quenched compared to the relative optical properties of PTOTT-*b*-PEG in methanol and chloroform (Figure 4.9 A-B). Overall, the emission of PTOTT-*b*-PEG in methanol is about 4 times less and its absorbance is red-shifted when compared to its optical properties in a better solvent for PTOTT-*b*-PEG such as chloroform (Figure 4.9 A-B). This indicates that the PTOTT chains in the nanoribbon structure are twisted and are tightly packed enough to cause quenching due to intermolecular interactions.[31]

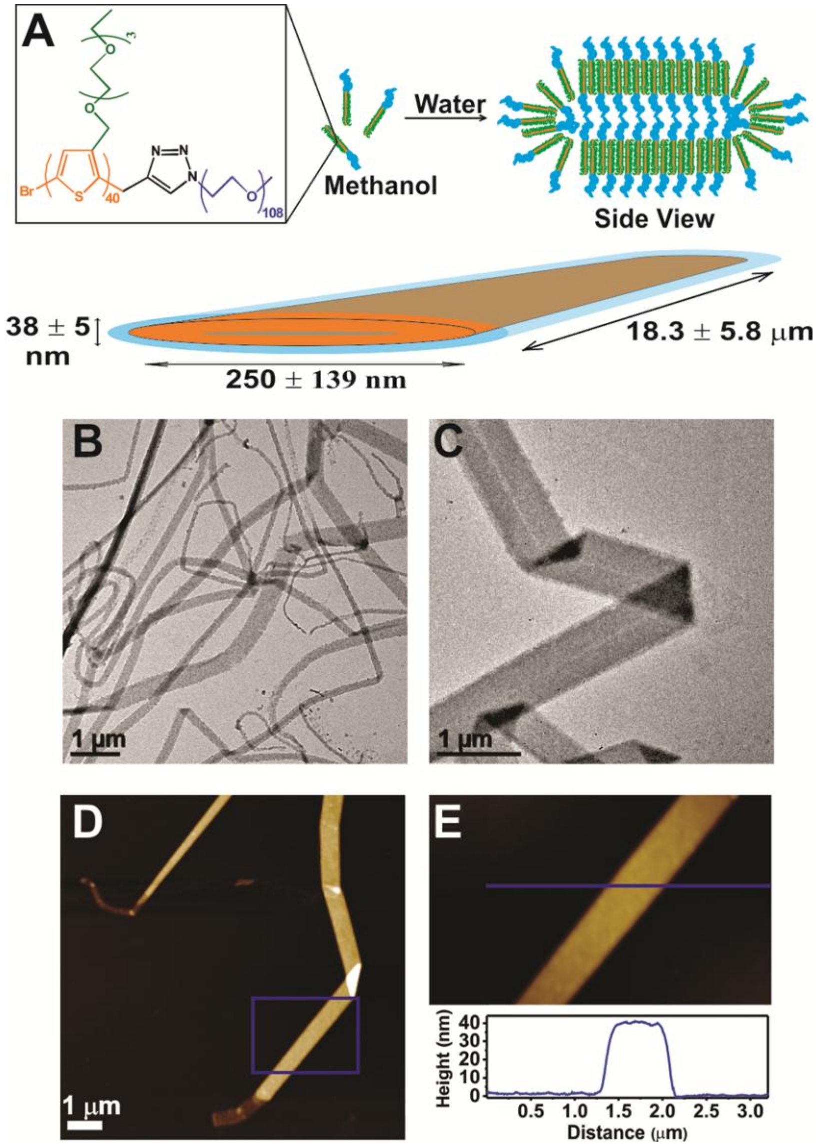

Figure 4.6. (A) Chemical structure of PTOTT$_{40}$-*b*-PEG$_{108}$ and schematic depiction of the self-assembly of PTOTT-*b*-PEG into nanoribbons from the common solvent methanol. (B), (C) TEM images of 2 μM PTOTT$_{40}$-*b*-PEG$_{108}$ in water self-assembled from methanol. (D), (E) AFM height images of 2 μM PTOTT$_{40}$-*b*-PEG$_{108}$ in water self-assembled from methanol and deposited on a silicon wafer.

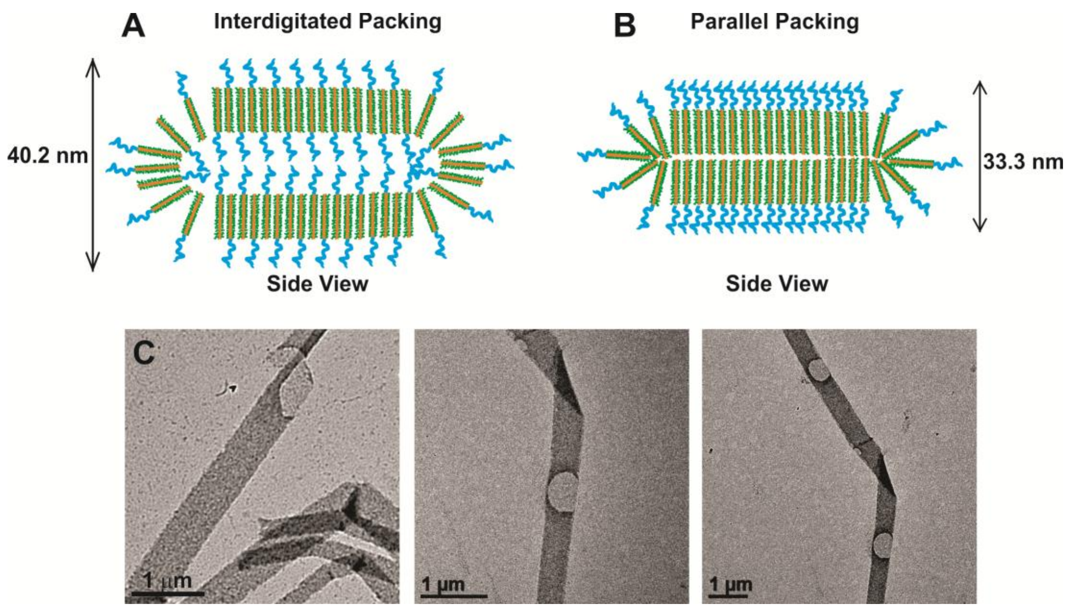

Figure 4.7. Schematic depiction of the two possible internal packing structures of PTOTT-*b*-PEG nanoribbons; (A) interdigitated packing of PTOTT and (B) parallel packing of PTOTT. (C) TEM images of broken PTOTT-*b*-PEG nanoribbons showing the double layered nature of the nanoribbon structure.

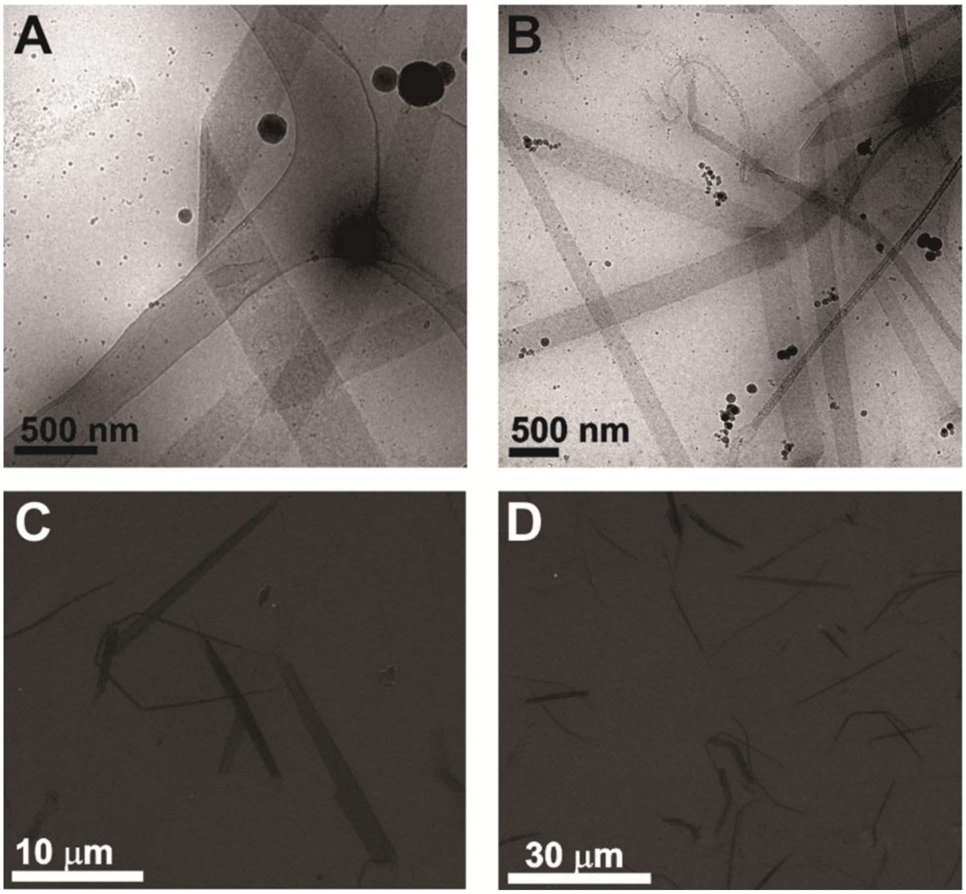

Figure 4.8. Cryo-TEM images (A, B) and SEM images (C, D) of 2 μM PTOTT-*b*-PEG nanoribbon assemblies in water that were self-assembled from methanol.

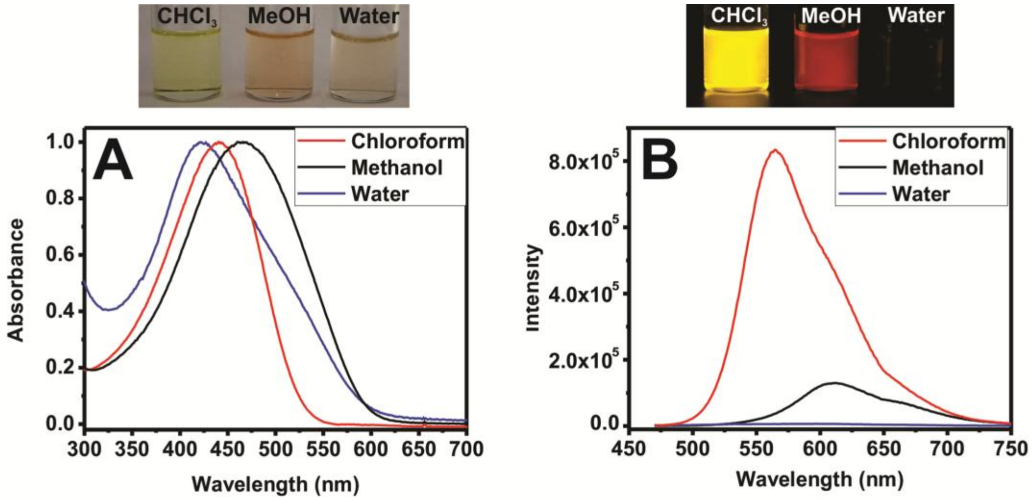

Figure 4.9. (A) Absorbance and (B) PL spectra of 2 μM PTOTT$_{40}$-*b*-PEG$_{108}$ dissolved in chloroform (red), methanol (black) and self-assembled into nanoribbons in water from methanol (blue). Pictures of solutions under ambient light (top-left) and under UV light (top-right) are given above the spectra.

4.5 Factors Controlling Self-Assembly and Optical Properties of PTOTT-*b*-PEG in Selective Solvents

4.5.1 Effect of Concentration. The initial concentration of PTOTT-*b*-PEG in methanol had a rather dramatic effect on its resultant self-assembled structure in water. With increasing concentration, the block copolymer morphology evolved from a lamellae structure, to a nanoribbon structure, to budding micelles on the nanoribbon, and finally to a mixture of quasi-spherical micelle-like aggregates and budded micelle nanoribbons (Figure 4.10). The lamellae structure found at lower concentrations of 0.5 μM (Figure 4.10 A) has a smaller height (7.5 ± 0.8 nm) relative to the nanoribbons (36 ± 5 nm) in Figure 4.10 B formed at larger concentration of 2 μM indicating that a parallel packing structure might be the more likely packing orientation for the lamellae.

The effect of block copolymer concentration on morphology is typically explained by an increase in the aggregation number of the polymer which is accommodated by a reduction of the stretching energy of the core via the adoption of lower curvature morphologies such as the bilayer structure.[32] Other block copolymer systems such as PS-*b*-PAA are known to change from spheres, to rods, to vesicles, and finally to bilayers with increasing concentration in order to relieve the stretching energy of the core.[33] In the case of PTOTT-*b*-PEG, the lamellae structure is most likely formed at lower polymer concentration because there is not enough material for the nanoribbon structure to be formed. As the aggregation number of the polymer increases, the nanoribbon structures starts forming because the larger core size of the nanoribbon lowers the total free energy of the system by reducing the interfacial energy between the core and the solvent. As the concentration increases further, the quasi-spherical micelle-like aggregates start forming on the nanoribbon structure because increasing the block copolymer concentration most likely interferes with the hydrogen bonding interaction that causes the nanoribbon structure formation. The fraction of hydrogen bonding between PEG and water decreases with increasing PEG concentration.[34] Therefore as the concentration of PTOTT-*b*-PEG increases, the hydrogen bonding interaction decreases and the quasi-spherical micelle-like aggregates found in polar aprotic solvents starts manifesting itself.

A similar morphological trend was identified via imaging aliquots of the block copolymer in methanol/water mixtures monitored at intermediate water addition stages (Figure 4.11). At 9 % water content, PTOTT-*b*-PEG self-assembles into vesicles (Figure 4.11 A). As the water % increases, the morphology evolves from vesicles to sheet-like structures (Figure 4.11 B), to finally nanoribbons (Figure 4.11 C,D). The layers composing the vesicles and sheets are significantly less electron dense than nanoribbons in TEM images, indicating that the assemblies formed at the intermediate water contents might adopt side-by-side parallel packing of PTOTT, which has been observed in other brush copolymers.[35-37] As the solvent quality for PTOTT becomes worse with further water addition, nanoribbons with face to face PTOTT packing emerge to minimize the interaction between polythiophene and water and reduce the interfacial energy. The effect of water content on the morphology can also be correlated with the change in aggregation number with lower water contents having smaller aggregation numbers, similarly to the effect of concentration.[38] It important to note that direct dialysis or slow addition of water without overnight incubation results in broken nanoribbons. Therefore, the slow addition of water allows for the self-assembly structure to reach its equilibrium morphology.

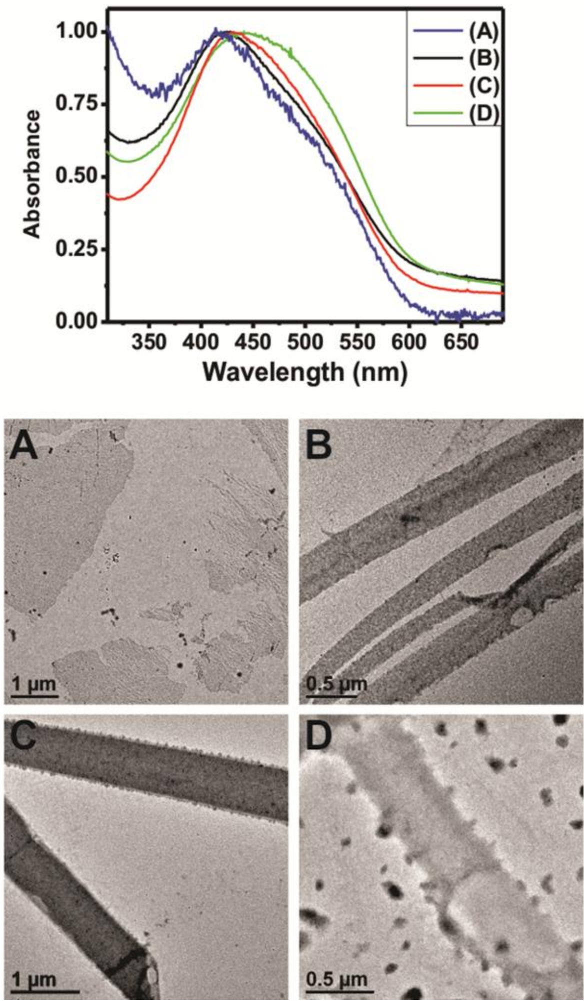

Figure 4.10. Absorbance spectra and corresponding TEM images of PTOTT$_{40}$-*b*-PEG$_{108}$ assemblies in water that were self-assembled from methanol at different concentrations of PTOTT$_{40}$-*b*-PEG$_{108}$; (A) 0.5 μM, (B) 2 μM, (C) 5.4 μM, and (D) 10 μM.

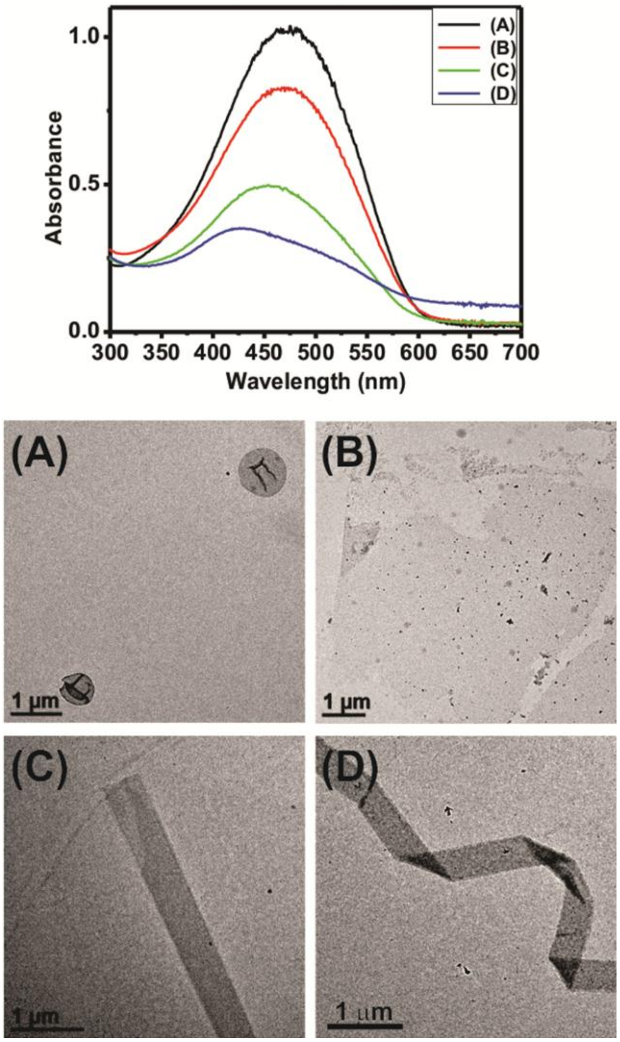

Figure 4.11. Absorption spectra and corresponding TEM images of 2 μM PTOTT-*b*-PEG block copolymer nanoribbon assemblies at a series of different water/methanol (v/v) contents: (A) 9 % water, (B) 23 % water after overnight incubation, (C) 56 % water, and (D) 100 % water.

4.5.2 Effect of Common Solvent. The initial common solvent plays a crucial role in determining the final structure of block copolymers in water. This phenomena has been demonstrated in other block copolymer systems such as PS-*b*-PAA[39] and PS-*b*-PEO[40] and is attributed to the difference in the relative solubility parameters of the interacting solvent and the block copolymer. The tetraethylene glycol side chain on the conjugated polymer imparts enhanced solubility on the block copolymer and allows for its dissolution in a number of different polar protic and polar aprotic solvents.

Interestingly, hydrogen bonding interactions along with the solubility parameters of the common solvents both play a critical role in dictating the resultant self-assembly structure of the polymer. The solubility parameters, hydrogen bonding strengths, and resultant morphologies are summarized in Table 2. TEM images and absorption characteristics of the resultant morphologies are further summarized in Figure 4.12. When polar aprotic solvents such as THF, DMF, dixoane, and acetonitrile are used as common solvents, PTOTT-*b*-PEG self-assembles into quasi-spherical micelle-like aggregates. In contrast, when PTOTT-*b*-PEG is self-assembled from polar protic solvents such as methanol, isopropanol, and ethanol the polymer self-assembles into the unique nanoribbon morphology. Despite the similarity of solubility parameters between low hydrogen bonding strength acetonitrile (24.3) and high hydrogen bonding strength isopropanol (23.5), the self-assembled morphologies for these solvents are quasi-spherical micelle-like aggregates and nanoribbons, respectively. This clearly demonstrates the dominant effect of the hydrogen bonding interactions in determining the self-assembled structure.

The nanoribbon structure that is formed in polar protic solvents is most likely a direct result of the competition between PEG-methanol, PEG-water, and water-methanol hydrogen bonding. In binary solvent mixtures of PEG homopolymer, the addition of water to methanol results in competition for hydrogen bonding sites along the PEG backbone resulting in the adoption of a pearl necklace conformation of PEG.[41] The competitive hydrogen bonding effect typically occurs in solvents that are co-nonsolvents. Co-nonsolvents are two good solvents that become poor for a polymer when mixed together. In one example, the co-nonsolvency effect between methanol and water resulted in a sharp depression of lower critical solution temperature (LCST) and the formation of a pearl necklace conformation of the poly(N-isopropylacrylamide) polymers.[42] In another example, poly(2-(methacryloyloxy) ethyl phosphorylcholine) polymer brushes were highly swollen in ethanol and in water, but became deswollen in mixtures of ethanol and water due to the co-nonsolvency effect.[43] The effect of competitive hydrogen bonding has also been demonstrated with the peptide (AAKLVFF) which forms twisted fibrils in water, nanotubes in methanol, and filamentous tapes in water/methanol mixtures.[44] The competitive hydrogen bonding effect is a key driving force in the complex amphiphilic brush copolymer self-assembly of PTOTT-*b*-PEG that manifests itself in the formation of supramolecular nanoribbons.

Table 2. Solubility parameters and hydrogen bonding strength of common solvents.

Common Solvent	Solubility Parameter (Mpa$^{0.5}$)	Hydrogen Bonding Strength	Initial λ (nm) [a]	Final λ (nm) [b]	Morphology in Water	D$_h$ (nm) [c]
THF	18.6	Medium	450	433	Micelles[d]	142 ± 52
Acetone	20.3	Medium	475	417	Micelles[d]	---
Dioxane	20.5	Medium	450	487	Micelles[d]	
2-Propanol	23.5	Strong	475	426	Nanoribbons	---
Acetonitrile	24.3	Poor	476	455	Micelles[d]	96 ± 31
DMF	24.8	Medium	460	485	Micelles[d]	110 ± 43
Ethanol	26.0	Strong	475	420	Nanoribbons	---
Methanol	29.7	Strong	465	428	Nanoribbons	---
Water	47.9	Strong	---	---	---	---

[a] Absorbance of PTOTT-*b*-PEG in common solvent.

[b] Absorbance of PTOTT-*b*-PEG water after self-assembly from common solvent.

[c] Hydrodynamic diameter determined by DLS analysis.

[d] Micelles denotes quasi-spherical micelle-like aggregates.

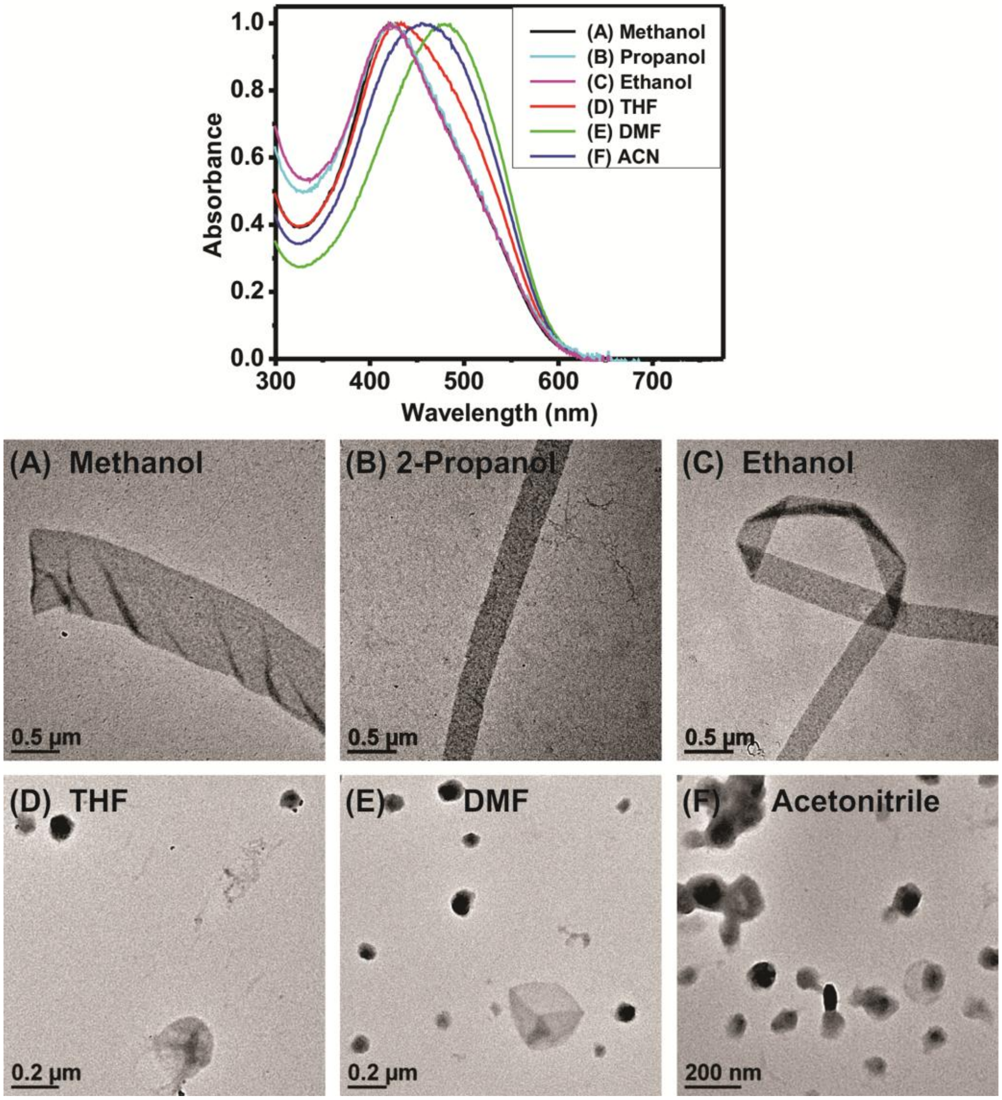

Figure 4.12. Absorption spectra and corresponding TEM images of 2 μM $PTOTT_{40}$-*b*-PEG_{108} assemblies in water that were self-assembled from different common solvents; (A) methanol, (B) 2-propanol, (C) ethanol, (D) THF, (E) DMF, and (F) acetonitrile.

4.5.3 Effect of Mixed Solvent. Further evidence of the prevailing effect of hydrogen bonding in achieving the unique nanoribbon morphology was attained by studying the morphology of PTOTT-*b*-PEG in mixed solvent systems. A mixture of nanoribbons and micelles was formed when PTOTT-*b*-PEG was self-assembled from a 50 % (v/v) mixture of acetonitrile and methanol (Figure 4.13). In contrast, a nanofiber morphology with a width of 14.2 ± 1.6 nm (the length of one PTOTT_{40} chain calculated with the monomer length of 0.4 nm[45] is 15.2 nm) was obtained when the block copolymer was assembled from a 50 % (v/v) mixture of DMF and methanol (Figure 4.13). Studies on binary mixtures of methanol and DMF have revealed that hydrogen bonding interactions and dipole association results in the formation of intermolecular complexes between the two solvents.[46-48] This new nanofiber morphology most likely consists of interdigitated fully stretched thiophene chains and occurs because the intermolecular complex between methanol and DMF interferes with the hydrogen bonding effect that typically yields the nanoribbon morphology.

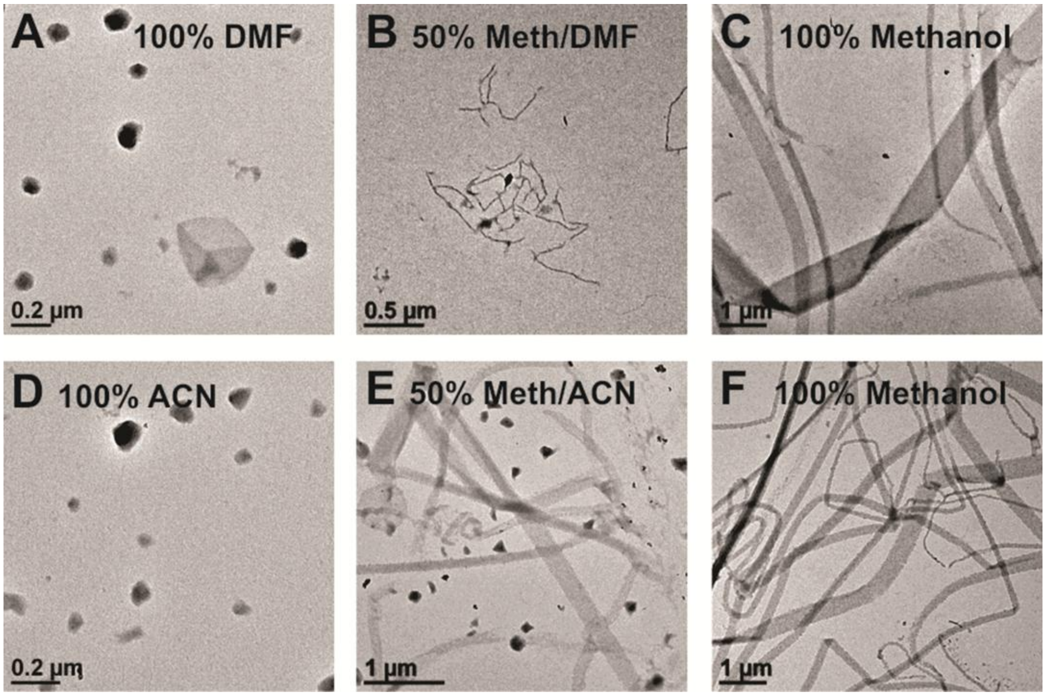

Figure 4.13. TEM images of 2 µM PTOTT$_{40}$-*b*-PEG$_{108}$ assemblies in water that were self-assembled from different common solvents; (A) 100 % DMF. (B) 50% DMF/methanol (v/v), (C) 100 % methanol, (D) 100 % acetonitrile, (E) 50% acetonitrile/methanol (v/v), and (F) 100 % methanol.

4.5.4 Effect of Temperature. The effect of temperature on the external structure of the PTOTT-*b*-PEG nanoribbons was investigated by heating the PTOTT-*b*-PEG nanoribbons in water for 15 hours in a 45 °C water bath. Interestingly, the TEM images of the nanoribbon structure after heating reveal a much more curved and snakelike nanoribbon structure when compared to the very straight nanoribbon structure found prior to heating the sample (Figure 4.14 B-C). The height of the nanoribbon does not change after heating, but the structure does become less flat and more curved. The optical properties of the nanoribbon structure did change after heating with a 52 nm red-shifted absorbance of the heated sample compared to the original sample (Figure 4.14 A), but the emission of the heated sample was similar to the spectra obtained prior to heating.

The width of heated curved nanoribbon was 156 ± 28 nm compared with the statistical width distribution prior to heating of 250 ± 139 nm. The smaller and more monodisperse widths of the nanoribbons after heating could be due to a compilation of factors. Heating the nanoribbons may have caused excess methanol or water entrapped in the nanoribbon structure to be expelled, thus resulting in a more compact structure and accounting for the change in width and optical properties. It is also possible that the rather large red-shift in the absorption after heating would indicate that the internal packing of the curved nanoribbons might have changed to a more compact planar structure after heating. The curved structure of the heated curved nanoribbons was retained after incubation for 30 days, thus indicating that the structure is retained once the sample is cooled to below room temperature. Furthermore, the rate of cooling was not found to have any effect on the structure, with slow cooling over the course of 5 hours yielding the same optical and morphological results as a sample that was quenched quickly in an ice water bath. This indicates that the curved nanoribbon morphology is stable and is not just a result of crystallization processes.

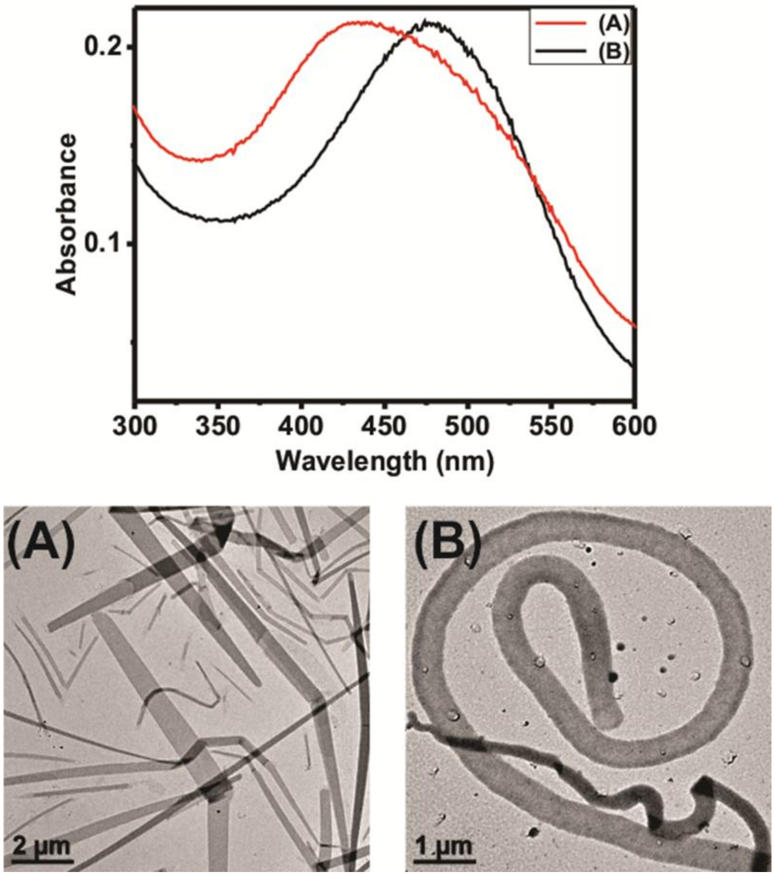

Figure 4.14. Absorption spectra and corresponding TEM images of 2 µM PTOTT-*b*-PEG block copolymer nanoribbon assemblies (A) before, and (B) after heating at 45° C for 15 hours.

4.5.5 Effect of Hydrophilic Block Length. The self-assembly characteristics of a block copolymer with a shorter hydrophilic block length PTOTT$_{40}$-*b*-PEG$_{63}$ was studied and compared to the self-assembly characteristics of the polymer with a slightly longer hydrophilic block, PTOTT$_{40}$-*b*-PEG$_{108}$. The TEM images and absorption characteristics of PTOTT$_{40}$-*b*-PEG$_{63}$ self-assembled from different common solvents are summarized in Figure 4.15. In general, the self-assembly behavior of PTOTT$_{40}$-*b*-PEG$_{63}$ behaves very similar to PTOTT$_{40}$-*b*-PEG$_{108}$ with polar aprotic solvents resulting in quasi-spherical micelle-like aggregates, and polar protic solvents such as methanol resulting in the nanoribbon formation. In Chapter 3, it was shown that rather slight changes in the hydrophilic length of PHT-*b*-PEG had a rather large effect on the length of the nanofibers that were formed. In this case, the PTOTT length is long enough that the hydrophobic interaction and hydrogen bonding interaction most likely dominates over the effect of hydrophilic block length.

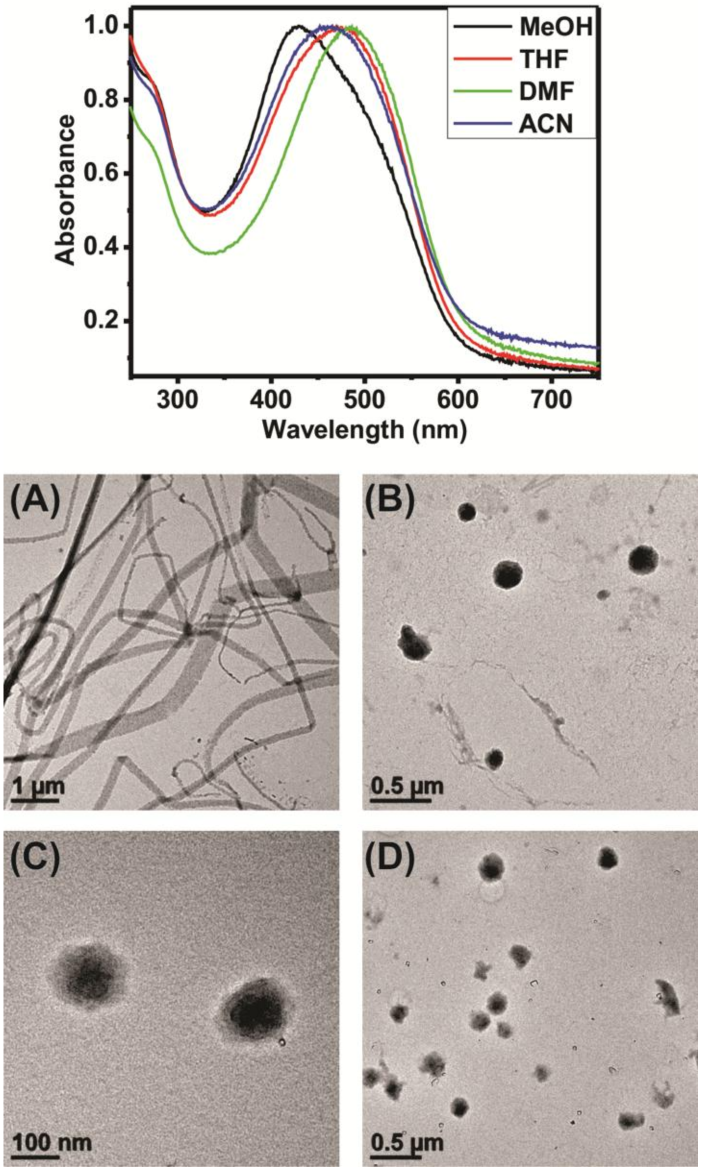

Figure 4.15. Absorption spectra and corresponding TEM images of PTOTT$_{40}$-*b*-PEG$_{63}$ assemblies in water that were self-assembled from different common solvents; (A) methanol (B) THF (C) DMF and (D) acetonitrile.

4.5.6 Comparison with PTOTT Homopolymer. The structure of PTOTT is such that the hydrophobic thiophene backbone and polar tetraethylene glycol side chains resembles an amphiphilic brush copolymer. Although the PTOTT homopolymer will not directly dissolve in an aqueous solvent, it can be self-assembled into aqueous solvents via slow-addition of water and dialysis into water from a common solvent. The absorbance characteristics and TEM images of the self-assembled morphologies of PTOTT homopolymers self-assembled from different common solvents are presented in Figure 4.16. The dominant morphology for self-assembled PTOTT homopolymer from both polar protic and polar aprotic solvents is micellar aggregates with rather red-shifted absorbances of ranging from 440 nm to 470 nm. The micellar morphology is most likely the dominant morphology irregardless of the common solvent because it allows for the hydrophobic thiophene to bury itself in the hydrophobic core of the micelle and avoid the unfavorable interaction with the polar aqueous solvent. Although quasi-spherical micelle-like aggregates are the dominant morphology, the structure formed from the common solvent THF shown in Figure 4.16 B does more closely resemble that of a vesicle structure and also has a blue-shifted absorbance peak at 420 nm which more closely matches that which is expected for a looser packing of polymer chains like those found in the nanoribbon and vesicle morphologies. Previous reports have shown that homopolymers can undergo self-assembly into stable aggregates such as vesicles if they possess sufficient amphiphilic character.[49] It is important to note that self-assembly of PTOTT homopolymers in polar protic solvents does not result in nanoribbon formation.

This means that the covalent attachment of PEG and its interaction with polar protic solvents is critical for the formation of nanoribbons.

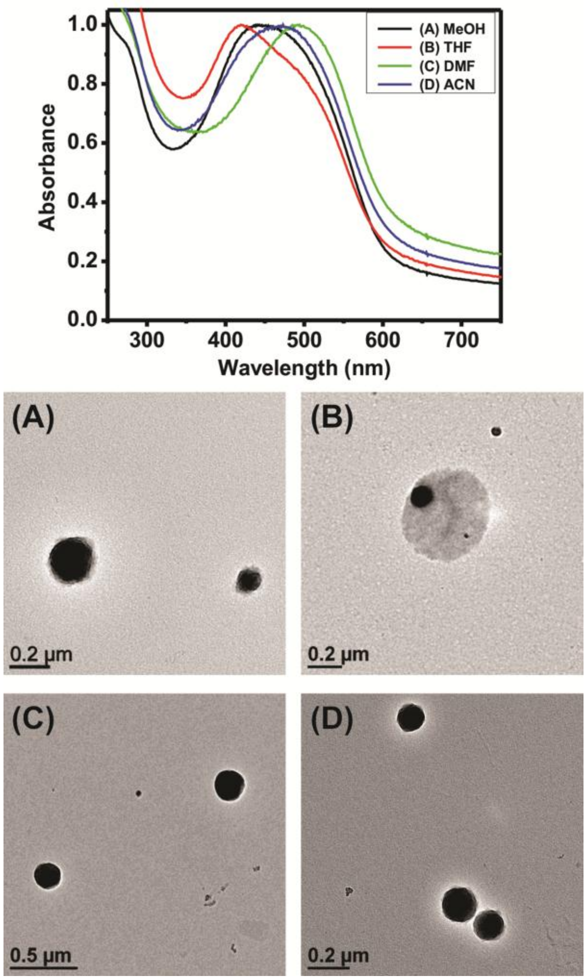

Figure 4.16. Absorption spectra and corresponding TEM images of 2 μM PTOTT$_{40}$ homopolymer assemblies in water that were self-assembled from different common solvents; (A) methanol, 443 nm (B) THF, 420 nm (C) DMF, 494 nm and (D) acetonitrile, 473 nm.

4.6 Conclusions.

As described above, the ability to control the molecular packing structure and the size of ordered domains is critical for fabricating high performance devices based on conjugated polymers. The self-assembly of PTOTT-*b*-PEG reported here generated various assembly structures including nanoribbons with elongated lateral dimensions reaching tens of micrometers. The formation of the distinctive nanoribbon structure was specifically formed due to combined energetic contributions from the conjugated pi-pi stacking interactions and the hydrogen bonding interaction between the polymers and the polar protic solvents. The nanoscale orientation of the nanoribbons was also tuned from a straight nanoribbon to a curved nanoribbon along with concurrent changes in the internal packing structure as evidence by optical measurements. This type of elongated nanoribbon structure has not been reported for amphiphilic conjugated block copolymers and could offer further insight into how internal packing structure affects the electronic properties of the conjugated block copolymer.

4.7 References

1. Tao, Y.; Ma, B.; Segalman, R. A., Self-Assembly of Rod-Coil Block Copolymers and Their Application in Electroluminescent Devices. *Macromolecules* 2008, 41, 7152-7159.
2. Palmer, L. C.; Stupp, S. I., Molecular Self-Assembly into One-Dimensional Nanostructures. *Acc. Chem. Res.* 2008, 41, 1674-1684.
3. Kim, J.-K.; Lee, E.; Jeong, Y.-H.; Lee, J.-K.; Zin, W.-C.; Lee, M., Two-Dimensional Assembly of Rod Amphiphiles into Planar Networks. *J. Am. Chem. Soc.* 2007, 129, 6082-6083.

4. Ryu, J.-H.; Hong, D.-J.; Lee, M., Aqueous Self-Assembly of Aromatic Rod Building Blocks. *Chem. Commun.* 2008, 1043-1054.

5. Patra, S. K.; Ahmed, R.; Whittell, G. R.; Lunn, D. J.; Dunphy, E. L.; Winnik, M. a.; Manners, I., Cylindrical Micelles of Controlled Length with a Π-Conjugated Polythiophene Core Via Crystallization-Driven Self-Assembly. *J. Am. Chem. Soc.* 2011, 133, 8842-5.

6. Lee, E.; Hammer, B.; Kim, J.-K.; Page, Z.; Emrick, T.; Hayward, R. C., Hierarchical Helical Assembly of Conjugated Poly(3-Hexylthiophene)-Block-Poly(3-Triethylene Glycol Thiophene) Diblock Copolymers. *J. Am. Chem. Soc.* 2011, 133, 10390-10393.

7. Iovu, M. C.; Jeffries-El, M.; Zhang, R.; Kowalewski, T.; McCullough, R. D., Conducting Block Copolymer Nanowires Containing Regioregular Poly(3-Hexylthiophene) and Polystyrene. *J. Macromol. Sci., Pure Appl. Chem.* 2006, 43, 1991-2000.

8. Kamps, A. C.; Fryd, M.; Park, S.-J., Hierarchical Self-Assembly of Amphiphilic Semiconducting Polymers into Isolated, Bundled, and Branched Nanofibers. *ACS Nano* 2012, 6, 2844-2852.

9. Wu, D.; Zhi, L.; Bodwell, G. J.; Cui, G.; Tsao, N.; Müllen, K., Self-Assembly of Positively Charged Discotic Pahs : From Nanofibers to Nanotubes. *Angew. Chem. Int. Ed.* 2007, 46, 5513-5516.

10. Guo, Y*., et al.*, Single-Crystal Microribbons of an Indolo 3,2-B Carbazole Derivative by Solution-Phase Self-Assembly with Novel Mechanical, Electrical, and Optical Properties. *Adv. Mater.* 2008, 20, 4835-4839.

11. Wang, M.; Mohebbi, A. R.; Sun, Y.; Wudl, F., Ribbons, Vesicles, and Baskets: Supramolecular Assembly of a Coil-Plate-Coil Emeraldicene Derivative. *Angew. Chem. Int. Ed.* 2012, 51, 6920-6924.

12. Kim, J.; Song, I. Y.; Park, T., Polymeric Vesicles with a Hydrophobic Interior Formed by a Thiophene-Based All-Conjugated Amphiphilic Diblock Copolymer. *Chem. Commun.* 2011, 47, 4697-9.

13. Oriol, L.; Sa, C.; Serrano, L.; Cicco, D.; Keller, P.; Li, M.-h., Self-Assembly of

Linear-Dendritic Diblock Copolymers : From Nanofibers to Polymersomes. *J. Am. Chem. Soc.* 2010, 132, 3762-3769.

14. Zubarev, E. R.; Pralle, M. U.; Sone, E. D.; Stupp, S. I., Self-Assembly of Dendron Rodcoil Molecules into Nanoribbons. *J. Am. Chem. Soc.* 2001, 123, 4105-4106.

15. Messmore, B. W.; Hulvat, J. F.; Sone, E. D.; Stupp, S. I., Synthesis, Self-Assembly, and Characterization of Supramolecular Polymers from Electroactive Dendron Rodcoil Molecules. *J. Am. Chem. Soc.* 2004, 126, 14452-14458.

16. Zhang, Y.; Dong, H.; Tang, Q.; Ferdous, S.; Liu, F.; Mannsfeld, S. C. B.; Hu, W.; Briseno, A. L., Organic Single-Crystalline P-N Junction Nanoribbons. *J. Am. Chem. Soc.* 2010, 132, 11580-11584.

17. Campaigne, E.; Tullar, B. F., 3-Thenyl Bromide - Thiophene, 3-Bromomethyl. *Organic Synthesis* 1953, 33, 96-98.

18. Ngwendson, J. N.; Atemnkeng, W. N.; Schultze, C. M.; Banerjee, A., A Convenient Synthesis of Symmetric 1,2-Diarylethenes from Arylmethyl Phosphonium Salts. *Organic Letters* 2006, 8, 4085-4088.

19. Koeckelberghs, G.; Vangheluwe, M.; Samyn, C.; Persoons, A.; Verbiest, T., Regioregular Poly(3-Alkoxythiophene)S: Toward Soluble, Chiral Conjugated Polymers with a Stable Oxidized State. *Macromolecules* 2005, 38, 5554-5559.

20. Jeffries-El, M.; Sauve, G.; McCullough, R. D., Facile Synthesis of End-Functionalized Regioregular Poly(3-Alkylthiophene)S Via Modified Grignard Metathesis Reaction. *Macromolecules* 2005, 38, 10346-10352.

21. Iovu, M. C.; Jeffries-El, M.; Sheina, E. E.; Cooper, J. R.; McCullough, R. D., Regioregular Poly(3-Alkylthiophene) Conducting Block Copolymers. *Polymer* 2005, 46, 8582-8586.

22. Liu, J.; Loewe, R. S.; McCullough, R. D., Employing Maldi-Ms on Poly(Alkylthiophenes):‚Äâ Analysis of Molecular Weights, Molecular Weight Distributions, End-Group Structures, and End-Group Modifications. *Macromolecules* 1999, 32, 5777-5785.

23. Szwarc, M.; Levy, M.; Milkovich, R., Polymerization Initiated by Electron Transfer to Monomer - a New Method of Formation of Block Polymers. *J. Am. Chem.*

Soc. 1956, 78, 2656-2657.

24. Hiki, S.; Kataoka, K., A Facile Synthesis of Azido-Terminated Heterobifunctional Poly(Ethylene Glycol)S for "Click" Conjugation. *Bioconjugate Chem.* 2007, 18, 2191-2196.

25. Campaigne, E. E.; Tullar, B. F., *Org. Synth.* 1953, 33, 96-98.

26. Zdyrko, B.; Varshney, S. K.; Luzinov, I., Effect of Molecular Weight on Synthesis and Surface Morphology of High-Density Poly(Ethylene Glycol) Grafted Layers. *Langmuir* 2004, 20, 6727-6735.

27. Brinkmann, M.; Wittmann, J. C., Orientation of Regioregular Poly(3-Hexylthiophene) by Directional Solidification: A Simple Method to Reveal the Semicrystalline Structure of a Conjugated Polymer. *Adv. Mater.* 2006, 18, 860-863.

28. Han, K.-H.; Lee, E.; Kim, J. S.; Cho, B.-K., An Extraordinary Cylinder-to-Cylinder Transition in the Aqueous Assemblies of Fluorescently Labeled Rod-Coil Amphiphiles. *J. Am. Chem. Soc.* 2008, 130, 13858-13859.

29. Battaglia, G.; Ryan, A. J., Bilayers and Interdigitation in Block Copolymer Vesicles. *J. Am. Chem. Soc.* 2005, 127, 8757-8764.

30. Danino, D.; Bernheim-Groswasser, A.; Talmon, Y., Digital Cryogenic Transmission Electron Microscopy: An Advanced Tool for Direct Imaging of Complex Fluids. *Colloids and Surfaces a-Physicochemical and Engineering Aspects* 2001, 183, 113-122.

31. Tung, Y.-C.; Wu, W.-C.; Chen, W.-C., Morphological Transformation and Photophysical Properties of Rod-Coil Poly[2,7-(9,9-Dihexylfluorene)]-Block-Poly(Acrylic Acid) in Solution. *Macromol. Rapid Commun.* 2006, 27, 1838-1844.

32. Zhang, L. F.; Eisenberg, A., Crew-Cut Aggregates from Self-Assembly of Blends of Polystyrene-B-Poly(Acrylic Acid) Block Copolymers and Homopolystyrene in Solution. *J. Polym. Sci., Part B: Polym. Phys.* 1999, 37, 1469-1484.

33. Zhang, L.; Eisenberg, A., Thermodynamic Vs Kinetic Aspects in the Formation and Morphological Transitions of Crew-Cut Aggregates Produced by Self-Assembly of Polystyrene-B-Poly(Acrylic Acid) Block Copolymers in Dilute Solution. *Macromolecules* 1999, 32, 2239-2249.

34. Dormidontova, E. E., Role of Competitive Peo−Water and Water−Water Hydrogen Bonding in Aqueous Solution Peo Behavior. *Macromolecules* 2002, 35, 987-1001.

35. Chang, H.-Y.; Lin, Y.-L.; Sheng, Y.-J.; Tsao, H.-K., Multilayered Polymersome Formed by Amphiphilic Asymmetric Macromolecular Brushes. *Macromolecules* 2012, 45, 4778-4789.

36. Zhang, J. X.; Qiu, L. Y.; Zhu, K. J., Solvent Controlled Multi-Morphological Self-Assembly of Amphiphilic Graft Copolymers. *Macromol. Rapid Commun.* 2005, 26, 1716-1723.

37. Ge, Z.; Liu, S., Supramolecular Self-Assembly of Nonlinear Amphiphilic and Double Hydrophilic Block Copolymers in Aqueous Solutions. *Macromol. Rapid Commun.* 2009, 30, 1523-32.

38. Shen, H.; Eisenberg, A., Morphological Phase Diagram for a Ternary System of Block Copolymer Ps 310 -B-Paa 52 / Dioxane / H 2 O. *Society* 1999, 9473-9487.

39. Yu, Y. S.; Zhang, L. F.; Eisenberg, A., Morphogenic Effect of Solvent on Crew-Cut Aggregates of Apmphiphilic Diblock Copolymers. *Macromolecules* 1998, 31, 1144-1154.

40. Bhargava, P.; Zheng, J. X.; Li, P.; Quirk, R. P.; Harris, F. W.; Cheng, S. Z. D., Self-Assembled Polystyrene-Block-Poly(Ethylene Oxide) Micelle Morphologies in Solution. *Macromolecules* 2006, 39, 4880-4888.

41. Shankar, R.; Klossner, R. R.; Weaver, J. T.; Koga, T.; van Zanten, J. H.; Krause, W. E.; Colina, C. M.; Tanaka, F.; Spontak, R. J., Competitive Hydrogen-Bonding in Polymer Solutions with Mixed Solvents. *Soft Matter* 2009, 5, 304.

42. Kinugasa, S.; Fudagawa, N.; Koga, Y., Aggregative Behavior of Poly(Ethy1ene Oxide) in Water and Methanol. *Macromolecules* 1994, 27, 6889-6892.

43. Edmondson, S.; Nguyen, N. T.; Lewis, A. L.; Armes, S. P., Co-Nonsolvency Effects for Surface-Initiated Poly(2-(Methacryloyloxy)Ethyl Phosphorylcholine) Brushes in Alcohol/Water Mixtures. *Langmuir* 2010, 26, 7216-26.

44. Castelletto, V.; Hamley, I. W.; Harris, P. J. F.; Olsson, U.; Spencer, N., Influence of the Solvent on the Self-Assembly of a Modified Amyloid Beta Peptide Fragment. I.

Morphological Investigation. *J. Phys. Chem. B* 2009, 113, 9978-87.

45. Samitsu, S.; Shimomura, T.; Heike, S.; Hashizume, T.; Ito, K., Effective Production of Poly(3-Alkylthiophene) Nanofibers by Means of Whisker Method Using Anisole Solvent: Structural, Optical, and Electrical Properties. *Macromolecules* 2008, 41, 8000-8010.

46. Ruckenstein, E.; Shulgin, I., Effect of a Third Component on the Interactions in a Binary Mixture Determined from the Fluctuation Theory of Solutions. *Fluid Phase Equilib.* 2001, 180, 281-297.

47. Stangret, J.; Kamieńska-Piotrowicz, E.; Szymańska-Cybulska, J., Analysis of Spectral Data by Complementary Methods. Inspection of the Molecular Complex in N,N-Dimethylformamide-Methanol Mixtures. *Spectrochim. Acta, Pt. A: Mol. Spectrosc.* 2005, 61, 3043-50.

48. Unger, M.; Harnacke, B.; Noda, I.; Siesler, H. W., Solvent Interactions in Methanol/N, N-Dimethylamide Binary Systems Studied by Fourier Transform Infrared-Attenuated Total Reflection (Ft-Ir/Atr) and Two-Dimensional Correlation Spectroscopy (2d-Cos). *Appl. Spectrosc.* 2011, 65, 892-900.

49. Blanazs, A.; Armes, S. P.; Ryan, A. J., Self-Assembled Block Copolymer Aggregates: From Micelles to Vesicles and Their Biological Applications. *Macromol. Rapid Commun.* 2009, 30, 267-277.

Chapter 5: Bioconjugated Nanostructures of Semiconducting Block Copolymer

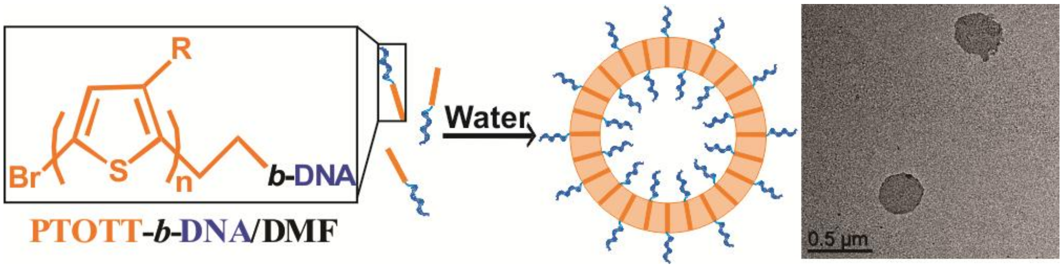

Herein, we describe the synthesis and self-assembly of amphiphilic semiconducting polymers composed of a poly(alkoxythiophene) derivative (i.e., poly(tetra-oxo-tridecanyl-thiophene)) and oligonucleotides. These functional bioconjugated polymers combine the excellent optoelectronic properties of semiconducting polymers with the bio-recognition properties and sequence programmability of DNA. This method offers a new approach to forming semiconducting nanostructures with controllable geometries by self-assembly and to interface nanomaterials with biological molecules. Due to the amphiphilicity of the molecule and the π–stacking of the rigid polythiophene, they self-assembled in aqueous solutions into distinct nanostructures which resulted in photoluminescence quenching of the semiconducting polymers.

5.1 Introduction

Polymer bioconjugates are composed of synthetic macromolecules that are covalently linked to biological moieties. The biological components can range in size from smaller monomers such as amino acids and sugars to larger oligomers such as oligodeoxynucleotides (ODN) and oligopeptides and to even more complex systems such as proteins, DNA, and enzymes. The systems composed of higher complexity proteins and enzymes are mainly looked at for their biological properties such as cell regulation, signal transduction, and immune responses; rather than for a structural purpose. On the other hand, the biological building blocks such as ODNs and oligopeptides are particularly interesting because they have the specific ability to self-organize and can be used in conjunction with synthetic polymers to create highly ordered synthetic nanomaterials.[1]

The development in the research of new polymerization methods (ATRP, RAFT, GRIM) and optimization of these synthetic techniques has led to a plethora of synthetic polymers that actually far exceeds the biological moiety toolbox.[2] The choice of the synthetic polymer for bioconjugate systems also yields numerous complementary properties that can yield a highly responsive biohybrid structure. Some of the functional properties of polymers include: biodegradability, stimuli sensitivity (pH, temperature, light irradiation, chemical environment), biocompatibility, conductivity and mechanical strength.[3, 4]

DNA-based polymer hybrids are a new emerging class of advanced functional polymers materials that are expected to exhibit a high level of structural control and specific biorecognition.[5, 6] Some of the DNA block copolymers synthesized by other research groups have been examined for possible applications such as gene therapy[7, 8], nanoreactors for DNA template organic reactions[9], and drug delivery[10]. On the other hand, conjugated polymers have unique optoelectronic properties and high extinction coefficients and are one of the most promising materials for a multitude of applications such as electrochromic devices, energy storage, chemical sensors, and biomedical applications.[11] Therefore, utilizing these distinct functions of conjugated polymers should delve into a new realm of applications that combine the optoelectronic properties of the conjugated polymer with the self-recognition and sequence programmability of the DNA strand. In addition there is a need for more fundamental studies on the role of hydrophobic blocks of DNA amphiphiles on determining the morphology of aggregates, their size, stability and hybridization into micelles.[12]

Previous work in the Park lab has demonstrated a DNA-*b*-PS/nanoparticle hybrid structure with enhanced DNA binding properties.[13] Other groups have built higher ordered structures of DNA block copolymer amphiphiles with enhanced melting properties through sequence specific hybridization with other nanomaterials.[14] Hermann *et al.* synthesized DNA-*b*-PPO which is a low Tg block copolymer that has been shown to change from spherical to rodlike aggregates upon hybridization with a longer repetitive complementary DNA strand.[15] Remarkably, these rodlike aggregates showed a significantly higher cellular uptake, thus demonstrating that control over the morphology of the DNA-block copolymer aggregate will be crucial towards gene delivery applications.[16] Towards this end, using a DNA conjugated block copolymer should result in very distinct morphologies compared to those of the typical coil DNA-block copolymer systems due to the added energetic contributions from the tendency towards liquid crystalline ordering of the rigid conjugated polymer.[17] The DNA conjugated block copolymer also affords a new opportunity to build higher ordered supramolecular structures by utilization of the π-π packing interaction of the conjugated backbone.

A number of groups have reported on the synthesis of conjugated rod-coil block copolymers.[18-20] However, very few groups have looked at the covalent attachment of conjugated polymer to DNA. Leclerc *et al.* utilized positively charged poly(thiophene) based DNA detection systems (noncovalent systems) centered on the conformational perturbations of the polymer chains and the resultant color change.[21, 22] Also, Kim *et al*. reported the synthesis of a DNA conjugated polymer hybrid that contains charged side chains to give it water solubility and used the signal amplifying property of the conjugated polymer to detect trace amounts of target DNA.[23] The first published example of a conjugated DNA block copolymer, poly(9,9-di-n-octylfluorenyl-2,7-diyl) (PFO-*b*-DNA), was very recently published.[24] In this work the PFO-*b*-DNA was used to functionalize SWNTs and subsequently facilitate sequence specific assembly in nanoelectronic devices. Although this work provides a very interesting approach towards sequence specific directing of carbon nanotubes, it does not allude to the self-assembly properties of the DNA conjugated block copolymer in it of itself. In fact, there are very little fundamental studies on the role of hydrophobic blocks in DNA amphiphiles on determining the structure, size, or stability of aggregates.

The DNA conjugated block copolymer system presented herein, PTOTT-*b*-DNA, is therefore one of the first reported amphiphilic conjugated polymer hybrids. This conjugated DNA block copolymer system is interesting because it is capable of exploiting both the recognition properties of the DNA and the responsiveness of the polymer to tailor the structural and physiochemical properties of the system. Most reports of DNA block copolymer hybrids self-assembly into micellar structures.[1, 14, 25] Herein, we present the self-assembly of a DNA conjugated block copolymer into more complex vesicle nanostructures which retain the binding capabilities of the DNA block and the structural function of the conjugated block. The tunability and adaptability of the system is also demonstrated via encapsulation of nanoparticles and salt dependent morphological transitions.

5.2 Experimental Section

5.2.1 Synthesis and Characterization of PTOTT-Phosphoramidite. The di-brominated tetra-oxo-tridecanyl-thiophene monomer was synthesized using modified literature procedures[26, 27,28] as was described in detail in Chapter 4.2.1 – 4.2.3 of this dissertation. Allyl-terminated PTOTT was synthesized following a modified GRIM synthesis method of the corresponding monomers followed by hydroboration/oxidation to convert the allyl end-groups to hydroxyl groups.[29] The PTOTT homopolymers and the end-functionalities were confirmed by NMR and the molecular weight of the polymers determined by GPC. The hydroxyl-terminated PTOTT was then reacted with chlorophosphoramidite in the presence of an amine to yield the corresponding phosphoramidite-PTOTT derivatives (Scheme 6).

Scheme 6. Synthesis of PTOTT-Phosphoramidite.

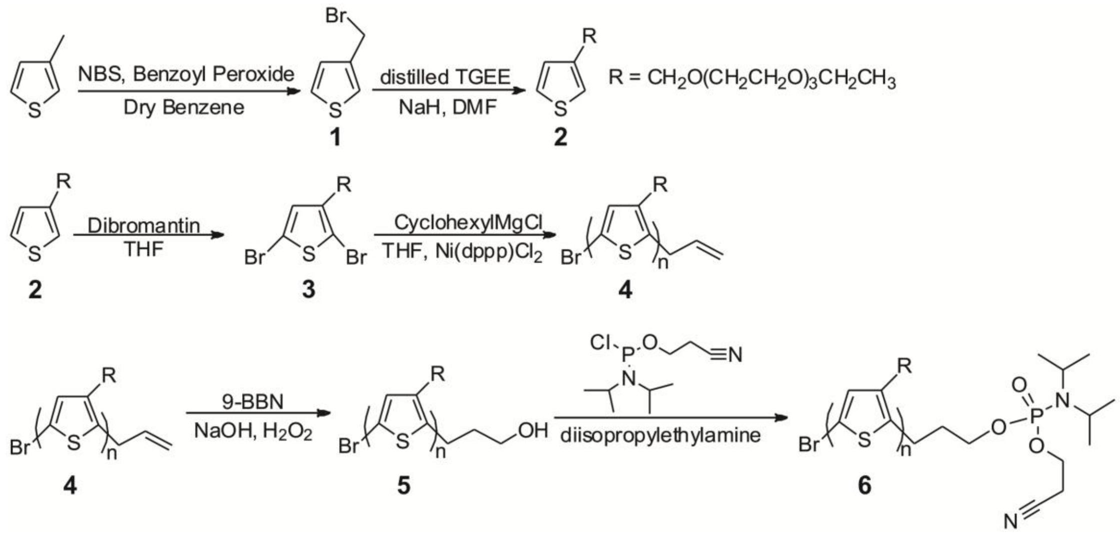

5.2.1.1 Synthesis of allyl-terminated poly(tetra-oxo-tridecanyl-thiophene) (PTOTT-allyl) (4).

2,5-dibromo-TOTT (1.93 g, 4.47 mmol) was weighed into a 250 mL 3-neck round bottom flask and was dissolved in freshly distilled THF (100 mL). The reaction set-up was flushed with argon. Cyclohexylmagnesium chloride (2.0 M / diethyl ether, 4.79 mL, 9.58 mmol) was added into the flask and the reaction was allowed to proceed for 30 minutes. Solid Ni(dppp)Cl_2 was then added under high argon flow, and the mixture was allowed to stir for another ten minutes. End-group termination was then achieved by adding allylmagnesium bromide (1.0 M/ diethyl ether, 2.40 mL, 2.40 mmol). The termination reaction was allowed to proceed for an additional 30 minutes before it was quenched with hexanes (20 mL). The reaction mixture was then concentrated using rotary evaporation and then the product was precipitated into hexanes, filtered, and purified by soxhlet extraction with hexanes and chloroform. The solvent was removed by rotary evaporation and the blood-red product was dried under vacuum overnight to yield 1.02 g (83%) of PTOTT-allyl.

1H NMR (500 MHz, $CDCl_3$): δ_H 1.17 (t, J = 6.97 Hz, 3H), 3.49 (q, J = 6.92 Hz, 2H), 3.55 (t, J = 4.61 Hz, 2H), 3.61-3.68 (m, 8H), 3.72 (s, 2H), 4.65 (s, 2H), 5.21 (m), 5.95 (m), 7.24 (s, 1H); GPC: Mn = 22000, Mn(corrected[30]) = 11000, PDI = 1.17.

5.2.1.2 Synthesis of hydroxyl-terminated poly(tetra-oxo-tridecanyl-thiophene) (PTOTT-hydroxyl) (5).

Conversion of the allyl end-group to the hydroxyl end-group was achieved following a modified literature procedure.[19] In a typical experiment, PTOTT-allyl (1.02 g, 0.09 mmol) was added to a 250 mL 3-neck round bottom flask and was dissolved in freshly distilled THF (70 mL). The reaction set-up was flushed with argon. 9-Borabicyclo(3.3.1)nonane (9-BBN) (1.8 mL, 0.9 mmol) was added into the flask and the reaction was allowed to proceed for 24 hours at 40°C. 6 M NaOH (0.9 mL) was then added to the reaction flask and the reaction solution was mixed for another 15 minutes. The solution was then cooled to room temperature, upon which 33 % hydrogen peroxide (0.9 mL) was added to the reaction flask. The reaction then proceeded for another 24 hours at 40°C. The reaction solution was then dried down using rotary evaporation. The solid product was redissolved into a minimal amount of chloroform (1 – 2 mL), precipitated into hexanes, filtered and then dried. The dried product was then washed with DI water and then the blood-red product was dried under vacuum overnight to yield 0.95 g (93%) of PTOTT-hydroxyl.

1H NMR (500 MHz, $CDCl_3$): δ_H 1.17 (t, J = 6.97 Hz, 3H), 1.94 (m), 3.49 (q, J = 6.92 Hz, 2H), 3.55 (t, J = 4.61 Hz, 2H), 3.61-3.68 (m, 8H), 3.72 (s, 2H), 3.95 (t), 4.65 (s, 2H), 7.24 (s, 1H); GPC: Mn = 22000, Mn(corrected[30]) = 11000, PDI = 1.17.

5.2.1.3 Synthesis of phosphoramidite-terminated poly(tetra-oxo-tridecanyl-thiophene) (PTOTT-phosphoramidite) (6).

The synthesis of PTOTT-phosphoramidite was synthesized following a modified literature procedure.[14, 31] In a typical experiment, PTOTT-hydroxyl (150 mg, 0.015 mmol) was added to a 25 mL 3-neck round-bottom flask. The reaction flask was vacuumed and purged with argon (x 3). 10 mL of freshly distilled THF was added to the reaction flask followed by anhydrous diisopropylethylamine (0.1 mmol, 0.045 mL) and then 2-cyanoethyl N,N-diisopropylchlorophosphoramidite (0.1 mmol, 0.058 mL). The reaction proceeded for 2 hours under argon. The product was then dried under vacuum on the schlenk line and then redissolved into 10 mL of anhydrous DMF. The crude PTOTT-phosphoramidite product (119 mg, 80% yield) was used in the DNA-coupling synthesis (within 2 hours of being synthesized) without further purification.

5.2.2 Synthesis and Characterization of PTOTT-*b*-DNA. PTOTT-*b*-DNA was synthesized by coupling the activated PTOTT-phosphoramidite to the 5’ end of the DNA which was synthesized on a solid support using a DNA synthesizer. After a series of washing steps to remove unreacted homopolymer, the protecting groups on the DNA were deprotected and the PTOTT-*b*-DNA product was cleaved from the solid support (Scheme 7). At this step, failure DNA strands and unreacted DNA were washed away by direct dissolution into water followed by centrifugation to isolate PTOTT-*b*-DNA aggregates.

Scheme 7. Synthesis of PTOTT-*b*-DNA.

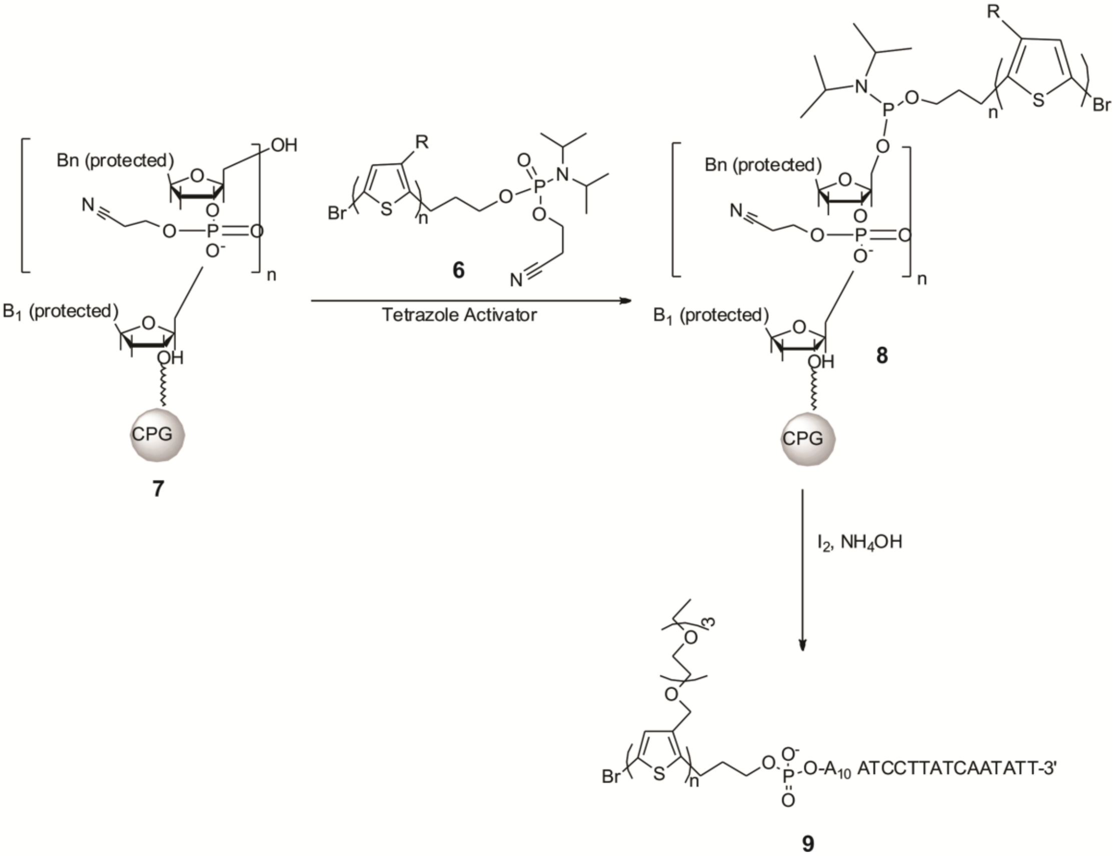

5.2.2.1 Solid State DNA Synthesis (7). A 10 μmol scale synthesis of oligonucleotide strand 5 ′ - A_{10} ATCCTTATCAATATT-3 ′ was carried out using a standard solid state DNA synthesis on an ABI instrument.

5.2.2.2 Synthesis of PTOTT-*b*-DNA **(9).** Block copolymers composed of an oligonucleotide block (DNA) and a PTOTT block were synthesized by coupling PTOTT-phosphoramidite to oligonucleotide grown on 1000 Å controlled pore glass (CPG) beads following modified literature procedures.[14, 31] PTOTT-phosphoramidite was activated with a 0.5 M tetrazole activator solution and was then immediately added via the cannula transfer technique under argon flow to a 50 mL 3-neck round bottom flask containing CPG-DNA in 2 mL of anhydrous acetonitrile. The coupling reaction proceeded under argon for 10 hours. The CPG beads were then washed with anhydrous DMF and acetonitrile to remove the uncoupled PTOTT. The phosphate group on the DNA was then oxidized with a 0.02 M solution of I_2/THF followed by a series of washes with acetonitrile. The PTOTT-*b*-DNA product and failure DNA strands were then deprotected and cleaved from the CPG beads via incubation in concentrated ammonium hydroxide at 55°C for 6 hours. Excess DMF was then added to the filtered ammonium hydroxide solution followed by an extraction with chloroform and water to isolate the DNA-*b*-PTOTT product in the organic phase (DNA failure strands localize to the aqueous phase). The organic phase was dried over anhydrous $MgSO_4$ and then dried under argon flow to yield the PTOTT-*b*-DNA product as an orange solid (25 % yield).

5.2.3 Materials, Measurements and Instrumentation. All reactions were carried out using standard Schlenk techniques under an inert atmosphere of pre-purified nitrogen or argon, using oven-dried glassware. Commercial chemicals 3-methylthiophene, sodium hydride, 1,3-dibromo-5,5'-dimethylhydantoin (dibromantin), [1,3-bis(diphenylphosphino)propane]dichloronickel(II) (Ni(dppp)Cl_2), cyclohexylmagnesium chloride, vinylmagnesium bromide, benzene, and anhydrous *N*,*N*-dimethylformamide (DMF) were purchased from Aldrich and used without further purification. *N*-Bromosuccinimide (Aldrich, 99%) was recrystallized from water, dried under vacuum, and stored over Drierite. Triethylene glycol monoethyl ether (TGEE) (Aldrich, tech.) was dried and vacuum-distilled over phosphorus pentoxide. Tetrahydrofuran was freshly distilled from sodium/benzophenone to ensure anhydrous conditions, and all other reagents were used without further purification.

IR spectra were obtained on a Perkin-Elmer system 2000 FTIR spectrometer. Electronic absorption spectra were acquired on an Agilent 8453 spectrophotometer. Photoluminescence spectra were acquired on a Spex Fluorolog 3 utilizing a R928 PMT detector. Proton NMR spectra were obtained on a Bruker-DMX500 interfaced to an Aspect 3000 computer in $CDCl_3$ solvent at ambient temperature. TEM was performed on a JEOL 1400 electron microscope operating at 120 kV accelerating voltage. GPC measurements were carried out at room temperature at a flow rate of 1.0 mL/min on a Shimadzu LC-10AT liquid chromatography system equipped with a series of two PLgel 10μm 10E6A columns, an SPD-10AVvp absorbance UV/VIS detector, and a refractive index detector (RID-10A) calibrated against linear polystyrene standards in THF.

Dynamic light scattering (DLS) measurements were taken on a Malvern Zetasizer Nano Series. Matrix assisted laser desorption ionization time-of-flight mass spectrometry (MALDI-TOF/TOF MS) spectra were obtained on a Bruker Flex Series MALDI-TOF/TOF MS. Spectra were recorded in the positive-ion reflectron mode with an accelerating voltage of 20 kV. The MALDI samples were prepared via the sandwich method by first depositing 1 μL of a 40 mg/mL DCTB matrix chloroform solution, followed by the deposition of 1 μL of a 1 mg/mL PTOTT chloroform solution on top of the matrix, and finally depositing another 1 μL of a 40 mg/mL *trans*-2-[3-(4-*tert*-Butylphenyl)-2-methyl-2-propenylidene]malononitrile (DCTB) matrix chloroform solution on top of the sample. After each of the solutions (1 μL) were deposited on the stainless steel sample target they were then air dried prior to the addition of the next solution. Oligonucleotides were synthesized in a 10.0 μmol scale on an automated DNA synthesizer (ABI, Applied Biosystems, Inc.). The purity of PTOTT-*b*-DNA was analyzed by polyacrylamide gel electrophoresis (PAGE) using a 15 % polyacrylamide gel at 100 V for 60 min. The gels were stained with ethidium bromide and imaged using an Amersham Biosciences Storm 860 phosphorimager.

5.3 Synthesis and Characterization of PTOTT-*b*-DNA

One of the greatest challenges in the preparation of biopolymer hybrids is that efficient coupling yields using phosphoramidite chemistry requires hydrophobic polymers to be soluble in more polar solvents such as acetonitrile.[32] Fulfilling the polar solubility requirement for conjugated polymer can be rather difficult because most conjugated polymers tend to be rather hydrophobic and are not typically soluble in such polar solvents. Towards this end, a modified synthetic procedure[26, 29, 33] was used to synthesize an acetonitrile soluble poly(alkoxythiophenes) derivative; poly(tetra-oxo-tridecanyl-thiophene) (PTOTT). The tetraethylene glycol side chains impart enough polarity to the conjugated polymer and allows for sufficient solubility in typical polar solvents such as acetonitrile and methanol, thus allowing for efficient coupling yielding.

A conjugated DNA block copolymer, PTOTT-*b*-DNA was synthesized by coupling a short 25 base pair DNA chain (5′-A_{10}ATCCTTATCAATATT-3′) to a hydroxyl-functionalized PTOTT using standard phosphoramidite chemistry. Allyl-terminated PTOTT was synthesized following a modified GRIM synthesis method of the corresponding monomers followed by hydroboration/oxidation to convert the vinyl end-groups to hydroxyl groups.[29] The PTOTT homopolymers and the end-functionalities were confirmed by NMR and the molecular weight of the polymers determined by GPC. The hydroxyl-terminated PTOTT was then reacted with chlorophosphoramidite to yield the corresponding phosphoramidite-PTOTT derivatives (Scheme 6). The activated PTOTT-phosphoramidite was then coupled to the 5′ end of the ODN which was synthesized on a solid support using a DNA synthesizer. After a series of washing steps to remove unreacted PTOTT homopolymer, the phosphate groups on the DNA were oxidized and the PTOTT-*b*-DNA product was cleaved from the solid support (Scheme 7). At this step, failure DNA strands were washed away by direct dissolution into water followed by centrifugation to isolate PTOTT-*b*-DNA aggregates. The DNA conjugated block copolymer $PTOTT_{25}$-*b*-DNA was successfully synthesized in a relatively high yield of 20 %.

The successful synthesis of $PTOTT_{25}$-*b*-DNA was confirmed by DNA gel electrophoresis as shown in Figure 5.1. Gel electrophoresis is an experimental technique that uses an electric potential to cause migration of charged samples through the gel based on their charge density and molecular weight. The ds-DNA-*b*-PTOTT sample in Lane 1 has a lower gel shift then the ds-DNA control in Lane 2 of the gel. Therefore, the higher MW of the ds-DNA-*b*-PTOTT along with the aggregated nature and increased charge of the ds-DNA-*b*-PTOTT results in smaller migration through the gel and confirms that all of the failure DNA strands were removed in the purification procedure described above. Further confirmation that the DNA was covalently attached to the polymer was also verified by self-assembly and hybridization studies as will be described in the next section.

Figure 5.1. 15 % polyacrylamide gel stained with ethidium bromide; Lane 1: double stranded DNA-*b*-PTOTT block copolymer, Lane 2: double stranded DNA control.

5.4. Self-Assembly of PTOTT-*b*-DNA

5.4.1. Morphology and Optical Properties. The chemical structure of PTOTT-*b*-DNA has many unusual features that distinguish it from more typical coil-type DNA block copolymers. In particular, the PTOTT moiety is not only a conjugated polymer, but it is also a conjugated polymer with structural characteristics reminiscent of an amphiphilic conjugated brush copolymer due to the hydrophilic oligomeric polar ethylene glycol side chains attached to the conjugated thiophene backbone of the polymer. Importantly, the PTOTT polymer still retains the desirable optoelectronic properties found in more structurally typical poly(alkylthiophenes) that have found applications in organic light electroluminescent diodes, solar cells, and photovoltaic cells.[34]

The PTOTT-*b*-DNA polymer was self-assembled into a distinct vesicle structure by the slow addition of water to a solution of the polymer in DMF followed by subsequent dialysis into water (Figure 5.2 A). The TEM images in Figure 5.2 B-C shows the well-defined vesicle structure with a width of 218 ± 80 nm by TEM and a hydrodynamic diameter of 208 ± 44 by DLS. The internal composition of the vesicle walls is most likely composed of the rigid interdigitated thiophene segments packed in an oriented radial arrangement in order to maximize the contact of the charged hydrophilic DNA segments with water.

The distinct vesicle structure of PTOTT-*b*-DNA is notable because it has not been widely reported for other DNA block copolymers and is most likely a direct result of the pi-pi stacking interaction of the rigid thiophene backbone of the PTOTT block. Amphiphilic block copolymers are known to form various structures such as micelles, vesicles, bilayers, or rod-like micelles.[35] However, previous reports of DNA block copolymers are typically composed of coil-like hydrophobic blocks that tend to self-assemble into micelles in aqueous solutions.[14, 36] The vesicle morphology has only been reported for one other DNA block copolymer system, polybutadiene-*b*-DNA, which is also considered a rigid rod.[37, 38] In general, other biocompatible vesicles, such as PEG-*b*-Poly(caprolactone) and PEG-*b*-poly(lactide), are being looked at for applications such as the in-vivo delivery of drugs, gene's and other active agents.[39]

The DMF solution of well-dissolved PTOTT-*b*-DNA absorbs at 450 nm and is highly fluorescent as shown pictorially in Figure 5.3 A and in the photoluminescence (PL) spectra in Figure 5.3 B. However, upon self-assembly into vesicles in water, via the slow addition/dialysis method, the fluorescence of the conjugated PTOTT chains becomes efficiently quenched. The absorbance of PTOTT-*b*-DNA vesicles shows a peak at 260 nm arising from the DNA[40] and a peak at 480 nm arising from the PTOTT (Figure 5.3 A**)** The absorbance of the PTOTT-*b*-DNA vesicles shown in Figure 5.3 A is red-shifted compared to the relative optical properties of PTOTT-*b*-PEG in DMF. This indicates that the PTOTT chains in the vesicle structure are tightly packed in a planar arrangement that causes efficient PL quenching due to intermolecular interactions.[41]

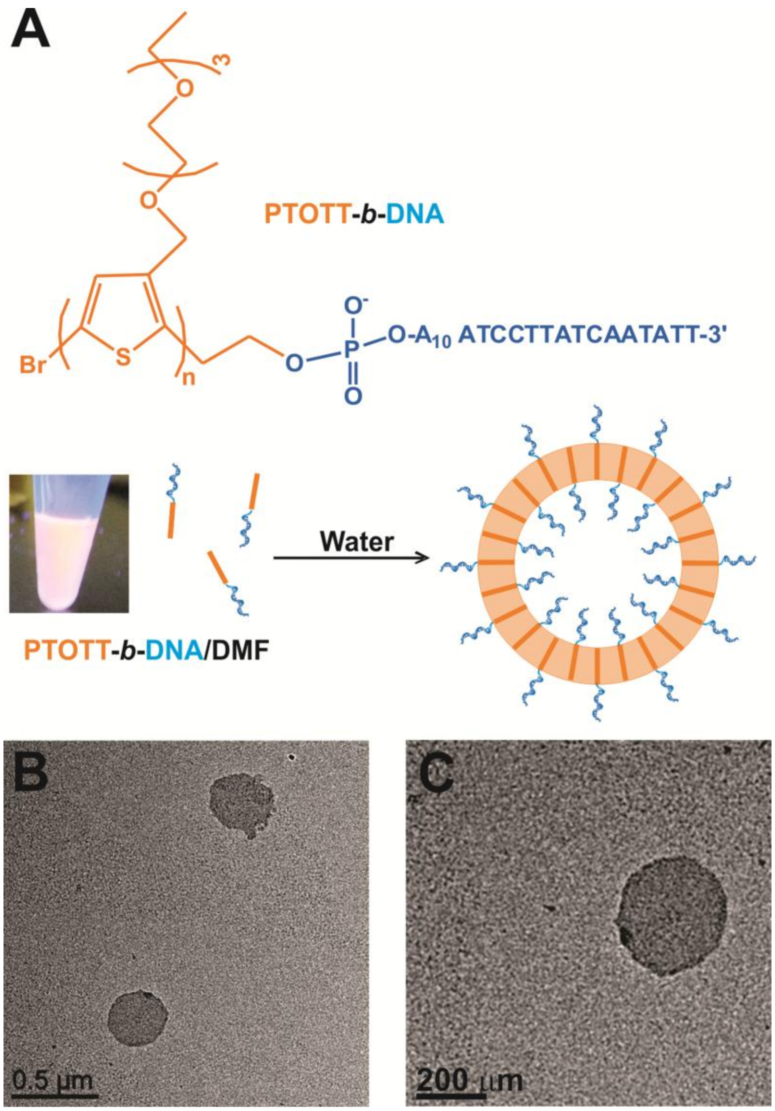

Figure 5.2. (A) Chemical structure of PTOTT-*b*-DNA and schematic depiction of the self-assembly of PTOTT-*b*-DNA into vesicles. (B,C) TEM images of PTOTT-*b*-DNA vesicles.

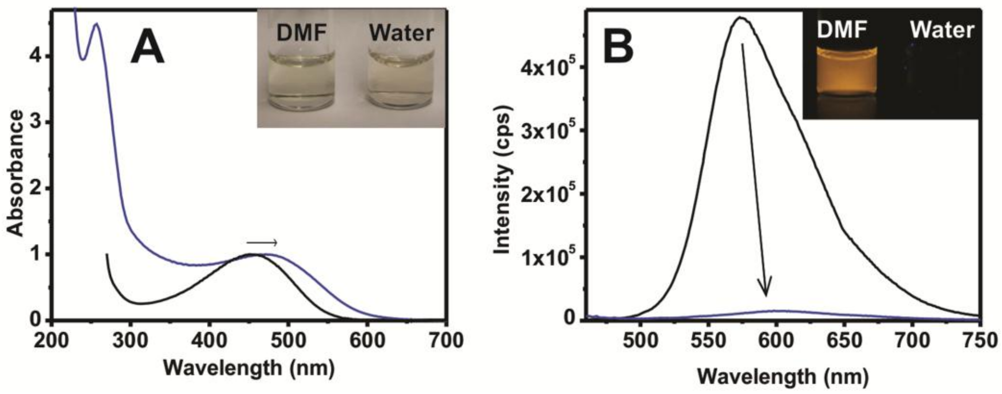

Figure 5.3. (A) Absorbance and (B) PL spectra of 3.5 μM of PTOTT-*b*-DNA dissolved in DMF (black), and self-assembled into vesicles in water (blue). PL spectra were collected using an excitation wavelength of 440 nm. Pictures of PTOTT-*b*-DNA solutions under ambient light (top-left) and under UV light (top-right) are given above the spectra.

5.4.2 Effect of Concentration. The initial concentration of PTOTT-*b*-DNA in DMF had a rather dramatic effect on its subsequent self-assembled structure in water. With increasing concentration, the block copolymer morphology evolved from a rod-like layered structure to a vesicle structures with a vesicle size that further increased with increasing polymer concentrations (Figure 5.4). The average diameter of vesicles as measured by TEM analysis increased from 218 ± 80 nm at 4 μM concentration, to 468 ± 159 nm at 7 μM concentration, and finally to a dual distribution of 1087 ± 230 nm and 2490 ± 940 nm at a 20 μM concentration of PTOTT-*b*-DNA. The vesicle structure seems to be the most stable morphology over a rather large concentration range spanning 4-20 μM. At lower polymer concentrations of 1 μM, the PTOTT-*b*-DNA has a much lower aggregation number and adopts a rod-like lamellae structure. As the aggregation number of the polymer increases, the vesicle structure is the most favorable morphology as it serves to lowers the total free energy of the system by reducing the interfacial energy between the core and the solvent.

The effect of block copolymer concentration on morphology is typically associated with an increased aggregation number of the polymer which is accommodated by a reduction of the stretching energy of the core via the adoption of lower curvature morphologies such as bilayer structures.[42] Other block copolymer systems such as PS-*b*-PAA are known to change from spheres, to rods, to vesicles, and finally to bilayers with increasing concentration in order to relieve the stretching energy of the core.[43] In this case, the effect of concentration on the self-assembly process is complicated by the rigidity and pi-pi stacking interaction along with the amphilicity of the PTOTT segment of the PTOTT-*b*-DNA polymer; therefore yielding morphological trends that are not typically observed for coil-coil polymers.

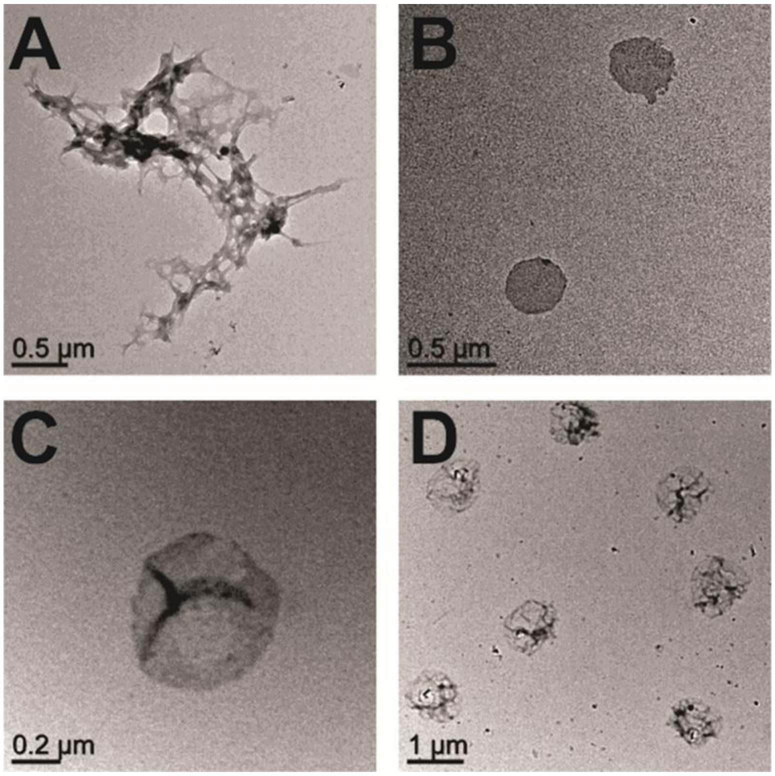

Figure 5.4. TEM images of PTOTT-*b*-DNA assemblies in water that were self-assembled from DMF at different concentrations of PTOTT-*b*-DNA; (A) 1 μM, (B) 4 μM, (C) 7 μM, and (D) 18 μM.

5.4.3 Effect of Salt on Assembly Structure. The PTOTT-*b*-DNA vesicles undergo a unique phase transitions from vesicles to collapsed vesicle membranes upon addition of salts as shown in the TEM images in Figure 5.5. When dried 0.3 M PBS is added to PTOTT-*b*-DNA vesicles in water the vesicle structure (Figure 5.5 A) collapses into a vesicle membrane structure as shown in Figure 5.5 B. The same collapsed vesicle membrane structure is obtained (Figure 5.5 C) when salt is added in a less harsh condition; via slow water addition with 0.1 M PBS and then complete dialysis into 0.1 M PBS. The salt induced morphology change was also found to be somewhat reversible. When the collapsed vesicle membrane in 0.3 M PBS was dialyzed back into water, the morphology returned to a mixture of vesicles and lamellae as shown in Figure 5.5 D,E. Although the vesicle structure found after dialysis looked more broken then the original structure, this is still a good indication that tuning salt conditions could be a useful technique to reversibly tune the morphology of PTOTT-*b*-DNA.

The salt induced morphological transition occurs in PTOTT-*b*-DNA because the added salts effectively screen the negative charges on the phosphate backbone of the DNA thus causing a transition to a lower curvature morphology. It is known that the morphologies of charged diblock copolymer amphiphiles in solution are determined by a delicate balance of non-covalent forces that are further complicated by the steric and electrostatic interactions of the charged coronal blocks.[44] Early work from Eisenberg *et al.* demonstrated that with increasing salt contents, the morphology of PS-*b*-PAA can be tuned from spheres to rods, to vesicles, to large compound vesicles.[45] Later work by Discher *et al.* showed that the morphologies such as tethered vesicles, encapsulated vesicles, or large compound vesicles formed from a charged diblock copolymers of PAA-*b*-PBD in water could be controlled by tuning the ionic strength and pH of the solution.[46] This is the first example of a DNA block copolymer assembly that exhibited a morphological change dependent on the salt concentration.

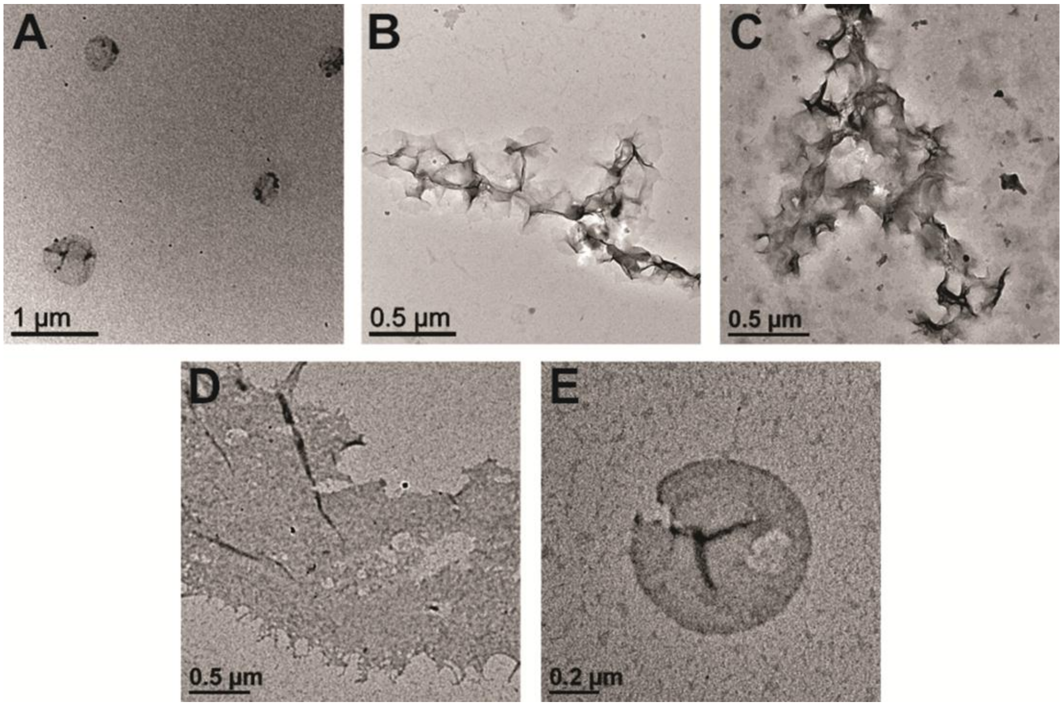

Figure 5.5. TEM images of PTOTT-*b*-DNA assemblies in (A) water, (B) in 0.3 M PBS, (C) self-assembled into 0.1 M PBS, and (D,E) dialyzed back into water after being in 0.1 M PBS.

5.4.4 Hybridization with Complementary DNA. The accessibility of the DNA for duplex hybridization events on the surface of the PTOTT-*b*-DNA vesicles were investigated in this system. The PTOTT-*b*-DNA vesicles were hybridized with a complementary DNA strand in 0.3 M PBS. The sequence specific hybridization event was monitored by UV and compared with the melting curve of a ds-DNA control as shown in Figure 5.6. Preliminary binding studies do show evidence of DNA hybridization, but enhanced binding is not observed (Figure 5.6). In fact the melting temperature (Tm) of ds-DNA-*b*-PTOTT is very similar to that of ds-DNA with respective T_m of 56.4 °C and 56.9 °C. The absorbance change for ds-DNA-b-PTOTT was smaller (32 %) when compared to the ds-DNA control sample (43 %). This smaller change in absorbance could occur because the DNA strands in the core of the ds-DNA-b-PTOTT vesicle membrane structure are not available to bind with the complementary DNA strand. It was originally hypothesized that hybridization with complementary DNA might additionally change the conformation of PTOTT and subsequently effect the optical properties of the system. However, no changes in absorption and emission were observed after hybridization with a complementary DNA strand. Continuing efforts are being made to tune the morphology of the PTOTT-*b*-DNA in an effort to adjust the DNA density on the surface and study the binding efficiency of the resultant morphologies.

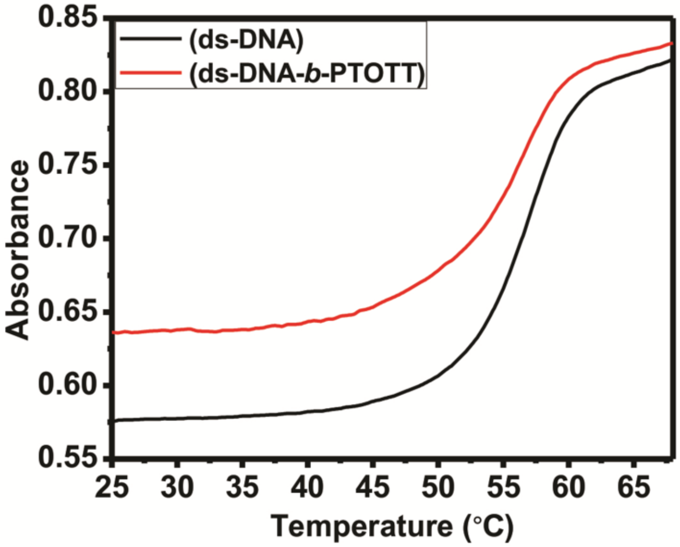

Figure 5.6. Melting curve of 2.5 μM ds-DNA control (black) and 2.5 μM ds-DNA-*b*-PTOTT in 0.1 M PBS.

5.4.5 Comparison with PTOTT Homopolymer. The structure of PTOTT is such that the hydrophobic thiophene backbone and polar tetraethylene glycol side chains resembles an amphiphilic brush copolymer. Although the PTOTT homopolymer will not directly dissolve in an aqueous solvent, it can be self-assembled into aqueous solvents via slow-addition of water and dialysis into water from a common solvent. The absorbance characteristics and TEM images of the self-assembled morphologies of PTOTT homopolymers self-assembled from DMF at different concentrations are presented in Figure 5.7. The average diameter of the PTOTT homopolymer micelles as measured by TEM analysis increased from 89 ± 13 nm at 1 μM concentration, to 210 ± 40 nm at 4 μM concentration, to 279 ± 53 nm at 7 μM concentration, and 338 ± 43 nm at a 20 μM concentration of PTOTT. In comparison to PTOTT-*b*-DNA vesicles, the size of the homopolymer micelles did not depend as closely on the polymer concentration. This suggests that the vesicle morphology is much more dependent on the aggregation number than the closely packed homopolymer assemblies. The PTOTT homopolymer micelle-like aggregates are stable in water and do not undergo any sort of morphology transition when salts are added to the system. This confirms that the charged DNA block is necessary to form vesicles and that the salt induced morphology transitions are a direct result of salt induced screening of the charged DNA block.

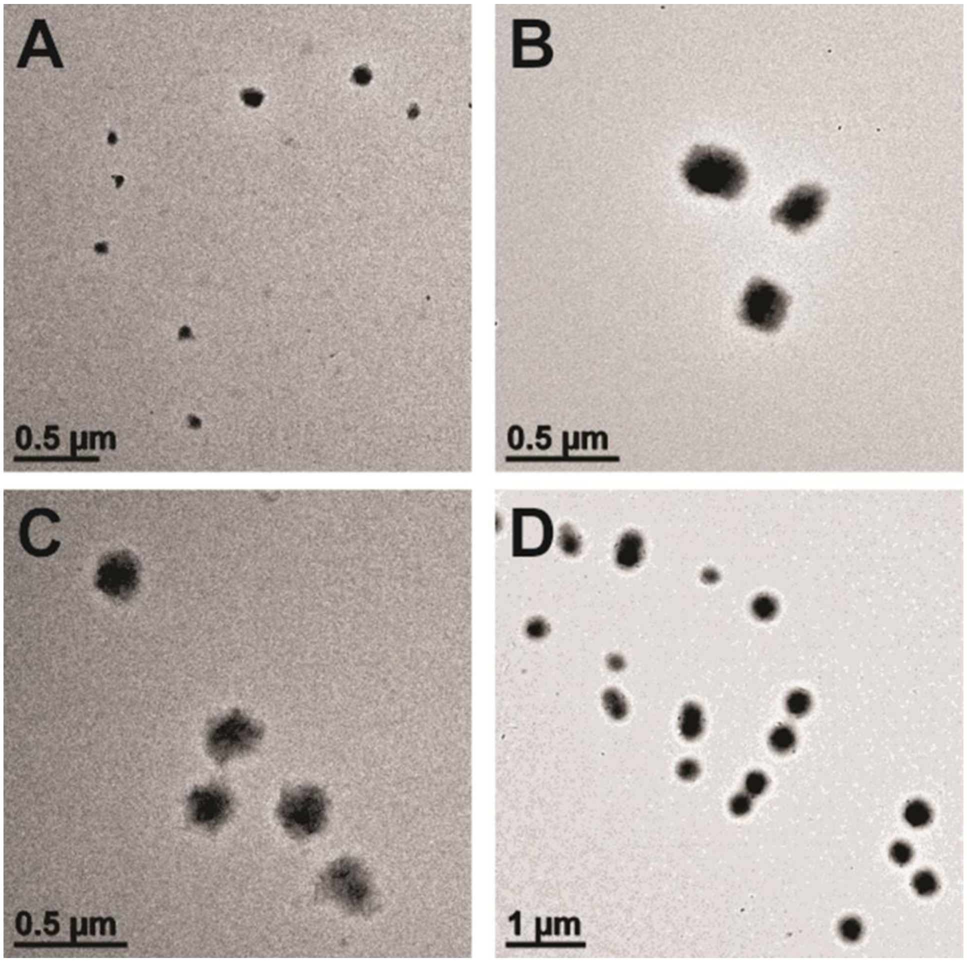

Figure 5.7. TEM images of PTOTT homopolymer assemblies in water that were self-assembled from DMF at different concentrations of PTOTT; (A) 1 μM, (B) 4 μM, (C) 7 μM, and (D) 18 μM.

5.4.6 Encapsulation of Nanoparticles. A hybrid nanomaterial structure of PTOTT-*b*-DNA and hydrophobic iron oxide nanoparticles was formed via self-assembly of the conjugated DNA polymer with the magnetic nanoparticles. The magnetic nanoparticles were incorporated into the PTOTT-*b*-DNA structure as evidenced by the TEM images in Figure 5.8 which clearly show nanoparticles located only in PTOTT-*b*-DNA assemblies. It is unclear from the TEM images where the nanoparticles are located within the PTOTT-*b*-DNA vesicle, but it is likely that the hydrophobic particles would preferentially locate within the hydrophobic PTOTT membrane of the vesicle structure. Another member of the Park group was the first to demonstrate encapsulation of nanoparticles into a DNA block copolymer micelle of DNA-*b*-PS.[13] Other groups such as Eisenberg *et al.* have incorporated gold nanoparticles functionalized with poly(styrene)-*b*-PAA (PS-*b*-PAA) into the walls of PS-b-poly(ethylene oxide) (PS-*b*-PEO) vesicles due to hydrophobic interactions.[47] The exact location of the nanoparticles in this case was easier to distinguish due to the electron density of the polymers and the collapsed nature of the vesicles. However, the incorporation of nanoparticle within DNA block copolymer vesicles present herein is important because it demonstrates the functionality of the system which should prove useful in the pursuit of many applications.

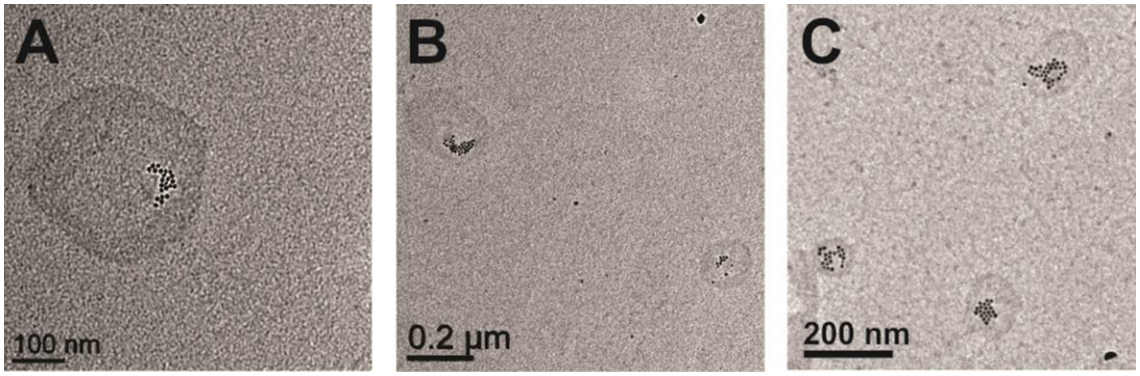

Figure 5.8. TEM images of PTOTT-*b*-DNA with magnetic nanoparticles incorporated into the vesicle structure.

5.5 Conclusions

The DNA conjugated block copolymer system presented herein, is one of the first reported amphiphilic conjugated polymer hybrids. The self-assembly of this amphiphilic conjugated DNA block copolymer into a distinct vesicle structure reveals the structural importance of the conjugated block in determining the morphology of the bioconjugated nanostructure. The work presented herein also reveals a unique salt-dependent morphology transition due to the salt screening the negative charges on the phosphate backbone of the DNA therefore causing a destabilization of the vesicle structure. DNA hybridization studies revealed that the recognition properties of the DNA block are retained in the vesicle structure. Furthermore, the functionality of the system is also demonstrated by the incorporation of hydrophobic particles into the bioconjugated PTOTT-*b*-DNA vesicle structure. It is expected that having the conjugated hydrophobic thiophene covalently attached to the DNA strand could lead to more complex self-assembled structures that could prove useful in drug delivery or nanoelectronic applications.

5.6 References

1. Kwak, M.; Herrmann, A., Nucleic Acid Amphiphiles: Synthesis and Self-Assembled Nanostructures. *Chem. Soc. Rev.* 2011, 40, 5745-5755.
2. Braunecker, W. A.; Matyjaszewski, K., Controlled/Living Radical Polymerization: Features, Developments, and Perspectives. *Prog. Polym. Sci.* 2007, 32, 93-146.
3. Lutz, J.-F.; Börner, H. G., Modern Trends in Polymer Bioconjugates Design. *Prog. Polym. Sci.* 2008, 33, 1-39.
4. Tian, H.; Tang, Z.; Zhuang, X.; Chen, X.; Jing, X., Biodegradable Synthetic

Polymers: Preparation, Functionalization and Biomedical Application. *Prog. Polym. Sci.* 2012, 37, 237-280.

5. Fuks, G.; Talom, R. M.; Gauffre, F., Biohybrid Block Copolymers: Towards Functional Micelles and Vesicles. *Chem. Soc. Rev.* 2011, 40, 2475-2493.

6. Alemdaroglu, F. E.; Herrmann, A., DNA Meets Synthetic Polymers - Highly Versatile Hybrid Materials. *Organic & Biomolecular Chemistry* 2007, 5, 1311-1320.

7. Liu, H. P.; Zhu, Z.; Kang, H. Z.; Wu, Y. R.; Sefan, K.; Tan, W. H., DNA-Based Micelles: Synthesis, Micellar Properties and Size-Dependent Cell Permeability. *Chemistry-a European Journal* 2010, 16, 3791-3797.

8. Kwak, M.; Musser, A. J.; Lee, J.; Herrmann, A., DNA-Functionalised Blend Micelles: Mix and Fix Polymeric Hybrid Nanostructures. *Chemical Communications* 2010, 46, 4935-4937.

9. Alemdaroglu, F. E.; Ding, K.; Berger, R.; Herrmann, A., DNA-Templated Synthesis in Three Dimensions: Introducing a Micellar Scaffold for Organic Reactions. *Angewandte Chemie-International Edition* 2006, 45, 4206-4210.

10. Alemdaroglu, F. E.; Alemdaroglu, N. C.; Langguth, P.; Herrmann, A., DNA Block Copolymer Micelles - a Combinatorial Tool for Cancer Nanotechnology. *Adv. Mater.* 2008, 20, 899-902.

11. Tran, H. D.; Li, D.; Kaner, R. B., One-Dimensional Conducting Polymer Nanostructures: Bulk Synthesis and Applications. *Advanced Materials* 2009, 21, 1487-1499.

12. Fuks, F.; Talom, R. M.; Gauffre, F., Biohybrid Block Copolymers: Towards Functional Micelles and Vesicles. *Chem. Soc. Rev.* 2011.

13. Chen, X. J.; Sanchez-Gaytan, B. L.; Hayik, S. E. N.; Fryd, M.; Wayland, B. B.; Park, S. J., Self-Assembled Hybrid Structures of DNA Block-Copolymers and Nanoparticles with Enhanced DNA Binding Properties. *Small* 2010, 6, 2256-2260.

14. Li, Z.; Zhang, Y.; Fullhart, P.; Mirkin, C. A., Reversible and Chemically Programmable Micelle Assembly with DNA Block-Copolymer Amphiphiles. *Nano Lett.* 2004, 4, 1055-1058.

15. Ding, K.; Alemdaroglu, F. E.; Boersch, M.; Berger, R.; Herrmann, A., Engineering

the Structural Properties of DNA Block Copolymer Micelles by Molecular Recogntition. *Angewandte Chemie-International Edition* 2007, 46, 1172-1175.

16. Alemdaroglu, F. E.; Alemdaroglu, N. C.; Langguth, P.; Herrmann, A., Cellular Uptake of DNA Block Copolymer Micelles with Different Shapes. *Macromolecular Rapid Communications* 2008, 29, 326-329.

17. Klok, H. A.; Lecommandoux, S., Supramolecular Materials Via Block Copolymer Self-Assembly. *Advanced Materials* 2001, 13, 1217-1229.

18. Alemseghed, M. G.; Gowrisanker, S.; Servello, J.; Stefan, M. C., Synthesis of Di-Block Copolymers Containing Regioregular Poly(3-Hexylthiophene) and Poly(Tetrahydrofuran) by a Combination of Grignard Metathesis and Cationic Polymerizations. *Macromolecular Chemistry and Physics* 2009, 210, 2007-2014.

19. Iovu, M. C.; Jeffries-El, M.; Sheina, E. E.; Cooper, J. R.; McCullough, R. D., Regioregular Poly(3-Alkylthiophene) Conducting Block Copolymers. *Polymer* 2005, 46, 8582-8586.

20. Wang, H. B.; Wang, H. H.; Urban, V. S.; Littrell, K. C.; Thiyagarajan, P.; Yu, L. P., Syntheses of Amphiphilic Diblock Copolymers Containing a Conjugated Block and Their Self-Assembling Properties. *J. Am. Chem. Soc.* 2000, 122, 6855-6861.

21. Hoeben, F. J. M.; Jonkheijm, P.; Meijer, E. W.; Schenning, A. P. H. J., About Supramolecular Assemblies of Pi-Conjugated Systems. *Chem. Rev.* 2005, 105, 1491-546.

22. Ho, H. A.; Bera-Aberem, M.; Leclerc, M., Optical Sensors Based on Hybrid DNA/Conjugated Polymer Complexes. *Chemistry-a European Journal* 2005, 11, 1718-1724.

23. Lee, K.; Povlich, L. K.; Kim, J., Label-Free and Self-Signal Amplifying Molecular DNA Sensors Based on Bioconjugated Polyelectrolytes. *Advanced Functional Materials* 2007, 17, 2580-2587.

24. Kwak, M*., et al.*, DNA Block Copolymer Doing It All: From Selection to Self-Assembly of Semiconducting Carbon Nanotubes. *Angewandte Chemie (International ed. in English)* 2011, 50, 3206-10.

25. Chen, X.-J.; Sanchez-Gaytan, B. L.; Hayik, S. E. N.; Fryd, M.; Wayland, B. B.; Park, S.-J., Self-Assembled Hybrid Structures of DNA Block-Copolymers and

Nanoparticles with Enhanced DNA Binding Properties. *Small (Weinheim an der Bergstrasse, Germany)* 2010, 6, 2256-60.

26. Campaigne, E.; Tullar, B. F., 3-Thenyl Bromide - Thiophene, 3-Bromomethyl. *Organic Synthesis* 1953, 33, 96-98.

27. Ngwendson, J. N.; Atemnkeng, W. N.; Schultze, C. M.; Banerjee, A., A Convenient Synthesis of Symmetric 1,2-Diarylethenes from Arylmethyl Phosphonium Salts. *Organic Letters* 2006, 8, 4085-4088.

28. Koeckelberghs, G.; Vangheluwe, M.; Samyn, C.; Persoons, A.; Verbiest, T., Regioregular Poly(3-Alkoxythiophene)S: Toward Soluble, Chiral Conjugated Polymers with a Stable Oxidized State. *Macromolecules* 2005, 38, 5554-5559.

29. Sheina, E. E.; Khersonsky, S. M.; Jones, E. G.; McCullough, R. D., Highly Conductive, Regioregular Alkoxy-Functionalized Polythiophenes: A New Class of Stable, Low Band Gap Materials. *Chemistry of Materials* 2005, 17, 3317-3319.

30. Liu, J.; Loewe, R. S.; McCullough, R. D., Employing Maldi-Ms on Poly(Alkylthiophenes):‚Äâ Analysis of Molecular Weights, Molecular Weight Distributions, End-Group Structures, and End-Group Modifications. *Macromolecules* 1999, 32, 5777-5785.

31. Alemdaroglu, F. E.; Ding, K.; Berger, R.; Herrmann, A., DNA-Templated Synthesis in Three Dimensions: Introducing a Micellar Scaffold for Organic Reactions. *Angewandte Chemie (International ed. in English)* 2006, 45, 4206-10.

32. Lutz, J. F.; Borner, H. G., Modern Trends in Polymer Bioconjugates Design. *Prog. Polym. Sci.* 2008, 33, 1-39.

33. Ritter, S. K.; Noftle, R. E., Cleavage of Substituents Upon Oxidative Polymerization of Substituted Thiophenes. *Inorg. Chim. Acta* 1999, 287, 232-237.

34. de Cuendias, A.; Hiorns, R. C.; Cloutet, E.; Vignau, L.; Cramail, H., Conjugated Rod-Coil Block Copolymers and Optoelectronic Applications. *Polym. Int.* 2010, 59, 1452-1476.

35. Choucair, A.; Eisenberg, A., Control of Amphiphilic Block Copolymer Morphologies Using Solution Conditions. *European Physical Journal E* 2003, 10, 37-44.

36. Fuks, G.; Mayap Talom, R.; Gauffre, F., Biohybrid Block Copolymers: Towards

Functional Micelles and Vesicles. *Chem. Soc. Rev.* 2011, 40, 2475-93.

37. Cottenye, N.; Syga, M.-I.; Nosov, S.; Müller, A. H. E.; Ploux, L.; Vebert-Nardin, C., Biological-Like Vesicular Structures Self-Assembled from DNA-Block Copolymers. *Chemical communications (Cambridge, England)* 2012, 48, 2615-7.

38. Teixeira Jr, F.; Rigler, P.; Vebert-Nardin, C., Nucleo-Copolymers: Oligonucleotide-Based Amphiphilic Diblock Copolymers. *Chem. Commun.* 2007, 1130-1132.

39. Ahmed, F.; Discher, D. E., Self-Porating Polymersomes of Peg–Pla and Peg–Pcl: Hydrolysis-Triggered Controlled Release Vesicles. *J. Controlled Release* 2004, 96, 37-53.

40. Tataurov, A. V.; You, Y.; Owczarzy, R., Predicting Ultraviolet Spectrum of Single Stranded and Double Stranded Deoxyribonucleic Acids. *Biophys. Chem.* 2008, 133, 66-70.

41. Tung, Y.-C.; Wu, W.-C.; Chen, W.-C., Morphological Transformation and Photophysical Properties of Rod-Coil Poly[2,7-(9,9-Dihexylfluorene)]-Block-Poly(Acrylic Acid) in Solution. *Macromol. Rapid Commun.* 2006, 27, 1838-1844.

42. Zhang, L.; Eisenberg, A. D. I., Crew-Cut Aggregates from Self-Assembly of Blends of Polystyrene-B-Poly (Acrylic Acid) Block Copolymers and Homopolystyrene in Solution. 1999, 1469-1484.

43. Zhang, L.; Eisenberg, A., Thermodynamic Vs Kinetic Aspects in the Formation and Morphological Transitions of Crew-Cut Aggregates Produced by Self-Assembly of Polystyrene-B-Poly (Acrylic Acid) Block Copolymers in Dilute Solution. 1999, 2239-2249.

44. Discher, D. E.; Ahmed, F., Polymersomes. *Annu. Rev. Biomed. Eng.* 2006, 8, 323-41.

45. Zhang, L.; Eisenberg, A., Morphogenic Effect of Added Ions on Crew-Cut Aggregates of Polystyrene-B-Poly(Acrylic Acid) Block Copolymers in Solutions. *Macromolecules* 1996, 29, 8805-8815.

46. Geng, Y.; Ahmed, F.; Bhasin, N.; Discher, D. E., Visualizing Worm Micelle Dynamics and Phase Transitions of a Charged Diblock Copolymer in Water. *The journal of physical chemistry. B* 2005, 109, 3772-9.

47. Mai, Y.; Eisenberg, A., Controlled Incorporation of Particles into the Central Portion of Vesicle Walls. *J. Am. Chem. Soc.* 2010, 132, 10078-10084.